# Static and Dynamic Analysis of Nonlinear Valve Springs Based on Finite Element Analysis and Machine Learning Algorithm


Submitted by:

**ZEWEN GU**

This dissertation is submitted for the degree of Doctor of Philosophy

2022

**Lancaster University**

Engineering Department

# Declaration

This thesis has not been submitted in support of an application for another degree at this or any other university. It is the result of my own work and includes nothing that is the outcome of work done in collaboration except where specifically indicated. Many of the ideas in this thesis were the product of discussion with my supervisor Prof. Jianqiao Ye and Dr. Xiaonan Hou.

Excerpts of this thesis have been published in the following conference manuscripts and academic publications.

1. ***Non-linear finite element model for dynamic analysis of high-speed valve train and coil collisions.***

- Authors: Zewen Gu, Xiaonan Hou, Elspeth Keating, Jianqiao Ye
- Journal: *International Journal of Mechanical Sciences*
- Year: 2020

2. ***Advanced static and dynamic analysis method for helical springs of nonlinear geometries.***

- Authors: Zewen Gu, Xiaonan Hou, Jianqiao Ye
- Journal: *Journal of Sound and Vibration*
- Year: 2021

3. ***Analysis and design method of nonlinear helical springs using a combining technique: Finite Element analysis, constrained Latin Hypercube sampling and Genetic Programming.***

- Authors: Zewen Gu, Xiaonan Hou, Jianqiao Ye
- Journal: *Proceedings of the Institution of Mechanical Engineers, Part C: Journal of Mechanical Engineering Science*
- Year: 2021

ZEWEN GU and full qualifications
Lancaster University, UK

# Abstract

The valve spring is a fundamental type of helical spring which is essential for enabling the opening and closure of a valve in a car engine. Nowadays, it is increasingly common to use valve springs of nonlinear geometry in high-speed car engines for better dynamic performance. However, practical issues such as malfunction and pre-failure are also raised by spring researchers and manufacturers using and analysing these nonlinear springs. It is commonly stated that existing spring models and empirical formula do not allow for the analysis of these nonlinear springs. To tackle such difficulties, it is imperative that all the varied geometric parameters of a nonlinear spring be clarified in order to facilitate efficient and generalizable analysis. Past research efforts have mainly emphasized the analysis of standard valve springs of constant geometric parameters and the development of spring models for low-speed static conditions. However, these models do not take into account the full breadth of conditions and consequently are considered to be insufficient and compromised in accuracy. Therefore, it remains a challenge to effectively leverage such models in the analysis and design of nonlinear valve springs.

This thesis aims to address the existing gaps and present a comprehensive study on the analysis of nonlinear valve springs and their dynamic response in high-speed engines. An advanced spring formula is developed based on simplified curved beam theory to formulate the relationships between the nonlinear spring geometry (varied coil diameter, varied pitch and coil clash) and the mechanical properties of a beehive valve spring. These nonlinear considerations deliver a higher predictive accuracy than the existing spring formulas by comparing FE and experimental results. The new spring formula is coupled with the distributed parameter model to simulate the dynamic spring

responses. However, whilst it accurately simulates the dynamic responses at lower engine speeds (lower 5000-rpm), it fails to simulate the significant abnormal spring forces at high engine speeds (over 8000-rpm). On the contrary, the FE springs model is developed, of which static and dynamic simulation results fit well with the experimental data at both low and high engine speeds. More importantly, analysis of the dynamic FE results explains how the violent coil clash leads to significant abnormal spring forces. In the last part, a machine learning model, based on genetic programming techniques and the FE results, is developed to aid the design of nonlinear helical springs. The model enables researchers to analyse nonlinear helical spring properties directly using information extracted from FE results data, bypassing the necessity to unravel the complex inner relationships between the nonlinear spring parameters.

# Acknowledgements

I would like to express my deepest and most sincere gratitude to my supervisors, Prof. Jianqiao Ye and Dr. Xiaonan Hou, for their continuous support of my research and class work during my academic career. I should really be thankful for their surgical advice and expert guidance on my academic and living aspects. I am very fortunate to have such approachable and devoted mentors, especially those who paid patience and delivered ideas to every single problem I met. I believed these professional guides and advice for my life had made a huge step for me towards being an academic researcher.

I would also like to thank my parents, my sister and especially the companion of my wife. I am only able to be writing this PhD thesis due to the support of my parents and the wise advice of my sister Dr. Chongyan Gu. Especially, I am very gratefully for the unconditional love of my wife Xiaoxuan Ding. They had always stayed by my side in the journey when I pursued the completion of the PhD. Words will never be sufficient to express my gratitude and my respect.

I wish to thank my sponsor company Force Technology Ltd. and the Centre of Global Eco-Innovation organization. Steve Williams and Simon Lonsdale from Force Technology have given me the best technical support they can do and be always gentle and lovely to me.

Finally, I am grateful to my colleagues and friends I met at Lancaster University and everyone that has made my time as a PhD student in Lancaster University an outstanding, fruitful and enriching experience.

# List of Tables

# List of Figures

# Nomenclature

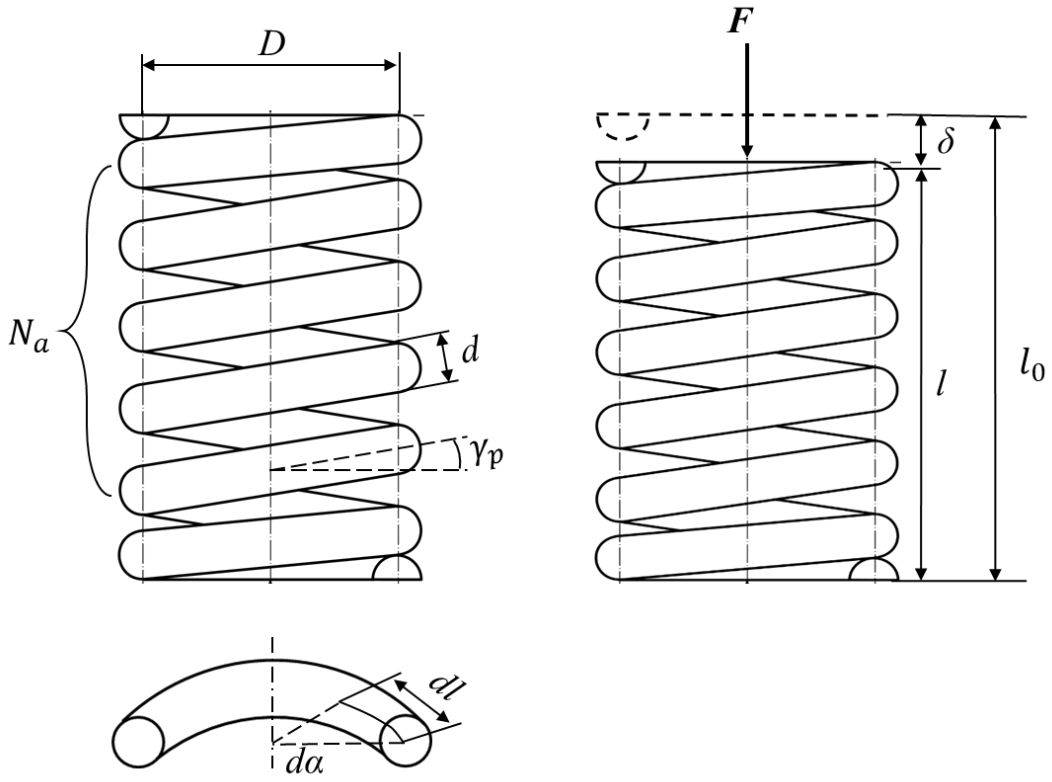


**Helical Spring Terminology**

| | |
|---|---|
| $\alpha/\alpha_0$ | Coil rotating radius (cylindrical polar coordinates) / Total coil radius of single helical spring |
| $\alpha_e/\alpha_i$ | the coil rotating radius of the first/last untouched spring element |
| $d/d_o/d_i$ | Wire diameter / Wire diameter of outer spring / Wire diameter of inner spring |
| $l_0/l$ | Free length / current length of helical spring |
| $\gamma_p$ | Pitch angle |
| $D$ | Coil diameter of helical spring |
| $N_a$ | Number of active coils of helical spring |
| $R$ | Radius of circular helix coil |

**Analytical Model Notations**

| | |
|---|---|
| $\beta$ | Total angle of twist of spring wire at loading end |
| $\delta$ | Axial displacement of spring loading end |
| $\varphi$ | Torsion of helical curve in the Cylinder coordinates system |
| $f$ | First order natural frequency |
| $g$ | Acceleration of gravity |
| $\xi$ | Viscous damping ratio |
| $\kappa$ | Curvature of helical curve in the Cylinder coordinates system |
| $k$ | Spring stiffness |
| $m$ | Active mass of helical spring |
| $\omega$ | Angular speed of valve cam |
| $\rho$ | Material density |
| $\tau/\tau_m$ | Shear stress / maximum shear stress |
| $F$ | Applied longitudinal load |
| $G$ | Material shear modulus |
| $M$ | Torque moment |

**Abreviation**

| | |
|---|---|
| *cLHS* | Constrained Latin hypercube sampling |
| *DOHC* | Double overhead camshaft |
| *FEA* | Finite element analysis |
| *GP* | Genetic programming |
| *GA* | Genetic algorithm |
| *IC* | Internal combustion |

| | |
|---|---|
| *LHS* | Latin hypercube sampling |
| *ML* | Machine learning |
| *NF* | Nature frequency |
| *SOHC* | Single overhead camshaft |
| *SC* | Super clean |

# Contents

# 1 Introduction

## 1.1 Background

As one of the most commonly used components in mechanical systems, the helical spring, with its unique coiled shape and large flexibility, can transfer kinetic energy into potential energy. Its uses are manifold and range from low-speed working conditions, like vehicle suspension and shock absorption, to high-speed conditions such as an engine valve train and high-speed machine tool. The first and most fundamental law for depicting the properties of a helical spring is Hook's law which British physicist Robert Hooke proposed in 1676. This law was effective for the relatively simple working conditions of helical springs in earlier periods, and back then significant errors in estimating their properties were considered acceptable. However, mechanical systems are much more complicated today, contributing to more complex working conditions for the helical springs inside the systems. In addition, the demand for a more precise estimation of spring properties has also increased. In efforts to achieve these, engineers and researchers have contributed to unveil the latent relationships between spring properties and spring materials and between spring properties and spring structures. Then, categories of analytical and numerical models, such as distributed parameters, lumped mass, finite element, and multi-body models, were presented to analyse helical springs. Despite being only used in static or quasi-static conditions, these models succeed in improving the precision of estimating spring properties to a higher level.

The phenomenon of severe spring failure and damage were observed during the 1930s when significant increments in car engine speeds were introduced. Malfunctions of car engines occurred due to the breakage of valve springs, which traditional static spring theories fail to explain. In an IC (internal combustion) engine, a valve spring is

usually defined as a helical spring used to hold closed the engine valve after the valve is opened mechanically. When an engine is operating, the inside valve springs, when compressed repeatedly, perform as elastic objects to periodically store and release mechanical energy. The valve spring acts as the most flexible part in a cam-train system, and its failure leads to the malfunction of the IC engine. It was later found that the dynamic effects of helical springs, for example spring surge, could be the culprit of these failures. When the operating speeds of a valve spring are high, the dynamic effects can be much larger than with static results.

To consider these dynamic responses, researchers placed dynamic terms into the existing static spring models for analysis. On the other hand, spring designers discovered that the dynamic effects could be mitigated by modifying the basic structure of a helical spring, such as making the coil diameter varied and adding narrow pitches between spring coils. However, these changes turn a helical spring from linear to nonlinear. As a result, the traditional spring models and empirical spring formulas fail to estimate the properties of these nonlinear springs and, therefore, fail to simulate the nonlinear dynamic response at high speeds.

## 1.2 Aims and Objectives

The purpose of this thesis addresses a practical engineering problem encountered by one of our co-operators, Force Technology Ltd., a company specialising in the manufacturing of various ranges of helical springs. One of their products is the beehive valve spring which serves the high-speed engine of McLaren sports cars. The beehive spring has a varied coil diameter and a narrow pitch between coils. It is expected to work at engine speeds of up to 10,000 rpm. It is found that the dynamic spring forces at certain engine speeds are much higher than the forces at other speeds and the forces

under static compressions, therefore potentially leading to a decrease in the fatigue life of the spring and bringing about earlier failure of it. However, it is difficult to understand the problem by simply analysing the testing data. Besides, the traditional spring models also show their drawbacks in simulating the high-speed dynamic response of nonlinear helical springs. Therefore, it is imperative to develop a feasible and effective model for discovering the myth behind the significant dynamic spring forces. The main aims and objectives of this study are as follows:

1. To improve the exiting linear analytical models of helical springs by considering the nonlinear effects of unique spring designs.

2. To couple the developed analytical spring model with the distributed parameter spring model to include the nonlinear spring effects in the dynamic solutions.

3. To develop nonlinear static and dynamic finite element spring models for accurately simulating and explaining the nonlinear dynamic responses of a high-speed valve spring.

4. To investigate the cause of the abnormal high-frequency spike forces that appear in high engines by using the dynamic FE models.

5. To develop an innovative machine learning model based on the FE results for effectively and efficiently analysing and designing nonlinear helical springs with desired mechanical properties.

## 1.3 Thesis structures

The thesis is divided into seven chapters. This chapter introduces the development of traditional helical springs under various different working conditions. The rapid development of designs of helical springs brings nonlinearities into the helical spring geometries, and the nonlinearities result in new challenges and problems in the

applications and analysis of nonlinear helical springs. The motivation for solving problems raised by a spring manufacturer is also stated in this chapter.

Chapter 2 contains a literature survey. It establishes how researchers address the static and dynamic problems of helical springs. The characteristics of the existing analysis methods of helical springs and their differences are demonstrated and discussed.

Chapter 3 presents the setup of static spring compression tests and dynamic engine head tests. The basic layouts of various valvetrain mechanisms and the installation of valve springs in the studied valvetrain are also discussed.

Chapter 4 presents the development of an analytical spring model for analysing the high-speed dynamic effects of a beehive valve spring based on the distributed parameter model demonstrated in Chapter 2. Also, innovative spring formulas are developed for predicting the mechanical properties of helical springs with nonlinear geometries. It is then coupled with the developed analytical spring model to conduct high-speed dynamic simulations for the nonlinear beehive valve spring.

Chapters 5 and 6 are dedicated to describing the development of finite element (FE) spring models in Ansys. In Chapter 5, the nonlinear geometry of the beehive spring is represented by developing a 3D geometry model in Solidworks. The spring geometry model is imported into Ansys and meshed for developing an FE spring model. The FE model is simulated under static loadings, and the simulation results are compared with the results of the developed spring formulas and the experimental data. In Chapter 6, the FE model developed in Chapter 5 is simulated under high-speed dynamic loadings at 4200-rpm, 5600-rpm and 8000-rpm engine speeds. The dynamic FE simulation results are compared with the results of the analytical spring model and the engine head test at the same engine speeds.

In Chapter 7, a genetic programming model is proposed to implement nonlinear helical springs' design and analysis by combining machine learning techniques with the developed FE spring model. An advanced sampling technique is adopted to select numerical samples in the given design domain. A sensitivity analysis of the variable spring geometry parameters is also conducted to investigate the relationships between spring geometry parameters and essential mechanical properties.

The general conclusions are drawn in Chapter 8, where the recommendations of the future works follow. First, a reflective conclusion on how the present outcomes contribute to the research development in helical springs and how the developed methods are beneficial for the cooperated spring manufacturer is stated. Next, the developed novelty is summarized, and finally, a promising trend for future works is given.

# 2 Literature Review

## 2.1 Elementary Theory of Mechanical Springs

The research on mechanical springs dates back to 1678 when British physicist, Robert Hooke, discovered Hooke's law. It was then widely used in the centuries that followed. The dynamic characteristics of the high-speed spring were systematically studied from the early 1900s together with the development of IC engines. Berry presented his concerns on the practical problems of spring designs (Berry, 1938). The difficulties of spring products designed by engineers were, as he commented, 'merely incidental'. Elementary theories were presented to analyse the static and dynamic properties of mechanical springs during that era.

### 2.1.1. Helix curve theory

One of the theories that mechanical springs are based on is the theory of space curve. It treats the geometry of a mechanical spring, or the centre line of a spring rod, as a curve embedded in a three-dimensional space. At an early age, the notion of curvature was extended from a two-dimensional plane to a three-dimensional space, which contributes towards laying the solid foundation for deriving the formulae for mechanical spring properties (Serret, 1851, Frenet, 1852). When assuming a circular helix with radius *R*, the position vector $\boldsymbol{r}$ of a helix in Cartesian coordinates system (Figure 2-1a) can be described:

$$\boldsymbol{r} = \boldsymbol{x} + \boldsymbol{y} + \boldsymbol{z} \tag{2.1}$$

In order to write the position vector $\mathbf{r}$ of a point on the helix in the Cylinder coordinates system (Figure 2-1 (b)), we define coordinates vectors by:

$$\boldsymbol{x} = R \cdot \cos(\alpha) \cdot \boldsymbol{E_1} \tag{2.2}$$

$$\boldsymbol{y} = R \cdot \sin(\alpha) \cdot \boldsymbol{E_2} \tag{2.3}$$

$$\boldsymbol{z} = R \cdot \alpha_p \cdot \alpha \cdot \boldsymbol{E_3} \tag{2.4}$$

where $\boldsymbol{E_1}$, $\boldsymbol{E_2}$ and $\boldsymbol{E_3}$ are the coordinates vectors in the Cylinder coordinates system, and $\alpha$ is the cylindrical polar coordinates. The $\alpha_p = tan(\gamma_p)$, where $\gamma_p$ is the pitch angle. By substituting Eq.(2.2), (2.3) and (2.4) into Eq.(2.1), we got the position vector $\boldsymbol{r}$ below:

$$\boldsymbol{r} = R \cdot cos(\alpha) \cdot \boldsymbol{E_1} + R \cdot sin(\alpha) \cdot \boldsymbol{E_2} + R \cdot \alpha_p \cdot \theta \cdot \boldsymbol{E_3} \tag{2.5}$$

We can define unit vectors $\boldsymbol{e_r}$ and $\boldsymbol{e_\theta}$ by:

$$\boldsymbol{e_r} = \cos(\alpha) \cdot \boldsymbol{E_1} + \sin(\alpha) \cdot \boldsymbol{E_2} \tag{2.6}$$

$$\boldsymbol{e_\theta} = \cos(\alpha) \cdot \boldsymbol{E_2} - \sin(\alpha) \cdot \boldsymbol{E_1} \tag{2.7}$$

It is common to rewrite Eq. (2.5) as:

$$\boldsymbol{r} = R \cdot \boldsymbol{e_r} + R \cdot \alpha_p \cdot \alpha \cdot \boldsymbol{E_3} \tag{2.8}$$

According to Frenet-Serret Formulas, the unit tangent vector $\boldsymbol{e_t}$ can be computed by differentiating the position vector $\boldsymbol{r}$ with respect to the arc-length parameter $s$.

$$\boldsymbol{e_t} = \frac{\partial \boldsymbol{r}}{\partial s} = \frac{d\theta}{ds}(R \cdot \boldsymbol{e_\theta}) + R \cdot \alpha_p \cdot \boldsymbol{E_3} \tag{2.9}$$

As $\boldsymbol{e_t}$ is a unit vector, the norm of $\boldsymbol{e_t}$ should satisfy:

$$\| \boldsymbol{e_t} \| = 1 \tag{2.10}$$

By substituting Eq. (2.9) into Eq.(2.10), we can infer that

$$\frac{d\alpha}{ds} = \pm \frac{1}{R\sqrt{1 + \alpha_p{}^2}} \tag{2.11}$$

Now, we can represent the basis vectors of the Frenet triad as:

$$\boldsymbol{e_t} = \pm \frac{1}{\sqrt{1 + \alpha_p{}^2}}(\boldsymbol{e_\theta} + \alpha_p \boldsymbol{E_3}) \tag{2.12}$$

$$\boldsymbol{e_n} = -\boldsymbol{e_r} \tag{2.13}$$

$$\boldsymbol{e_b} = \pm \frac{1}{\sqrt{1 + \alpha_p{}^2}} \left( \boldsymbol{E_3} - \alpha_p \boldsymbol{e_\theta} \right) \tag{2.14}$$

Eventually, the curvature $\kappa$ and the geometric torsion $\varphi$ can be calculated by:

$$\kappa = \| \frac{\partial \boldsymbol{e_t}}{\partial s} \| = \frac{1}{R} cos^2(\gamma_p) \tag{2.15}$$

$$\varphi = \| \frac{\partial^2 \boldsymbol{e_t}}{\partial s^2} \| = \frac{1}{R} \cos(\gamma_p) \sin(\gamma_p) \tag{2.16}$$

The derived formulas for the curvature and the torsion were then widely used by the subsequent researchers to describe the geometry of a helical spring.

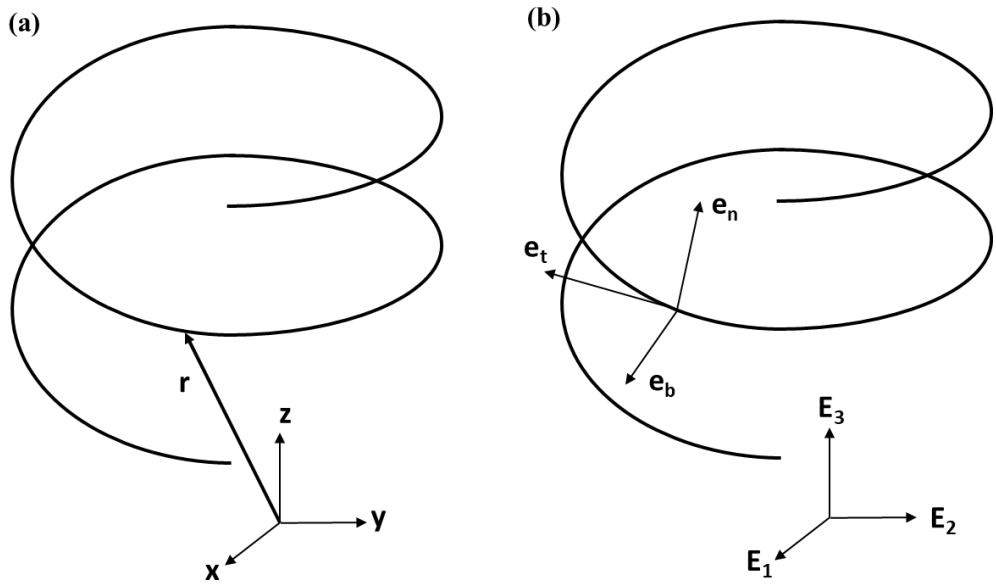


*Figure 2-1: (a). Helix and position vector* ***r*** *in Cartesian coordinates system. (b). Helix unit vector in the Cylinder coordinates system*

### 2.1.2. Beam deformation theory

Later, a comprehensive book of mechanical springs was published by Wahl (Wahl, 1944). In the book, the elementary theory is to assume a spring as a straight bar under torsion. In other words, the spring has a large spring index (the value of mean coil

diameter *D* over spring wire diameter *d*) and a small helix angle. A spring has a constant mean coil radius *R*, a constant wire diameter *d* and an applied loading *P* is shown in Figure 2-2(a). The cross-section of the spring wire is shown in Figure 2-2(b), where the distance between a point on the surface and the centre is denoted as $\rho$. The shear stress $\tau$ at a distance $\rho$ is:

$$\tau = 2\rho\tau_m/d \tag{2.17}$$

In this $\tau_m$ the maximum shear stress is on the surface of the cross-section of the spring wire. When denoting *M* to the total torque moment, the unit moment element *dM* taken up by the width $d\rho$ will be:

$$dM = 2\pi\rho^2 d\rho(2\rho\tau_m/d) \tag{2.18}$$

The total torque moment $F{\cdot}R$ will be:

$$F \cdot R = M = \int_0^{\frac{d}{2}} dM = \int_0^{\frac{d}{2}} \frac{4\pi\tau_m\rho^3}{d} d\rho = \frac{\pi d^3\tau_m}{16} \tag{2.19}$$

Then it can be re-written for calculating the maximum shear stress as:

$$\tau_m = \frac{16FR}{\pi d^3} \tag{2.20}$$

The deformation under torque moment will rotate the cross-section by a small angle $\theta$. According to the torsional beam theory, the value of $\theta$ is equal to $\tau_m/G$ as:

$$\theta = \frac{\tau_m}{G} = \frac{16FR}{\pi d^3 G} \tag{2.21}$$

where *G* is the shear modulus. The spring is considered a straight bar with a length $l = 2\pi nR$, where $N_a$ is the number of active coils (coils can deform during compression).

When the total angle $\beta$ is the angle of twist of the loading end, by using Eq.(2.21), it is:

$$\beta = \int_0^{2\pi nR} \frac{2\theta}{d} dl = \int_0^{2\pi nR} \frac{32FR}{\pi d^4 G} = \frac{64FR^2N_a}{Gd^4} \tag{2.22}$$

Here, the *dl* is the unit length of the spring coil. At last, since the effective moment arm is *R*, the total axial deformation $\delta$ at the loading end can be obtained by:

$$\delta = \beta R = \frac{64FR^3N_a}{Gd^4} \tag{2.23}$$

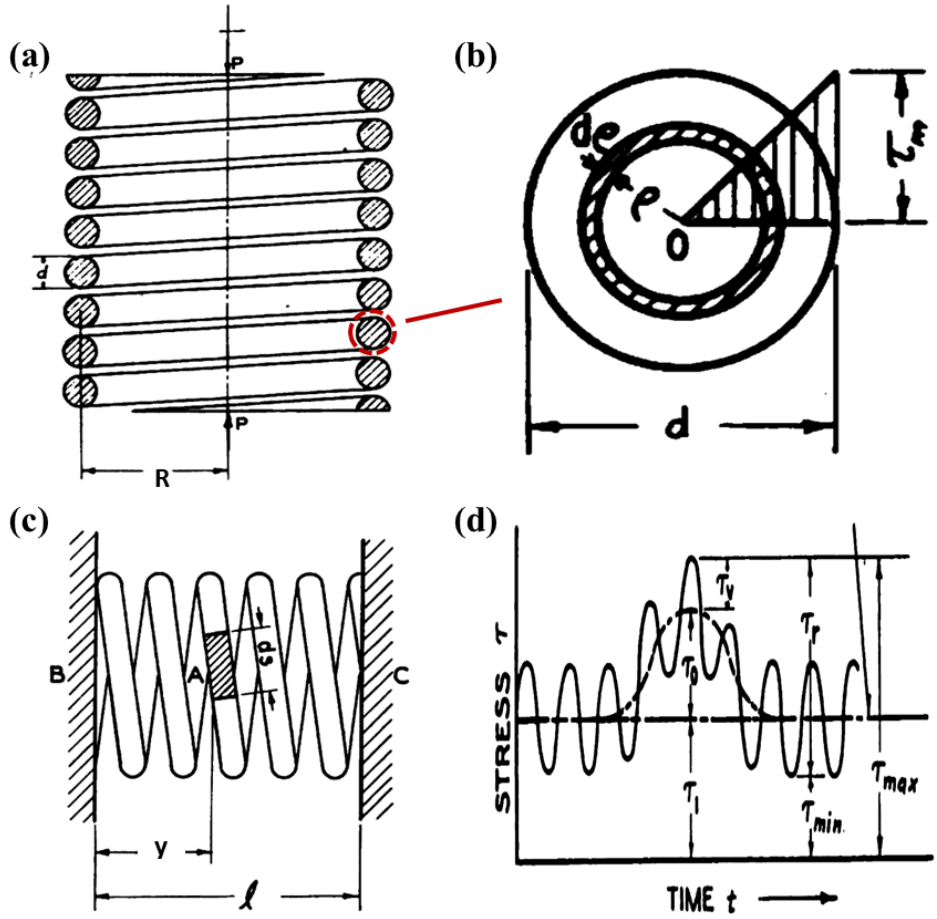


*Figure 2-2: (a). Helical spring with a large spring index and small pitch angle. (b). Cross-section of the spring wire. (c). Helical spring compressed by two parallel plates. (d). Static and dynamic stress of spring. Adapted from Wahl (1944).*

Eq.(2.23) derived in the study is the widely used formula for conveniently calculating the deflection or stiffness of a standard spring with a constant *R* and a constant $N_a$. Wahl (1944) commented that this formula is 'quite accurate even for fairly small spring indexes and large helix angles' compared with the ordinary stress formula. Besides, he highlighted the great importance of the dynamic effects of mechanical

springs due to surge or vibration in many applications - especially in the aircraft or automotive engine. Though in other applications loading was ‘tacitly’ assumed to be executing at a low rate, the phenomenon known as ‘spring surge’, which was explained by a wave travelling from the loading end to and then reflected by the fixed end. The travelling time depends on the natural frequency of the spring. He demonstrated that when the spring is subject to a rapid reciprocating motion, for instance, engine valve springs, it is essential to avoid the resonance generated between the natural frequency of the spring and the frequency of external loading. If it is not drawing enough attention, severe spring surging could cause more than 50% additional stress, which would probably lead to the malfunction of the spring.

In order to reduce surging stress, three recommendations were proposed. Firstly, Wahl (1944) suggested shaping the cam contour to make the spring operate with a low surging amplitude at specific harmonics. These harmonics of the cam are the ones causing resonance with the natural frequency of the spring. The second method increases the spring's natural frequency as high as possible, so resonance occurs at higher-order harmonics. Since the amplitudes of surging stress will reduce as the order of harmonic improves, the total stress of the spring will be lowered. The third way suggests a reduction or variation of the pitch of the coils at the lower end of the spring. It aims to close up end coils, and therefore change the natural frequency to weaken the resonance. Ultimately, it was concluded that the spring's natural frequency plays an essential role in reducing spring surges. Therefore, equations for calculating the natural frequency and dynamic characteristics of a vibrating spring were also developed.

Firstly, in order to describe the dynamic response of a helical spring, a differential equation of motion was derived. In Figure 2-2(c), the helical spring is compressed by

two flat plates, B and C. The spring element A has a *dl* length and is located at a distance of *x* from the end B. The weight of element A can be calculated by:

$$m_A = \frac{\pi d^2 \rho ds}{4g} \tag{2.24}$$

where $\rho$ is the weight of the spring material per unit of volume, and $g$ is the acceleration of gravity. By applying Newton's second law, the force to accelerate the element A can be written as:

$$F_a = m_A \frac{\partial^2 y}{\partial t^2} = \frac{\pi d^2 \rho ds}{4g} \cdot \frac{\partial^2 y}{\partial t^2} \tag{2.25}$$

In this equation, $y$ represents the deflection of A from its mean position at time $t$. Hence, it is a function of both $l$ and $t$. The acceleration of A can be therefore written as $\partial^2 y/\partial t^2$. By differentiating Eq.(2.23), the net force $F_b$ accelerating element A is expressed as :

$$F_b = \frac{\partial F}{\partial l} dl = \frac{\pi G d^4}{32R^2} \cdot \frac{\partial^2 y}{\partial l^2} \cdot dl \tag{2.26}$$

By including a damping force that is proportional to the velocity of motion, the damping force $F_d$ opposing $F_b$ can be written as:

$$F_d = \xi \frac{\partial y}{\partial t} dl \tag{2.27}$$

where $c$ is the damping ratio of which unit is force per unit length of the wire per unit of velocity. An equilibrium equation can be obtained by:

$$F_a = F_b - F_d \tag{2.28}$$

Finally, by substituting Eq,(2.25), Eq.(2.26) and Eq.(2.27) into Eq.(2.28), a differential equation could be obtained as:

$$\frac{\partial^2 y}{\partial t^2} + 2b \frac{\partial y}{\partial t} = a^2 \frac{\partial^2 y}{\partial x^2} \tag{2.29}$$

where

$$a = l\sqrt{\frac{kg}{m}} \tag{2.30}$$

$$b = \frac{\xi g}{2m} \tag{2.31}$$

$$k = \frac{Gd^4}{64R^3N_a} \tag{2.32}$$

$$M = \frac{\pi^2}{2} d^2 N_a R\rho \tag{2.33}$$

In these equations, the terms *k* and *m* refer to the stiffness of the spring and the total mass of spring's active part, respectively. Thus, when assuming no damping, Eq.(2.29) was reduced to:

$$\frac{\partial^2 y}{\partial t^2} = a^2 \frac{\partial^2 y}{\partial x^2} \tag{2.34}$$

As Wahl (1944) stated, this equation is in the same form as the well-known wave equation, where *a* is the velocity of motion of the wave. Eq.(2.34) was used to calculate the spring's natural frequency, as the neglect of damping was considered 'permissible'. At first, the deflection *y* at any point of the spring was assumed a combination of a function $\phi(x)$ of distance *x* only and a function $\varphi(t)$ of time *t* only. Hence,

$$y = \emptyset(x) \cdot \varphi(t) \tag{2.35}$$

Substituting it into Eq.(2.34),

$$\frac{d^2\psi}{dt^2} \cdot \emptyset(x) = a^2 \frac{d^2\emptyset}{dx^2} \cdot \psi(t) \tag{2.36}$$

This equation can only be satisfied when the following two equations are equal to a constant. $\omega^2$ is selected as a constant in the book.

$$\frac{d^2\psi}{dt^2} + \omega^2\psi(t) = 0 \tag{2.37}$$

$$\frac{d^2\phi}{dx^2} + \frac{\omega^2\phi(x)}{a^2} = 0 \tag{2.38}$$

By solving Eq.(2.37), Eq.(2.38) and substituting them into Eq.(2.35), a solution that satisfies Eq.(2.34) is found:

$$y = (A_1 sin\omega t + B_1 cos\omega t) \cdot (A_2 sin\frac{\omega x}{a} + B_2 cos\frac{\omega x}{a}) \quad (2.39)$$

where the boundary conditions of a problem will determine constant A1, A2, B1, B2. For instance, under the normal working conditions of an engine valve spring, both ends of the spring can be considered fixed at any time step *t*. Hence, at any *t*, it has $y = 0$ for $x = 0$; $y = 0$ for $x = l$. With these, the constant $B_2$ should be equal to *0*, which makes $sin(\omega l/a) = 0$. It produces a relation that $\omega = j\pi a/l$, where $j \epsilon N+$. Since $\omega = 2\pi f$ where *f* is the natural frequency, the expression of *f* is:

$$f = \frac{\omega}{2\pi} = \frac{j}{2}\sqrt{\frac{kg}{M}} = \frac{d}{2\pi R^3 n}\sqrt{\frac{Gg}{32\gamma}} \quad (2.40)$$

The *j* is usually assigned the value of one to calculate the lowest frequency or the first order of natural frequency. It is always the most critical frequency in analysing spring dynamics. After calculating the natural fFrequency of the spring, the dynamic stress of the spring was calculated. As shown in Figure 2-2(d), the maximum dynamic stress $\tau_{max}$ has a difference of $\tau_y$ to the maximum static stress ($\tau_0 + \tau_1$), where $\tau_1$ is the initial stress caused by the pre-compression. A simple equation was introduced to calculate the maximum dynamic amplitude of motion in the spring by:

$$y_{max} = \frac{2c_j f_j}{b\lambda} sin(2\pi f_j t + \phi) \quad (2.41)$$

In this equation, $c_j$ represents the amplitude of the valve lift curve, which is in resonance with the natural frequency $f_j$ of the spring. However, it is too simple an equation to explain the entire process of the dynamic response of the spring operation. Hence in the later years, this equation was not widely used by researchers. On the contrary, the formulae for calculating stiffness Eq.(2.23) and natural frequency Eq.(2.40)

of the spring were extensively adopted and utilised to research spring dynamics in the following decades.

## 2.2 Extensions on Elementary Theory

### 2.2.1. Coupling extension and rotation effects

In an early article (Geballe, 1958), the theories on extension and the twisting of springs were reviewed in detail. Static loading was applied on one end of the spring when the other end was fixed. The article aims to find the coupled oscillation of the springs. Considering that the dynamic effects of coupling extension and spring rotation were not analysed in previous studies, a dynamic model was proposed to include these effects (Wittrick, 1966). The existing spring formula obtained by deriving the equation of wave propagation Eq.(2.34) was used in the paper. It is shown that the two fundamental propagation waves, the extension wave and the rotation wave, can be treated independently. They are uncoupled and are only relative to the spring coil's radius and the spring's material properties.

In addition, specific formulae for calculating fundamental frequencies involving the surging effects of springs were given. For this purpose, one end of the spring is fixed when the other end is exposed to various conditions. By comparing the results of the proposed formulas with those of existing formulas, it was found that the two assumptions in existing simple formulas bring two corresponding errors. The first assumption is that the wire diameter $d$ is small compared with the diameter of spring coil $D$. This assumption is believed to cause an error in the order of $1/\gamma^2$. $\gamma$ is a parameter that satisfied $\gamma = r \cdot sec^2\alpha / k_T$, where $r \cdot sec^2\alpha$ is the radius of curvature of the helix and $k_T$ is the polar radius of gyration. The second assumption is of large wavelength, which brings an error in the order of $1/\lambda^2$. The parameter $\lambda$ represents the wavelength of a helix,

and it is equal to cosα times $N_a$, where α is the helical angle and $N_a$ is the active number of spring coils. It indicates that inaccuracy can be introduced when a large helical angle α and a few spring turns are accounted for. Despite these errors, the author demonstrated that the results of the simple formulas agree very well with the results of the set-up experiments, as long as the helical angle is small.

Jiang also drew similar conclusions when the coupled extensional-torsional vibration of helical springs was investigated (Jiang et al., 1991). The helical spring was affected by a constant helical angle and helix radius, although the deformation of the spring was assumed small in the study. A linear force-strain relationship and the equation of motion is derived from his previous paper and used in the article. First, the linearised equations of motion are solved by applying the method of Laplace transform and then the whole method is used to solve free vibration problems of the helical spring, which is where the spring is fixed at one end and subjected to an initial displacement at the other end. The displacement is then removed at time $t = 0$, which makes the spring vibrate freely. The simulated results, in fact, confirmed the outcomes of the previous study (Wittrick, 1966) that the extension wave and rotation wave could be treated separately. However, the ultimate combined vibration is complex due to the interaction effects between extension and rotation waves.

Later on, Jiang et al. (1992) published another paper (Jiang et al., 1992) to extend his spring theory on the forced motion of helical springs. The spring sample is made of spring steel with a constant helical diameter and pitch angle. Compared with the free vibration case, two additional factors, constant longitudinal force and rotational moment, are considered in the motion equations. The authors demonstrated that even under forced motion, the motions of the spring are formed by two separate waves, the extension wave and the rotation wave. Different from those in free vibrations, both of

the waves consist of two components. The first component is influenced by the frequency of the constant external loadings. The second component is the term which followed the natural frequency of the spring itself. In Jiang's last article, it was declared that neither friction force nor damping were considered. Besides these, both of his studies do not show a significant correlation between the numerical results and corresponding experimental data.

### 2.2.2. Effects of radial expansion

Another critical factor in designing a helical spring is the effects of dynamic radial expansions. Excessive wear can be caused between the spring body and its cylindrical constraint under high-speed loading. Therefore, it is important to investigate the longitudinal and dynamical radial effects on helical springs.

Stokes proposed a spring model to investigate the dynamic radial expansion of helical springs caused by longitudinal loading after realising that the previous static spring theory could not explain the radial interference between helical springs and the cradles (Stokes, 1974). As is well known, the significant difficulty lies in obtaining sufficient information on radial motion, of which vibration magnitudes is substantially smaller in comparison with longitudinal motion. A scheme of normalisation is used to solve the problem. Impact tests are conducted on a specially designed spring, and their results validate the proposed theory. The developed model, which is considered with no end effects and assumed as an infinite spring, possessed the minimum complexity. However, a drawback caused by the simplification is that significant error might be introduced near the spring ends as long as the ends are not squared and ground. This drawback makes the theory unable to apply to some types of spring, for instance the valve spring, of which the ends are ground in a valve train.

After observing a video of dynamic motions of helical springs, Costello gave a perspective that the end effects of helical springs are essential and should have been considered in analysing the radial expansion of the springs (Costello, 1975). Therefore, a theory which considered both radial effects and end effects of impacted helical springs was proposed in his article. In order to consider the end effects, the boundary conditions at both spring ends were defined in the model. The end at $x = h$ was fixed, while the end at $x = 0$ is subjected to an axial displacement but no rotation. This situation is very similar to that of a valve spring operating in an internal combustion engine. The coefficients in the paper are assumed constant, which makes the equations of motion become linear. It is noteworthy that the effects of contact between adjacent coils, or coil clash, were not included in the theory. This assumption is validated by test data obtained from Phillips and Costello's paper (Phillips and Costello, 1972). The results show that dynamic radial deflection could be much larger than the previous massless spring theory. In addition, the author demonstrated that the end effects played an important role in predicting the dynamic radial deflection of a helical spring.

### 2.2.3. Effects of varying pitch

Kato studied the dynamic properties of a varying pitch helical compression spring (Kato, 1974). The spring in the article is subjected to a sinusoidal excitation, and it is studied both theoretically and experimentally. The theoretical model is based on solving a one-dimensional wave equation when the boundary conditions change with time $t$. The author believed that the narrow pitch in the spring would better prevent the spring surge than with standard springs. The reason is demonstrated by the coils at narrow pitches repeatedly separating from each other. This results in reducing the number of active coils and therefore increases the natural frequency. Besides, the author declared that the

stress is lower when the coil closure end was excited than when the normal pitch end was excited. However, the experimental results display that the actual difference in the stress was negligible.

### 2.2.4. Linear model and natural frequency

Studies (Chen and Polvanich, 1975, Koster, 1975) were conducted to investigate the dynamic behaviour of a cam-driven mechanism. It was stated that the helical spring usually is one of the essential parts of the mechanism. It is constantly compressed and released to restore and release energy repeatedly. Its performance can be significantly influenced by the value of the rotating speed of the exciting cam. Nevertheless, to simplify and find feasible solutions, the helical spring was assumed to be a linear spring with stiffness but containing no mass. On the other hand, the longitudinal and the torsional vibrations of helical springs with small pitches and finite-length were analysed (Kagawa, 1968). It is assumed that the pitch of the spring is very small so that the longitudinal and the torsional vibrations can be considered separately. The assumption is believed ‘very reasonable for practical springs’. At the end of the article, the author concluded that the equation of motion for the longitudinal and torsional vibrations is the same form. In addition, he emphasised that regardless of the magnitude of the frequency range, the spring is better to be considered as a model of distributed parameters rather than a simple stiffness or a simple mass. The reason is that higher frequency spectra can exist, when the spring is driven by transient vibrations.

## 2.3 Existing Helical Spring Models

### 2.3.1. Static Spring Model

Calder and Jenkins developed a static spring stress model to illustrate strain-gage rosettes' function when measuring strains in the complex strain field of helical springs (Calder and Jenkins, 1988). The model is derived from the elementary spring equation Eq.(2.20). Experiments are also conducted on the spring sample with a 38mm length, a mean coil diameter of 117mm, a wire diameter of 15.9mm and a constant pitch angle of 7.3 degrees. A 4.45kN loading is applied to compress the spring when the rosette is bounded to the inner surface of the spring coil at the midweight. The strain readings obtained from the rosette were compared with the predictions achieved from the elementary spring model. The results demonstrated that the results based on the elementary theory show an excellent agreement with experimental results. A different application of the static spring equations was presented in the article by Readman et al. He approximated the shape of the helical spring coils by applying the theory of the curvature Eq.(2.15) and torsion Eq.(2.16) of a helix curve. The employed method successfully formulated the spring geometry (Readman et al., 2001).

Dragoni and Bagaria presented a theoretical model to describe the mechanical behaviours of helical springs. In their study (Dragoni and Bagaria, 2011), the helical spring is based on a hybrid construction formed of an inner polymer core and an outer annulus of dissimilar material. They claimed that existing theories for hollow springs could not deal with the hybrid construction due to the ignorance of the strength and stiffness of the inner core. Wahl's static spring equations are employed and modified to fit the case of biomaterial helical springs with a circular cross-section. Eq.(2.20) is adopted and rewritten as Eq.(2.42) to approximate the maximum shear stress that occurred on the biomaterial helical spring.

$$\tau_m = \frac{16MG_o d_o}{\pi[G_i d_i^4 + G_o(d_o^4 - d_i^4)]} \tag{2.42}$$

In the equation, $G_i$, $d_i$ and $G_o$, $d_o$ represents the shear modulus and wire diameter of the inner and outer materials, respectively. And similarly, Eq.(2.23) is rewritten as Eq.(2.43) to calculate the axial deformation of the biomaterial helical spring.

$$\delta = \frac{8FD^3 n}{G_i d_i^4 + G_o(d_o^4 - d_i^4)} \tag{2.43}$$

They concluded that the proposed model leads to closed-form equations for approximating the stresses and deflection of the biomaterial helical springs.

In another article (Liu and Geng, 2011), the cylindrical helical spring was selected as an example to apply the variation coefficient method for conducting the reliability sensitivity calculation. It is believed that the method could simplify mechanical reliability analysis by reducing the number of random variables. Wahl's static spring equations for calculating the maximum stress and deflection were employed in the study.

Later, another work (Shevale and Niranjan, 2016) was published on estimating the fatigue life of the helical springs where Wahl's static spring equations Eq.(2.23) and Eq.(2.20) are employed to calculate the spring deflection and the maximum stress. These results then contributed to the prediction of the fatigue life of the helical spring. In addition, a finite element model is generated in Ansys 16.0 to validate the analytical results. It is reported that the percentage errors were 2.64% and 2.61% between the finite element solutions and the analytical results for predicting the fatigue life and the maximum shear stress, respectively.

Dym demonstrated that the consistent application of Castigliano's second theorem could be applied on helical spring models to calculate the stiffness of the springs under axial forces and axially directed torque (Dym, 2009). It was also pointed out that the effects of varying end conditions were neglected in his method while he stated the end

conditions could be suitable to be modelled by the finite element method. He also highlighted that the coupling effects between the extensional and rotational response should not be ignored when calculating the stiffness of a helical spring.

### 2.3.2. Distributed Parameters Model

A distributed system is usually referred to as opposed to a lumped system. It is a system that shows state space is infinite-dimensional. Since more spatial variables exist in the system besides time variables, partial differential equations (PDEs) should be solved.

#### 2.3.2.1. Models based on the theory of helix curve (Love's theory)

In 1987, Lin and Pisano proposed a distributed parameters model for analysing the static response of a helical spring (Lin and Pisano, 1987). Their study aims to derive a more general model for calculating spring force than those using Eq.(2.15) and (2.16). The functions of curvature $\kappa$ and torsion $\tau$ are derived by the authors respectively:

$$\kappa(s,t) = \frac{1}{R(s,t)} cos^2[\gamma_p(s,t)] \tag{2.44}$$

$$\tau(s,t) = \frac{1}{R(s,t)} \cos[\gamma_p(\mathrm{s},\mathrm{t})]\sin[\gamma_p(s,t)] \tag{2.45}$$

By comparing these functions with Eq.(2.15) and (2.16), one can quickly find that the constants $\gamma_p$ and $R$ are replaced by functions $\gamma_p(s, t)$ and $R(s, t)$ with respect to variables $s$ and $t$. The relationship between the rotation angle $\psi(s, t)$ and torsion $\tau(s, t)$ is defined by:

$$\frac{\partial \psi(s,t)}{\partial s} = \tau(s,t) - \tau(s,0) \tag{2.46}$$

The axial displacement is stated as:

$$y(s,t) = \int_0^s \sin[p(\xi,t)]\, d\xi\,, 0 \le s \le L \tag{2.47}$$

where $L$ is the free length of the helical spring. Then with these geometric constraints, the dynamic equations of the spring were deduced from Hamilton's Principal:

$$\int_{t1}^{t2} \delta(\sum T_i - \sum U_i) dt = 0 \tag{2.48}$$

where $T_i$, $U_i$ are the kinetic energy and potential energy, respectively. By incorporating damping effects, the equation is extended to be:

$$\int_{t1}^{t2} \delta(\sum T_i - \sum U_i) dt + \int_{t1}^{t2} \sum \overline{F_i}\, \delta \overline{R_i} dt = 0 \tag{2.49}$$

where the second term is the work done by all kinds of damping forces. In the article, the authors stated that the nonlinear dynamic equations derived by them were challenging to be solved analytically for the general case. However, they mentioned that it is much easier to find a solution under static loading. It is because in a static case all the terms involving time derivatives are equal to zero. Then, the authors compared the static solutions based on the proposed model with experimental data, that of linear theory, that of Sayre-De Forest nonlinear formula and that of Lin-Pisano with a constant pitch. It was concluded that significant errors could be caused by using a linear model to estimate spring force considering varying pitches and large deformations. On the contrary, the proposed model well predicted the spring force under large spring compressions. Soon after that, they published another paper studying the differential geometry of general helical springs (Lin and Pisano, 1988).

Following their research, another paper (Lin and Pisano, 1990) was published to investigate the dynamic equations of valve springs. The traditional fixed boundary condition demonstrated that it does not present the actual situation at high engine speeds. Therefore, a new numerical model that is combined with the moving boundary

technique was proposed. Specifically, it was stated that the moving boundary technique could better describe the dynamic effects than the traditional methods have done. It is noteworthy that, unlike in previous papers where it was always ignored, the phenomenon of coil clash was highlighted and investigated in that article. The wave equation Eq. (2.34) is first applied to describe a valve spring's dynamic motions. When the term of damping is included, the equation is rewritten as Eq. (2.29). The wave speed is considered as a constant, which is related to the geometric and material properties.

A helical spring sample with constant wire diameter, helical diameter and pitch angle is chosen to test the numerical model in the experiment. It is observed that the equation could not represent the spikes on the spring force when its results compare with experimental data. The authors explained that the spikes are the results of coil clashes at the fixed spring end. In order to include the effects of coil clash into the numerical model, a moving boundary technique is proposed. The basic idea is to separate the last two coils at the fixed end into several segments. Then the displacements of every segment are traced at each step. As long as a recorded displacement was equal to the pitch at its position, the segment is considered to contact the fixed spring end. When the segment is moving rapidly, it is assumed that an extra clash force is generated. The magnitude of the extra clash force is given by a momentum balance:

$$F_{clash} = \frac{-M_{seg}V_{seg}}{dt} \tag{2.50}$$

where $M_{seg}$ and $V_{seg}$ are the mass and speed of each coil segment. At last, the calculated clash force is added to the total dynamic force calculated from solving the wave equation.

In the second part of the article, a numerical model is developed based on a nonlinear wave equation. The spring force formula adopted in the article is derived by Love (1972) as:

$$F = \frac{GJ}{R}\cos(\Delta\tau) - \frac{EI}{R}\sin(\Delta\kappa) \tag{2.51}$$

where $\Delta\tau$ is the change in curvature and $\Delta\kappa$ is the change in torsion. Besides, the application of Hamilton's Principle and the calculus of variation (Lin and Pisano, 1987) was used in the article. By applying the energy theory presented in their previous papers, three energy terms, four energy terms, and all six energy terms are considered in the developed numerical model. The numerical solutions are compared with experimental data at 602-rpm and 2372-rpm cam speeds (1204-rpm and 4744-rpm engine speeds). It was found that the accuracy of the numerical solutions is higher when involving more energy terms. In addition, the numerical model could simulate the spikes of spring force better than the results from the model without using the moving boundary technique. However, though it was claimed that the proposed method could successfully predict the clash force, the author did not provide enough proof in conclusion.

Using the dynamic spring model established by the above study, a computer-based optimal design tool for helical springs was developed (Lin et al., 1993). The derived dynamic model is firstly post-processed by Fast Fourier Transform and Constraint Evaluation. It helps to find out the severe level of the resonant oscillation. Then, another optimisation subroutine called the controlling program is applied. The program minimises the largest spectral power of the harmonic components of the spring force. An automobile engine valve spring is selected as a case study. As a result, the resonant harmonic power is reduced by roughly 47%, which gave the new design the ability to run higher engine speeds.

Another research based on Love's theory was conducted by Jiang (Jiang et al., 1989). He proposed a theory to deal with static and dynamic analysis of helical springs, as he found that previous studies established no exact force-strain relationships and equations of motions of helical springs. Two sets of force-strain relationships are proposed for

calculating small and large deformation of springs, respectively. A spring that has a helical angle $10^o$ and the ratio of spring diameter and wire diameter $R/r = 0.125$ is taken as an example to test his theory. Firstly, the spring is compressed by a static loading. The author illustrated that the linear theory was accurate only when considering a very small strain in spring deformation. In addition, by changing the value of the helical angle, it is found that the linear theory might underestimate the stiffness and therefore overestimate the deformation of the spring.

Moreover, it was stated that the relationship between torque and rotational strain is linear even when considering large deformation. Despite these findings, the author failed to provide adequate validations of experimental results. In the second part, the nonlinear equations of motion are derived. However, as was stated by the author, the nonlinear equations are 'difficult to solve in normal circumstances'. They can be simplified only by assuming small deformation. No corresponding experimental results and numerical solutions were presented in this part.

The theory of the helix curve is also widely used by researchers interested in analysing the free vibrations of helical springs. Unlike the forced motion of helical springs, for instance, the operation of a valve spring, the free vibrations would involve no external loading. A paper was published to investigate the parameters of helical springs that would influence the vibration frequency (Yildirim, 1996). Firstly, scalar equations of motion are formulated in a three-dimensional space for a spatial curve, which could be represented as a compact form by:

$$\frac{\partial\{S(s,t)\}}{\partial s} = [A]\{S(s,t)\} + [B]\frac{\partial^2\{S(s,t)\}}{\partial t^2} + \{P(s,t)\} \qquad (2.52)$$

where *S(s, t)* represents the state vector consisted of 12 component vectors, A(s) is referred to as the differential matrix and $\{P(s,t)\}$ is the vector of external loadings. When denoting the angular frequency by $\omega$, the form of the harmonic solution is:

$$\{S(s,t)\} = \{S^0(s)\}\sin(\omega t) \tag{2.53}$$

The zero superscript $S^0$ meant it is a function of only the coordinate s. As the studies only concern the free vibrations of helical springs, the external loading is assumed to equal to zero, $\{P(s,t)\} = 0$. Eq.(2.52) is therefore transformed to be:

$$\frac{d\{S^0(s,t)\}}{ds} = [A^0(\omega, s)]\{S^0(s)\} \tag{2.54}$$

When assuming the helical spring as a helix curve, the cylindrical coordinate based on Love's theory was adopted in the study. Thus, the homogeneous solution of the spring equations is finally given by:

$$\{S^0(\theta)\} = [F(\theta, \omega)]\{S^0(0)\} \tag{2.55}$$

where *[F (θ, ω)]* is the dynamic transfer matrix. The natural frequencies calculated by the analytical model were validated by the experimental data and the finite element method from other literature. The author concluded that the proposed method shows a significant efficiency in giving out precise results while reducing execution time.

In the author's later study (Yildirim and İnce, 1997), the same method is extended to address the vibrational problems of helical springs having arbitrary shapes, for instance, conical, barrel and hyperboloidal. It concentrates on the effects of the number of active turns, the helix pitch angle and the ratio of D/d on the natural frequencies. It was also found that the proposed method is efficient for calculating the free vibrational frequencies of helical springs with irregular shapes. Therefore, the proposed transfer matrix method is also treated as a benchmark method for the following researchers.

Besides, Yildrim extended his previous theory and applied the method to free vibration uniaxial composite helical springs (Yildirim, 2001). The coil material is carbon-epoxies which have $0^o$ and $90^o$ fibre directions, respectively. Yildirim claimed that his proposed transfer matrix method is also suitable for simulating the

unidirectional composite helical springs. However, no corresponding experiments were conducted in the study to confirm his findings.

Moreover, Yildirim applied his previous proposed transfer matrix method to calculate the critical buckling loads for a helical spring (Yıldırım, 2009). After comparing the results with the previous benchmark studies, he announced that the transfer matrix method could accurately predict the critical buckling loads for helical springs.

More recently, Yildirim integrated his previous research findings and developed a set of linearised disturbance dynamic equations to study the buckling and vibration analysis of helical springs in a comprehensive manner (Yıldırım, 2012). The proposed method dealt with the axial and shear deformation effects and rotatory inertia effects for cylindrical and non-cylindrical helical springs having straight or circular rods. The results obtained by the method were compared with those of previous literature, and Yildirim claimed that his model conceived the most comprehensive equations.

Researchers later used the method (Kacar and Yildirim, 2016) to predict the natural frequencies and buckling loads of composite helical springs that were noncylindrical and unidirectional. They summarized that the developed method should work for any helical springs having symmetric cross-sections, such as circle, square and rectangle.

It was argued that the common methods of treating a helical spring as a simple massless force element had failed to reflect its dynamic performance in practical applications. Hence, a method for simulating the dynamic performance of a helical spring was proposed (Lee and Thompson, 2001). In that article, the curvature and torsion of the helix curve were formulated by employing Love's beam theory, Eq.(2.15) and Eq.(2.16). A finite element model composed of 432 Euler-Bernoulli beams and the spring model based on the transfer matrix method was also developed to validate the

proposed dynamic stiffness method. The conducted case study is an automotive suspension spring of which significant dynamic stiffening occurred at the frequency of 40 Hz. It was then reported that the spring's calculated natural frequencies and stiffness show good agreement with the results obtained from the finite element model and the transfer matrix method. Especially, they emphasised that the dynamic stiffness method is particularly suited to the direct calculation of the transfer stiffness, which could be easily applied in another, for instance, multi-body, model of a whole vehicle.

Another method, the pseudospectral method, was proposed (Lee, 2007a, Lee, 2007b) to analyse the free vibration of cylindrical helical springs. The method was used firstly to represent the helix spring curve using Love's theory and then to show the series of expansions of Chebyshev polynomials to approximate the helical springs' displacements and rotations. The simulated spring was analysed under four different boundary conditions: fixed-fixed, free-free, fixed-free and hinged-hinged. The results from the pseudospectral method were also compared with those obtained by applying the transfer matrix and dynamic stiffness methods. It was found that the pseudospectral method can predict the natural frequency of the springs as accurately as the other two methods.

Temel and Calim investigated helical springs' forced and free vibration under impulsive loads in the Laplace domain (Temel and Calim, 2003). The governing equations were derived from the Timoshenko beam theory. Specifically, they managed to transfer the differential equations into the canonical form by applying the complementary functions method. The results obtained from their method were reported to concur closely with the results of previous methods and the finite element method. More importantly, it was found that a significant reduction of the computation time was achieved via this method.

After that, the same method was applied to analyse the dynamic behaviour of composite coil springs, which have an arbitrary shape (Çalım, 2009). The composite material was assumed homogeneous, linear elastic and anisotropic. The helical spring was simulated under both free and forced vibrations, and the results were validated by both previous literature and the finite element method. It was reported that the helix pitch angle is directly proportional to the vibration period while, on the contrary, it makes a negligible contribution to the displacement amplitude.

Another study (Frikha et al., 2011) was conducted to investigate the effect of axial load on the propagation of elastic waves in helical beams. Love's spring theory was employed to formulate the motion of the loaded helical beams. Four parameters (helix angle, helix index, Poisson ratio and axial strain) were determined to administer the problem. It was found that the effect of loading could be significant in a low-frequency loading range, which was caused by the deformation of the geometry under the axial load. Therefore, the author concluded that the effects of stress and geometry deformation should not be neglected in the dynamic analysis of helical beams.

A comparative study was conducted to assess the validity ranges of alternative theories for describing the dynamic behaviour of helical springs (Sorokin, 2009). The location of the dispersion curves was selected to evaluate the accuracy of these methods. It was reported that the standard Bernoulli-Euler theory could not provide a precise prediction while the refined Bernoulli-Euler theory validated only for low-frequency dominantly flexural waves. On the other hand, the Timoshenko theory is proved effective in describing dominantly flexural waves in high-frequency range.

As a continuation of his study, Sorkin proposed to analyse the vibrational energy transmission of helical springs by the Green's matrix method (Sorokin, 2011). The geometry of the helix curve is formulated by employing Love's theory. Then the

eigenfrequencies and the dynamic transfer functions are successfully calculated by using his proposed method. The results are compared with the results based on the FE method, and it was stated that Green's matrix method works well for finding exact solutions of problems with free and forced linear vibrations of elastic helical springs.

In order to allow for the free vibration analysis of helical springs having non-circular cross-sections, explicit analytical expressions based on Love's theory were developed to calculate the natural frequencies of the springs (Yu and Hao, 2011). Various types of cross-sections (elliptic, rectangular and uniform equilateral triangle) of helical springs were involved and formulated into the dynamic equations of the helical springs. The simulated results were validated by those obtained from the finite element method, which showed a close correlation. It should be highlighted in their study that the warping effect is considered in the spring model for the first time. For typical springs, the ends are often not uniform (with a varying cross-section), which few studies had paid attention to.

In addition, a wave and finite element method were proposed for describing the dynamic response of such helical springs (Renno and Mace, 2012). In that model, the spring was regarded as a curved waveguide and was formulated based on Love's theory, except that the non-uniform ends were modelled by the standard finite element method. It was found that the dynamic stiffness of the helical spring, approximated by the proposed wave finite element method, agrees more closely with the value of a real spring than that approximated by other methods without considering the non-uniform ends.

More recently, a coupled technique for modelling the vibration of helical springs was proposed (Hamza et al., 2013a, Hamza et al., 2013b). At first, the impedance method was employed to predict the natural frequencies of the spring. Then, numerical

solutions of axial and rotational strains of the spring were achieved by applying the finite difference scheme of Lax-Wendroff when the external loading was a harmonic forced axial velocity.

#### 2.3.2.2. Models based on deformed beam (Wahl's theory)

Paranjpe (1990) published a paper that combined Wahl's spring model with Coulomb damping instead of Viscous damping. In his study (Paranjpe, 1990), three distributed spring models were developed: the first one was an undamped spring model, which is in the same form as Eq.(2.34), the second was to couple the spring model with a viscous damping term which is in the same form as Eq.(2.29), and in the last spring model the viscous damping term was replaced by a Coulomb damping term as:

$$\frac{\partial^2 y}{\partial t^2} + f(x, \dot{y}) = a^2 \frac{\partial^2 y}{\partial x^2} \tag{2.56}$$

where $f(x, \dot{y})$ represents the Coulomb damping term. The spring force at 3000-rpm cam speed based on the three models were simulated and compared. The author concluded that the undamped spring model results in a continuous vibration without energy dissipation. On the contrary, the amplitude of the spring forces simulated by the two damped spring models was reduced progressively by the effects of the damping terms, which was considered more realistic. It showed that the vibration of the spring force, based on Coulomb damping, always stops very fast after the external loading has ceased. In contrast, the viscous damping based spring model allowed the spring force to vibrate continuously with a reducing amplitude when the external loading was removed. According to real engine test results, the dynamic spring force based on viscous damping should be more credible, though Paranjpe argued that the Coulomb

damping could be more suitable for developing the dynamic spring model as it generates no additional energy costs.

Although Paranjpe's study did not prove the feasibility of the Coulomb damping-based model for developing a dynamic spring model, his study triggered an interest from subsequent researchers to adopt his method for analysing springs with Coulomb friction devices.

Another study (Sefler and Pisano, 1993) investigated an automotive valve spring's experimental and modelling results that slide over the non-destructive elastomeric sleeve. In that study, Eq.(2.29) was used to simulate the dynamic effects of the spring, in which the viscous damping described the damping effects of the spring itself. On the other hand, the Coulomb friction term $f(x, \ddot{y})$ was also added into the dynamic equation to include the damping effects of the non-destructive elastomeric sleeve. The valve spring with dampers was tested and simulated at three different cam speeds: 1000-rpm, 2000-rpm and 2500-rpm.

In order to estimate the compression force of the spring over the dampers and therefore to calculate the Coulomb friction force over the dampers, the spring dilation was firstly estimated by:

$$R(x,t) = \frac{\Delta x}{\Delta \alpha}\cos[tan^{-1}(\frac{\partial}{\partial x}y(x,t))] \tag{2.57}$$

where $R$ is the radius of the spring coil and $\alpha$ is the radius of the helical curve. The dynamic spring model with the considerations of the viscous damping, Coulomb damping of the dampers and the spring dilation was then developed to simulate the dynamic forces of the valve spring. In this aspect of the experiment, a piezoelectric force transducer was placed beneath the spring to monitor the generated spring force. The results showed that high-frequency peak forces occurred at, and only at, 2500-rpm cam speed. This was explained by the evidence of the coil clash phenomenon. In

addition, the developed spring model succeeded in fitting the force curve at both 1000-rpm and 2000-rpm cam speeds. The simulation result correlated closely with the experimental force curve at 2500-rpm cam speed except that it failed to simulate the peak forces caused by the coil conflict phenomenon (spring contact). Lastly, the importance of damping terms in a spring model was highlighted, in that both the damping introduced by the spring itself and the external damper could reduce the amplitude of the dynamic vibrations of springs.

Following the above studies, the Eq.(2.29) proposed by Wahl, which comprised the viscous damping term, has been widely applied by researchers to analyse the dynamic response of helical springs. For instance, a distributed parameter spring model was developed based on Wahl's equation to investigate the dynamic effects of valve springs subjected to impact loading (Yang et al., 1996). The model was applied in two situations: 1. only one single spring was subject to impact loading, 2. the moving end of the spring was connected to a button. By applying the model, he successfully found that maximum stress occurred at the fixed end and discovered that coil clash happened when the loading velocity exceeded a threshold value. In addition, Champion and Champion modelled small deviations from the linear mechanical behaviours of helical springs subjected to vertical loading. Finally, in the study (Champion and Champion, 2011), the wave equation proposed by Wahl was used to develop a nonlinear model for simulating the helical spring under small-amplitude oscillations. They concluded that the developed model proved the departure from the linear behaviour of springs observed in static extension and oscillation situations.

In order to include the effects of the variable natural frequency and variable damping ratio, a new method was proposed (Liu and Kim, 2011) to predict the spring surge phenomenon. First, the valve spring sample was placed into a vibration exciter to test

and record the variable natural frequency. Then, the damping ratio ζ was determined by applying the half-power bandwidth method. In order to estimate the amplitude of the spring surge, Wahl's equation was used to simulate the internal vibration of the valve spring. The harmonic balance method was adopted to approximate the solution of the equation. In addition, a cylinder head of a car engine that was directly driven by an electric motor was used to test the spring surge amplitude. The analytical results were then compared with the experimental data collected from the test rig. It was found that the analytical results agreed with the test results, irrespective of using a constant damping ratio of 0.016 or the variable damping ratio. However, it was reported that a mismatch between analytical results and test results could be observed when employing a constant natural frequency of 490 Hz. They pointed out that the mismatch could be eliminated by using the variable natural frequency. Notably, no coil clash phenomenon was reported in the article though the maximum cam speed reached around 3000-rpm in the engine head test.

Another paper (Kobelev, 2014) addressed the practical problem of the load dependence of transverse vibrations for helical springs. Based on Wahl's spring equations, equations for describing transverse vibrations and explicit formulas for predicting the natural frequency were developed in that paper. These equations finally aided the analysis of the buckling of the studied helical spring. Another paper was later published (Hamza et al., 2015) to address the vibrations of a helical spring under axial compression by using Wahl's dynamic spring equation. It aimed to display the different effects between the slow axial waves and the fast angular waves.

Besides the analysis of the helical springs, the distributed parameter spring model was also favoured by researchers who investigated the whole valve train mechanism. However, few studies were conducted on introducing the dynamic spring model into

the valve train system, though the significance of the dynamic behaviour of a valve spring in a valve train had been realised for a long time (Ünlüsoy and Tümer, 1994). Therefore, a study was conducted (Ünlüsoy and Tümer, 1994) on coupling the cam follower system's lumped mass model and the valve spring's distributed parameter model. A method was proposed to address the difficulties in solving the coupled partial and ordinary differential equations. To achieve this, Wahl's wave equation for helical spring dynamics was adopted when Newton's law governed the lumped mass model of the cam follower system. As a result, the whole valve train system was successfully simulated, and the importance of the distributed parameter spring model, which gave out an accurate estimation of spring resonance, was highlighted in their study.

Similarly, a model was developed by coupling the distributed parameter spring model with the valve train's lumped mass system to investigate the valve train's vibrational behaviour (Lee and Patterson, 1997). Whilst Wahl's wave equation was used to formulate the dynamic spring, it was pointed out that the nonlinear effect of coil clash had been neglected. It was reported that the distributed parameter model and the lumped mass model could be solved simultaneously without iterations, and the coupled model could give accurate results of vibrational behaviour when compared with the experimental data.

In addition, another curved beam method for developing a valve spring model into a lumped mass model of valve train was presented (Huber et al., 2010, Clauberg and Huber, 2013). In both of their studies, the valve spring was approximated as a curved beam, and then partial differential equations were generated by deriving the equations of motion. Specifically, the motion of each unit mass of the spring coil was assumed to consist of three components: the translation, the small rotation, and the warping. Expressions for the displacement, the stress and the strain were derived according to

these assumptions. Finally, six coupled differential equations were derived to describe the behaviour of the spring by the equations of motions.

As these studies looked for the incorporation of the spring model into the multi-body model of valve trains, only the degree of freedom along the extensional direction was of interest. As a result, these differential equations were reduced to a partial differential equation in the same form as the well-known Wahl's one-dimensional wave equation. A test rig powered by an electric motor was built to test the static and dynamic spring forces. The test data then validated the analytical model. Clauberg and Huber demonstrated that the static analytical results had an excellent agreement with the data of the static compression test. In addition, a real engine test was also conducted to record the dynamic spring force generated at around 1200 rpm cam speed. It appeared that though the effect of internal vibrations on the spring were significant, the analytical results were able to fit the experimental curve well. The authors concluded that the developed spring models could aid both static and dynamic simulations of a valve train mechanism.

### 2.3.3. Lumped Parameters Model

The lumped parameters spring model, which the multibody model is inspired by, is commonly used to study the dynamic behaviour of interconnected rigid or flexible bodies. Basically, the motion of bodies is described by their kinematic behaviour, while the dynamic behaviour is usually calculated from the equilibrium of applied forces and the rate of change of momentum. To be specific, these bodies are usually connected by springs and dampers. Nowadays, the multibody system can usually provide the ability to simulate the arbitrary motions of thousands of interconnected bodies. Initially, the multibody system was not employed by researchers who investigated the dynamic

performance of helical springs. However, it was one of the most popular methods employed for simulating the dynamic valve train mechanism, which usually consists of interconnected components that can be treated as rigid bodies. Among these components, the valve spring is the most flexible and is usually modelled by methods for simulating continuous body, for instance the distributed parameters method.

Pisano and Freudenstein developed a dynamic model for a high-speed cam-follower system (Pisano and Freudenstein, 1983). In that model, the cam, cam-follower, rocker arm and rocker arm pivot are assumed to be rigid, and the mass of the pushrod was divided into halves while the valve spring was modelled by the distributed parameter method. This combination of methods allowed the dynamic response to be obtained by solving a coupled set of ordinary and partial differential equations. Besides, a lumped parameters dynamic model of the same valve spring was generated to compare with the distributed parameter spring model results. One-half of the mass of the valve spring was used in the lumped parameter spring model.

Then, the results based on both methods were validated by the results of valve train tests at 600-, 1800- and 2550-rpm cam speeds. It was reported that the dynamic model combined with the distributed parameter spring model performs well when predicting the system's overall response. On the contrary, by replacing the distributed spring model with the lumped parameter spring model, the dynamic model is unable to make accurate predictions. Therefore, the author concluded that the distributed parameter spring model plays an essential role in the accuracy of the results predicted by the dynamic model. Later on, it was claimed by researchers (Chan and Pisano, 1987) that in such a valve train system, the dynamics of finger-followers and hydraulic tappets should not be neglected. Hence, they developed a dynamic model considering both the effects of the finger-follower and the hydraulic tappet for predicting the dynamic response of the

valve train system. The spring model was greatly simplified by adding one-third of the spring mass to the valve mass, and the spring was eventually replaced by a spring constant in the dynamic model. The authors also emphasised that incorporating the distributed parameter spring model into the whole dynamic model should be part of the continuing works for their study.

Similarly, in another paper (Guo et al., 2011), the kineto-elastodynamics method was used to investigate the dynamic characteristic of a valve train system. It aimed to build an effective but simple dynamic model for the entire valve train system. All the components in the system were modelled by the lumped mass approach except that the valve spring was modelled by the distributed parameter method, as shown in Figure 2-3a. A 4-cylinder diesel engine mounted on a stationary test bench and derived by a motor was used to verify the simulation accuracy. The simulation and experiment were conducted at a range of cam speed from 700-rpm to 2000-rpm. It was reported that the simulation results of the valve force are very close to the experimental results at any tested cam speed.

In a later study (Guo et al., 2014), the dynamic behaviour of a pushrod valve train system was simulated by developing a rigid-flexible coupled dynamic model. It was stated that the valve spring is ‘a major source of compliance’ in valve trains, to which great attention should be paid. The tappet, upper retainer and valve head were treated as rigid bodies whilst the other components: the pushrod, rocker arm, valve spring and valve stem, were modelled as continuous flexible bodies. It was worth noting that the valve spring was modelled by the distributed parameter method where Wahl’s spring wave equation described the displacement of the spring coil elements. It was shown that the agreement between the results based on the rigid-flexible coupled dynamics model and the experimental results is good.

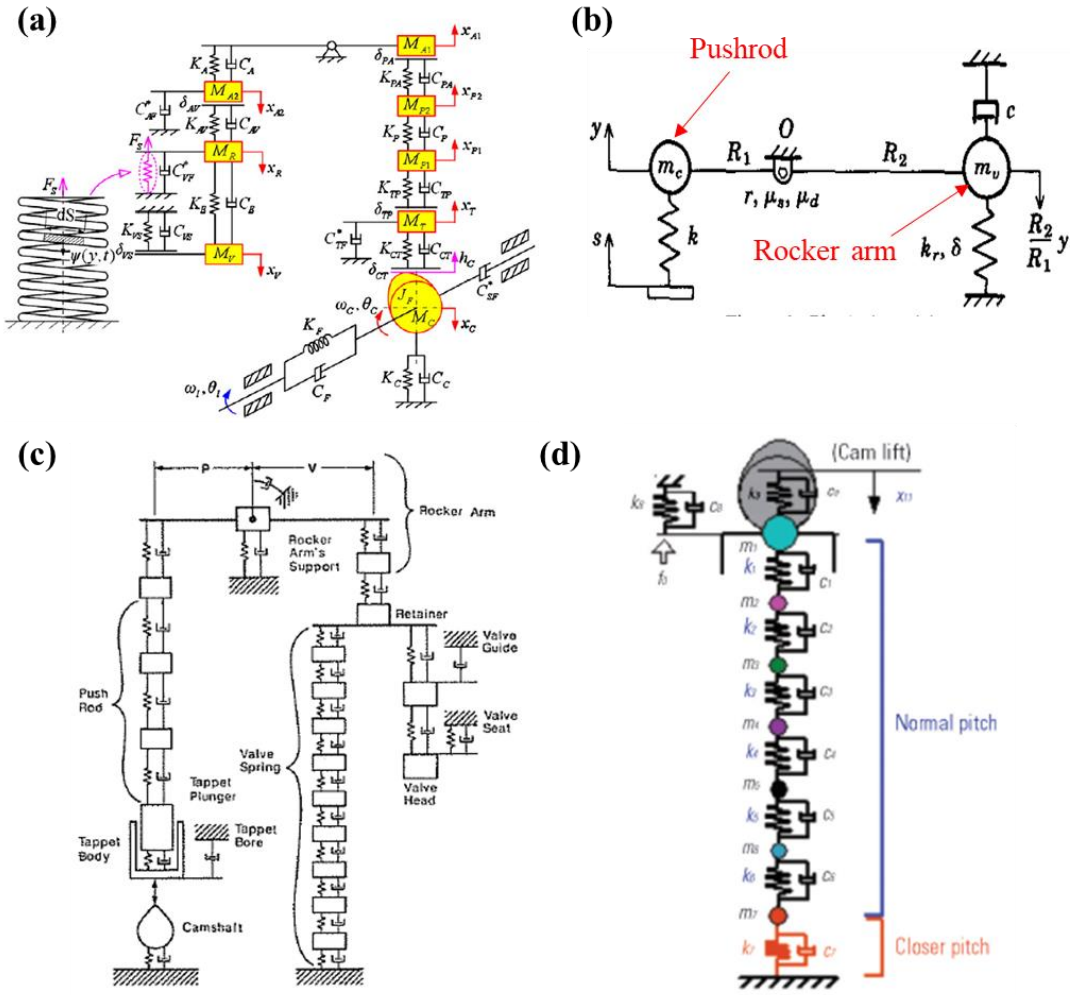


*Figure 2-3: (a). Dynamic model of pushrod valve train system (Guo et al., 2011). (b). Single-degree-of-freedom dynamic model for the overhead cam mechanism (Ünlüsoy and Tümer, 1994). (c). Analytical model for the valve train system (Seidlitz, 1989). (d). Lumped parameters model for the valve train system (Kitada and Kuchita, 2008).*

Though the distributed parameter spring model was proved effective when coupled with the lumped mass model of the entire valve train system, the valve spring was still replaced by a linear constant of spring stiffness in a valve train model due to the purpose of simplicity. A study (Ünlüsoy and Tümer, 1994) investigated the dynamic behaviour of an overhead cam mechanism where it was assumed that the Coulomb friction could significantly influence the behaviour. As shown in Figure 2-3b, the pushrod and the rocker arm were lumped to be point masses and connected with ideal springs and

dampers while the valve spring was simplified to be a spring stiffness having a value $k_r$ and under the preload $P$.

In addition, a similar method was proposed (Dresner and Barkan, 1995) where a cam follower system was modelled by using lumped parameter approach. The valve spring was also treated as a constant stiffness in the whole cam-follower system. Besides, a study (Dalpiaz and Rivola, 2000) was conducted to simulate the dynamic behaviour of a motorbike engine's desmodromic valve train by employing the lumped parameters method where the valve spring was assumed as an ideal spring having a constant stiffness. Experimental results validated the simulation results. However, some discrepancies were observed. The phenomenon was explained by the fact that the rocker stiffness should not be constant as assumed in the model.

Moreover, Teodorescu published a paper (Teodorescu et al., 2007) where the contribution of the multi-body method in the design analysis of valvetrain systems was highlighted. The tappet, pushrod, rocker arm and valve were all lumped as point masses connecting with springs and dampers while the valve spring was simply replaced by a constant stiffness and one-third of which actual mass was added to the mass of the valve. A motored test rig was built using a laser doppler vibrometer to validate the simulation results.

More recently, a study (Calabretta et al., 2010) investigated the friction generated among the valvetrain components after realising that the valve train could contribute significantly to the overall engine friction at low engine speeds. Therefore, the lumped parameters model for a valve train system was proposed to quantify the lost power between the components. In that model, the valve spring was also treated as a stiffness constant without mass. According to the above literature, it can be concluded that the valve spring is always simply replaced by a stiffness constant when the dynamic

response of the valve spring is not concerned and when only the dynamic response at low engine speeds is concerned. In short, assuming the valve spring as a stiffness constant usually cannot give out an accurate prediction of the dynamic response of the valve spring compared to the distributed parameter method, though it did contribute to simplifying the entire dynamic model of a valve train system and in the process saved a lot of computing time.

Besides the distributed parameters method, valve springs were also modelled by using the lumped parameters method. Compared to the distributed parameters spring model, the spring model based on the lumped parameters method could be more suitable to fit into a lumped parameters model of an entire valve train. In other words, the partial differential equations generated by the distributed parameter spring model and the ordinary differential equations governing the other components of the valve train system should be solved separately. On the contrary, the lumped parameters spring model is governed by the ordinary equations, which can be solved along with the governing equations of the whole valve train system. However, accurate results might not be obtained by assuming the valve spring as only one mass point. Hence, the valve springs were assumed as more than one mass by researchers.

For instance, Seidlitz developed a computer model for studying the dynamic behaviour of a valve train system by employing the lumped parameters model (Seidlitz, 1989). All the components (camshaft, tappet, pushrod, rocker arm, retainer and valve seat) of the valve train were assumed as at least one mass and the valve spring was composed of 9 masses connected by springs and dampers, as shown in Figure 2-3c. The stiffness of the two connecting springs at both ends of the valve spring was ten times as stiff as the connecting springs in the middle portion. An engine head test was also conducted to validate the results obtained from the simulation. The results showed that

the mathematical model could accurately simulate the dynamic behaviour of the valve train system.

Then, similar research was done by Roß and Arnold, who included the interacting effects of bending and torsional vibrations between each valve train into the developed lumped parameter model (Roß and Arnold, 1993). Each valve spring in a valve train system was discretised to 18 masses connecting by springs and dampers. They stated that the simulated results of camshaft bearing forces and camshaft displacements appeared to be very similar to the measuring results, which were not achievable by previous methods.

In order to include the spring surging effect under dynamic conditions and the contact compliance between the cam and the follower of a cycloidal cam-flat follower pair, a lumped parameters model incorporating the inertial elements was developed (Kushwaha et al., 2000). The valve train components (camshaft, cam, valve and follower) were assumed as one mass, while two masses represented the valve spring. It was believed that when the valve spring arrangement is clamped-clamped, the two masses connecting by springs and dampers should be enough to simulate the spring surge effect. Their model was validated by comparing with the results of previous literature. The results demonstrated that the valve train inertial imbalance increases at higher engine speeds so that the dynamic contact loads become larger.

Moreover, Kitada and Kuchita also published their study on analysing the dynamic vibration of an engine valve train by assuming the whole system as a lumped parameters model (Kitada and Kuchita, 2008). The model aims to include nonlinear effects like valve clearance and coil clash. For this purpose, the valve spring was not only discretised by six masses but also the closed coil at the lower end of the valve spring was represented by a connecting spring with a larger stiffness $k_{7,}$ as shown in Figure

2-3d. As a result, a spike spring force was observed at 4500 cam speed in the simulations results, which they explained was caused by the coil clash around the closed coil. However, no experiment was conducted to support their findings though the method could be an effective method to include the effects of valve clearance and coil clash in the dynamic simulation of the valve train system.

It can be concluded from the above literature that the lumped parameter method was usually employed for simulating the dynamic behaviour of valvetrain systems or finger-follower systems where valve springs act as essential parts. It is the simpler way to represent the valve spring by replacing the valve spring with a stiffness constant in the lumped parameters model of the valve train system. However, it usually cannot accurately predict the valve spring's dynamic response, for instance the effect of spring surge and coil clash. On the other hand, by employing the distributed parameters method to the model of valve springs, high accuracy of the simulation result can always be ensured. However, it is of great difficulty to observe jointly the distributed parameter spring model (governed by partial differential equations) and the lumped parameters model (governed by ordinary differential equations) of the other components in the valve train, and therefore must be solved separately. Hence, for simplicity, the valve spring and the other components were usually modelled using the lumped parameters method. In this case, the connecting stiffness and dampers of these discretised masses should be defined precisely to obtain accurate predictions of the dynamic response, which usually is considerably problematic especially when the valve spring contains nonlinear properties.

### 2.3.4. Finite Element Model

The distributed parameters method was proved able to accurately analyse the valve spring's dynamic response in most cases. However, it was claimed that the governing differential equations of the distributed parameters method were too challenging to be solved manually (Mottershead (1980)). Hence, the finite element method started to be employed by researchers to analyse the dynamic response of the valve spring due to its flexibility. The finite element method has been one of the most popular methods, which engineers and researchers use to solve engineering problems. The FEM is always treated as a special numerical method for solving partial differential equations, usually subdividing a large domain into smaller and simpler finite elements.

Mottershead published an article for addressing the eigenvalue problem of semi-infinite helical springs by using the finite element method (Mottershead, 1980). The natural frequencies and mode shapes of the helical spring were governed by Wittrick's differential equations. The valve spring was discretised into 12 elements per coil, each of which had twelve degrees of freedom: three rotations and three translations for each node on the element. The simulated natural frequencies of each mode were compared to the results obtained using Timoshenko's beam theory. It was found that the error between the two methods is lower than 1.6% from mode 1 to mode 5. In addition, the vibrational test of the spring was also conducted to validate the results of the finite element model. It was reported that no matter whether in the transverse or the longitudinal directions, the error between the finite element method and the spring test is always lower than +/-2.5%. Also, it was highlighted that the transverse motions of the valve spring were successfully simulated by the method, which was not able to be achieved with other spring theories. And, although the valve spring is meshed by a

relatively coarse density (six coils per element), the proposed method was more likely to give accurate results.

Following that study, Kim pointed out in his paper (Kim, 1999) that it was difficult to combine the method of Mottershead (1980) with other finite element codes due to the lack of symmetricity of the element matrices. Therefore, he developed a 3-D helical rod finite element method to analyse the dynamic behaviour of typical helical springs. The element matrices were derived from Galerkin's method, where the mass and stiffness matrices are symmetric. The finite element model was achieved and solved by using the commercial software iDEAS. An experimental test was also performed to validate the model. It was found that the two dominant natural frequencies in both analytical and experimental results were around 363.7Hz and 690.0Hz, which were very close to the first and second order longitudinal natural frequencies. It is explained that only the longitudinal vibration modes dominated as the external excitation is along the longitudinal direction. It was also found that the finite element model still gives accurate results, although each coil was modelled by only one element.

Cook recommended using the finite element method for formulating the deflection and state of stress in a closely coiled helical spring with an arbitrary cross-section shape (Cook, 1990). A helical spring having a rectangular cross-section shape was selected as a case study to test the finite element model. It was shown that the simulated results of both deflection and state stress were very close to the results of classical theories.

Later on, two different approaches for modelling a helical suspension spring which was used in a dynamic compressor, were discussed by researchers (Kelly and Knight, 1992). The first approach assumed the spring as a stiffness constant by applying Wahl's stiffness formula for helical springs. The other approach was to represent the helical spring as a finite element model with four linear beam elements for each coil. It was

suggested that the independent finite element spring model should be used when the spring surge existed in the frequency range of interest.

In addition, the cubic beam element was also employed (Stander and Du Preez, 1992) for analysing the vibrational behaviour of helical springs. The method was derived from the curved isoperimetric 3-dimensional beam finite elements. It was announced that the proposed finite element method is extremely suitable for the vibrational analysis of helical springs as arbitrary 3-dimensional beam elements can easily model them. Besides, coarse meshes of two to four elements per coil could also provide accurate results for the model analysis.

Suzuki et al. employed the finite element method to minimise helical springs' side force, and the finite element code was compiled in ABAQUS. In their study (Suzuki et al., 1996), the helical coil spring was modelled by 2-node linear beam elements when the spring seats were modelled by rigid surfaces. The results were validated by the test of a special six-point loading fixture on the helical spring. A good agreement between the side force of the finite element results and the experimental data was observed.

Moreover, Jiang and Henshall looked in to developing a general and accurate finite element model for analysing the static response of helical springs under axial loads. They pointed out that material nonlinearity and large deflection were usually not included in the Fourier series analysis, limiting the previous numerical spring models (Jiang and Henshall, 2000). Therefore, they developed accurate boundary conditions and used conventional finite element analysis instead of specific formulations so that the model could be directly implemented using commercial finite element software. Three-dimensional solid brick elements were applied to construct the helical spring, which consisted of eight nodes. The Von Mises equivalent stress distribution of the spring was simulated by applying both the proposed finite element model and the

previous analytical model, and they were seen to be in good agreement with each other. However, it was discovered that the discrepancy between the finite element results and the analytical results increases when the ratio of wire and coil diameter increases. The advantages of the proposed model were highlighted: it has a robust ability to include the effects of arbitrary cross-section, nonlinear material properties, and large deformation into the analysis of helical springs by adding multi-step loadings.

More recently, it was claimed that it is always hard to simultaneously solve the equations of the components of the valve train system derived by the finite element method. Hence, Lee demonstrated in his article (Lee, 2004) that by independently formulating the components by the finite element method, the dynamic equations of the valve train could be solved. In the model, the cam was treated as a rigid body, the rocker arm was modelled by 72 plane stress elements, the valve was represented by 341 axisymmetric elements and the valve spring which consists of five coils were modelled by 50 rod elements. The model was in the two-dimensional domain and simulated at 1000- and 3000-rpm cam speeds, respectively. It was noted that the effect of coil collisions inside the valve spring is considered in the model and is successfully simulated at 3000-rpm cam speed.

The introduction of the finite element method together with the rapid development of computer power lead to more widespread modelling of helical springs in the following years. Firstly, it was proposed to model the dynamic helical spring that is sleeved over a mandrel using a finite element analysis method (Rashidi et al., 2004). Rashidi claimed that the helical spring should have a variable Coulomb friction force during operation as it was expanded radially during compression. It was found that the results from spring vibration, as predicted by the spring model using variable damping

forces, were very close in comparison with the results obtained from the model using constant damping forces.

Then, a paper (Girgin, 2006) was presented to investigate the free vibration analysis of noncylindrical helices using the finite element method. The Timoshenko beam theory was used to derive the spring element matrix. It was demonstrated that although the formulation of his method is simple, it was effective at producing accurate solutions for the conical, barrel and hyperboloidal spring shapes.

In addition, the same method was also applied by researchers (Clauberg et al., 2012) who used the beam theory and finite element method to develop the model for the helical spring. The spring model was discretised using the finite element method when each element was assumed a curved beam. The numerical results also closely concurred with the results of the conducted static spring test.

In another study (Wang et al., 2010), the finite element spring mode generated in ANSYS software provided an accurate stress distribution of a normal helical spring and the natural frequency of the helical spring was also calculated. The finite element spring model's ability to address the nonlinear elastic behaviours was also highlighted; for instance, the large deformation occurred near spring resonance.

Then, Kaoua et al. adopted the finite element method to study the performance of twin helical springs under axial loading (Kaoua et al., 2011). The twin helical spring usually generated by double rolling a cylindrical coil had a more complicated geometry than the normal helical spring. It was reported that the finite element model can still accurately calculate the stress fields on the twin helical spring.

Mulla et al. dealt with the stress analysis of a helical spring in their paper (Mulla et al., 2012), which is used the front suspension of a three-wheeler automotive. The spring model was developed in ANSYS by tetrahedral elements and hexahedron elements,

respectively. It was found that spring models generated by the two elements can provide excellent accuracy in predicting static stress.

Similarly, Abidin et al. tried to investigate the static characteristics of the helical springs SUP12 used in an automotive (Abidin et al., 2013). The finite element model was generated in the software HYPERWORKS, in which the displacement conditions at the full rebound, curb length, and the full bump were simulated.

Besides, Gaikwad and Kachare (2013) developed a finite element for helical springs using NASTRAN, and the pre-processing of the model was conducted in HYPERMESH (Gaikwad and Kachare, 2013). Additionally, Sarkate (2013) developed a finite element model of helical springs, of which the geometry model was developed in Pro-E software (Sarkate, 2013). It was noted that the wire diameter is 13mm, which is very small compared to the mean diameter of the spring coil, which was 145mm. Nevertheless, it was reported that the model accurately predicts the helical spring's static stress compared to the analytical results.

Moreover, a finite element spring model was also developed using ANSYS for the static analysis of helical springs (Pattar et al., 2014). More recently, the helical suspension spring used in railroad vehicles was modelled using finite element analysis software ANSYS (Kumbhalkar et al., 2017).

These studies aimed to address the problem of vibrational response appearing in the helical spring, such as the harmonic or frequency response. The numerical model calculated the natural frequency of the helical spring, and this was validated by the experimental results.

The same method was also employed (Wu et al., 2017) to conduct the intake valve spring's static and modal finite element analysis. The static stress and deformation of the intake valve spring were successfully simulated. Then, similar FE spring models

were also employed by researchers who analysed the static stress of the helical spring with a non-circular wire cross section using CATIA V5 (Kanimozhi et al., 2018), who used the finite element spring model for validating the feasibility of using composite material in the design of helical springs (Mahadevan et al., 2018), who investigated the force-displacement response of the suspension spring in a three wheeler where high weight on one side was observed (Pawar and Desale, 2018), who investigated the damping capabilities of both helical springs with and with polyurethane cushion buffer (Jadhav et al., 2019), and who used the finite element model to conduct the comparative study of spring forces between the helical spring made by structural steel, S-Glass Epoxy composite and Epoxy-Carbon prepreg composite (Stephen et al., 2019).

Regardless of the software used to develop the finite element spring models, all the above studies achieve their goals of accurately simulating either the static or dynamic response of helical springs in various working conditions. In other words, the finite element method shows a robust ability in simulating the helical springs, especially the ones having nonlinear geometries or nonlinear behaviours. However, the finite element method is usually blamed for time costing. For instance, one-dimensional analytical spring models developed by researchers (Baghani et al., 2012, Okarmus et al., 2013) were reported as costing much less computational time than the approximated 1% of the time for three-dimensional finite element simulations.

## 2.4 Design and Optimization Methods of Helical Spring

### 2.4.1. Traditional Spring Analysis Methods

Besides the need to analyse static and dynamic spring responses, the spring models also play an essential role in the optimal design of helical springs. The first systematic and comprehensive spring design method was derived by Wahl (1944) in his book, where

the spring force, stress and natural frequency were formulated. In these formulas, the geometry parameters of the springs: coil diameter, wire diameter, number of active coils and pitch angle were considered. Though the formulas were simple and based on linear assumptions, they built a solid foundation for later researchers to conduct spring designs.

An optimised design for valve springs was conducted in order to reduce the spring loads and the installation height (Muhr, 1993). Wahl's spring formulas for calculating wire bending stress and wire torsional stress were adopted. It was then easy to find the optimal solutions of the formulas by fixing the unchanged parameters. It was reported that a 13% reduction in the spring loads and a 35% reduction in the installation height were eventually achieved by applying the design method.

A study (Ratle et al., 2004) was published on conducting a multi-objective optimal design of a helical spring by applying a non-dominated sorting genetic algorithm. The design domain contained five spring parameters: coil diameter, inner diameter, material thickness, helix pitch, number of active coils, and braid angle. Then, Wahl's spring stiffness was extended to Eq.(2.59), which was one of the objective functions. The other objective function was in the same form of Wahl's spring mass function.

$$Max \qquad k = \frac{Gd^4}{64nR^3}[1 + L(D, d, \alpha, n, \theta)] \tag{2.58}$$

$$Min \qquad m_A = \frac{\pi d^2 \gamma ds}{4g} \tag{2.59}$$

where the term *[1+L(D ,d, α, n, θ)]* represents the correlation factor for the stiffness formula, the *Max* and *Min* ahead of both the formulas show the objective is to search for the maximum stiffness *k* and minimum spring mass *m*. Good results were reported to have been obtained by applying the method.

The same method was also presented in another article (Shao et al., 2013) which looked for the minimum mass and the maximum natural frequency of the helical spring.

The strength, stiffness and fatigue life of the spring were set as boundary conditions. Similarly, Guo used the two objective functions of minimum spring mass and minimum spring stiffness error to conduct a helical spring's optimal design (Guo et al., 2010). The objective function of the minimum spring mass was also employed (Qimin et al., 2009a) to find the minimum mass for an automobile suspension spring. The spring mass was finally reduced by 16%, and the importance of the coefficients of the analytical expressions was also emphasized.

In addition, the objective function of minimum spring mass was also used (Qimin et al., 2009b) to optimise the design of a helical spring. In that article, the design domain consisted of three design variables: wire diameter, coil diameter and the number of active coils. The shear stress, maximum axial deflection, natural frequency, buckling, and fatigue life, which Wahl formulated, defined the constraint conditions. It was assumed that the coils were not in contact with each other in the study. The Particle Swarm Optimisation algorithm, that was coded in Matlab, was applied to solve the optimisation problem. It was reported that a spring mass as small as 5.5g was obtained.

Another study was conducted to find the optimal spring design under the objectives of maximum natural frequency and minimum mass (Qin-man et al., 2010). The particle swarm optimisation algorithm was applied to solve the optimisation problem, and as a result, the overall performance of the redesigned spring was better than the original design. Xi and Zhu addressed the problems caused by the negative impact of the inertia force of valve springs during high-speed valvetrain operations (Xi and Zhu, 2011). The objective function of the minimum spring mass was formulated based on Wahl’s spring mass formula. 12.44% of the spring mass was reduced by the optimal design, which also saved the spring's material and costs.

Moreover, the same optimisation objective functions of minimising spring mass and maximising the natural frequency were used (Zhang, 2012). The optimisation results of the spring were solved using the Genetic Algorithm. Sastry et al. presented the method of optimising helical springs by using the response surface method and design of experiments (Sastry et al., 2012). Wahl's spring formulas for calculating spring stress were used to derive the objective function. In the approach, a certain amount of design samples of the spring were required to accurately formulate the relationships between the spring geometry parameters and the output response. As a result, a significant reduction of the spring force was achieved.

The spring mass and the natural frequencies of the spring were also optimised in an article (Taktak et al., 2014) where four geometric parameters (wire diameter, middle helix diameter, active coils numbers and spring pitch) were chosen as design variables. The dynamic model of the helical spring was simulated in MATLAB in conjunction with the optimisation program. The author concluded that the presented method greatly reduces the spring's mass and increases the spring's first-order natural frequency, which is then higher than the working frequency.

Besides the widely used analytical spring model, the numerical method, such as the finite element method and lumped parameters method, were also applied to aid the optimal design of helical springs. It was realised that the conventional helical spring designs always have a shorter fatigue life than standard designs. Hence, a study presented an optimal method to redesign the helical spring by minimising the wire diameter, spring stiffness, avoiding spring surging and increasing the fatigue life (Pöllänen and Martikka, 2010). It was noted that the force and stress results were validated by the results of the finite element spring model and showed a good agreement.

In another study (Bakhshesh and Bakhshesh, 2012), the spring weight, stress and deflection of the helical spring made by four different materials (steel, E-glass/Epoxy, Carbon/Epoxy and Kevlar/Epoxy) were compared to find the best choice of material. The numerical spring model was developed by the finite element method in the software ANSY. It was demonstrated that the weight of spring was significantly reduced by using composite material compared to using steel. Then, a new approach was proposed to design helical springs by using the finite element method and the response surface optimisation method (Khurd and Kulkarni, 2014). In total, 78 numerical samples were generated in ANSYS with nine design parameters. The relationship between the design parameters and compressive stress was discovered by applying the response surface optimisation method. More importantly, the force and material property were found to significantly affect the compressive stress.

Lavanya et al. investigated the performance of suspension spring designs made from different materials (Lavanya et al., 2014). The numerical spring model was generated by using the finite element method in ANSYS. He drew the conclusion that the spring made by the low carbon structural steel resulted in lower spring stress than the spring made by chromo vanadium steel.

Besides the finite element method, researchers also used the lumped parameters method to optimise valve springs. Zheng et al. developed a lumped mass model for the valve mechanism and the valve spring was optimised by the Newton downhill method (Zheng et al., 2017). The aim of his study was to minimise the noise generated in the valve strain mechanism. It was found that the oscillation amplitude of the spring was reduced by 62.5%, which indicated that the noise of the valve train could be controlled and reduced by using the proposed method to optimise valve springs.

The traditional design methods for helical springs mostly rely on the analytical model based on Wahl's spring formulas. Numerical models like the finite element method and the lumped parameters method can be used to either generate numerical spring samples or validate the analytical results. However, it is common sense that the accuracy of the designed helical springs' performance hugely relies on the accuracy of the used analytical model (Sequenzia et al., 2011, Lin et al., 2012). In other words, the properties of the designed helical springs could fail to meet the initial requirements as the traditional spring formulas cannot consider the nonlinearities, for instance, varied spring pitch, coil clash and changing coil diameter.

### 2.4.2. Engineering Design and Analysis Methods Based on Machine Learning Models

Recently, due to the higher demand of involving nonlinearities in engineering designs and the emerging of artificial intelligence and machine learning techniques, new engineering design and analysis methods combining these emerging techniques have interested researchers and engineers alike. Unlike traditional methods that are usually difficult to involve nonlinearities and accuracy, they mainly rely on the quality of the chosen analytical formulas, new engineering design and analysis methods to directly look for the solutions from existing engineering results. Thus, it indicates that the nonlinearities are always considered as they already exist in the data of engineering results. On the other hand, however, enough results data should be guaranteed to achieve the precise design and analysis models. Therefore, experimental design methods are widely used to control the volume of the test or numerical samples.

#### 2.4.2.1. Design of Experiment

The design of experiment techniques, also called experimental design technique, was initially proposed for physical experiments and aimed to ease the effects of random errors (Alvarez, 2000, Simpson et al., 2001). It was later extended to the area for computer experiments to reduce the level of noise produced (Bonte et al., 2005). A design of experiment can select the sample points from a list of coordinates in the given design space. A design of experiment is usually composed of factors and levels which represent the input variables and the number of sampled configurations, respectively (Armani, 2014). Thus, the design of experiment is not subjected to a single method. Nonetheless, all the members in the design of experiment family have the same goal: to find the optimal number of input sets.

The most simple and basic design of experiment method is the full factorial design which the samples are all the combinations of factors at every level. The levels were assumed to have the same amount as the factors, which makes the number of design points equal to $N_l{}^{N_f}$ as shown in Figure 2-4(a), where $N_l$ is the number of levels and $N_f$ is the number of factors.

The central composite design also called the Box-Wilson central composite design, is an augmented factorial or fractional factorial design method containing centre points to estimate the curvature (Figure 2-4(b)).

The Box-Behnken design method was firstly proposed for estimating the coefficients in a second degree graduating polynomial (Box and Behnken, 1960). Its methodology is to place each factor equally in the three-level space. A simple sketch of the concept of the Box-Behnken design method is shown in Figure 2-4(c).

The Latin Hypercube design method was firstly proposed and treated as a stratified Monte Carlo sampling method (McKay et al., 1979). One of the most important features

of this method is that it considers all regions of the whole design space equally important. In other words, all the input factors can be very well represented regardless of the complication of the whole system. A simple case for a two-level Latin Hypercube design space and sampled points is shown in Figure 2-4(d). This feature makes it an excellent candidate for the early stage of designs where the complexity of the investigated system is not clear.

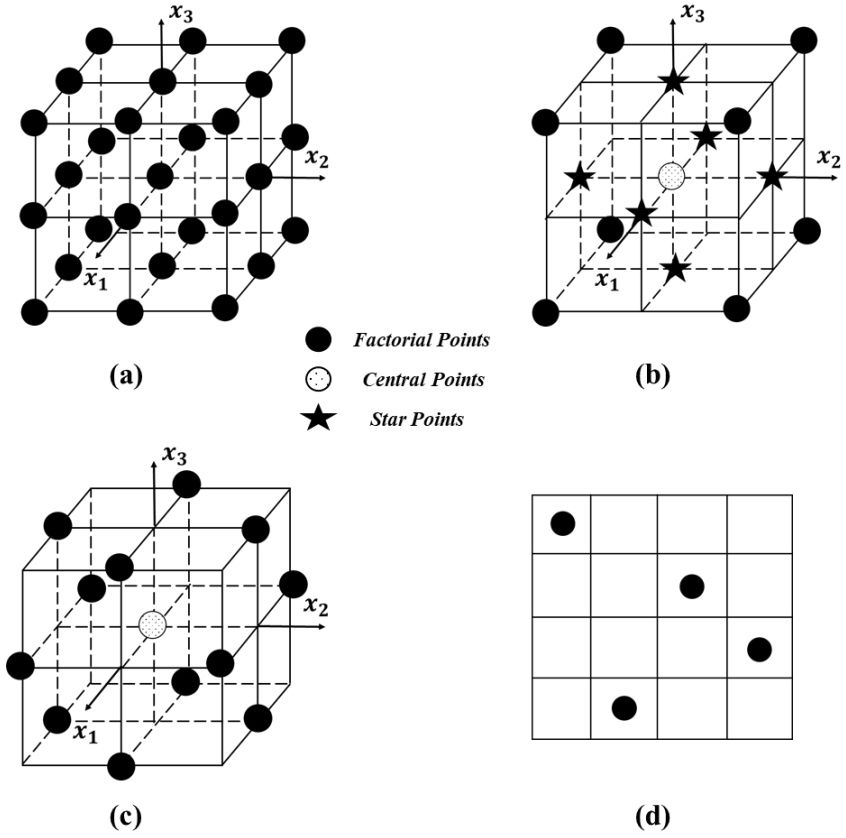


*Figure 2-4: Concept sketches of design of experiment techniques: (a). Full Factorial Design, (b). Central Composite Design, (c). Box-Behnken Design and (d). Latin Hypercube Design.*

The basic principles of the Latin hypercube method can be described as below:

1. The set of the input dimension $x = (x^1, x^2, \dots, x^d)^T$ is divided into N equal intervals where one sample is allowed for each interval, d is the number of input factors.

2. N scalar samples are then created by giving a certain dimension k.

3. The scalar samples were coupled with a random dimension to obtain an N-dimensional tuple.

4. Finally, the probability of the Latin Hypercube method can be calculated in the same way as the Monte Carlo (Morio and Balesdent, 2015).

Therefore, the sampled points selected by applying the Latin Hypercube method will be more representative than those selected by the random sampling method. Besides, it usually produces fewer samples by ensuring relatively high representativeness of input factors, which is particularly suitable for sampling computer and practical experiments for engineering applications. Nevertheless, it is still the responsibility of the user to choose an appropriate sized sample for a specific case when using the Latin Hypercube method (Ramu et al., 2010).

#### 2.4.2.2. Genetic Programming

Genetic Programming is a searching algorithm, commonly known as the concept firstly proposed by Cramer (1985). However, it did not draw much attention from researchers and engineers immediately, possibly due to the huge amount of computational resource required to calculate a solution at that time. However, with the rapid development of computers and their computational power, Genetic Programming has gathered considerable attention due to its robust ability to search for a suitable solution from a place where all possible solutions exist. Especially in engineering problems with complicated nonlinearities, which are usually difficult to formulate by analytical or physical models, Genetic Programming techniques reveal the inherent superiority of directing the search towards desirable or optimal solutions regardless of the complexity of the researched system (Armani (2014)). In other words, thanks to its main strength of being non-specific in nature, Genetic Programming is able to perform

a directed search on any entity. This has led to its wide use amongst engineering applications.

Genetic Programming can serve a varied range of tasks, among which the most common is symbolic regression (Barbosa and Bernardino, 2010). Symbolic regression is generally referred to as a type of regression analysis, and in the method, the initial research space is formed of mathematical expressions that contain randomly combined mathematical operators, functions, constants, and state variables. The search space in a symbolic regression is always infinite together with an infinite number of possible solutions. Nevertheless, in Genetic Programming, symbolic regression continually develops programs so that the terminal ends have a high-score of suitability. Genetic Programming is also used in the areas of machine learning techniques and artificial intelligence as it has the following properties listed below:

1. Genetic Programming can acquire knowledge from the structure of inputs (Schmidt and Lipson, 2009).

2. Genetic Programming can approximate relationships between variables without understanding the problem.

3. Genetic Programming can conduct sensitivity analysis studies on the input variables (Armani, 2014).

4. Genetic Programming has great potential to discover innovative solutions which researchers and engineers would struggle to achieve (Chellapilla, 1997, Schmidt and Lipson, 2009).

5. Genetic Programming can provide an explicit solution.

6. Genetic Programming has controllable compactness of the desired solution.

Typically, the drawbacks include:

1. Genetic Programming is always computationally expensive.

2. In some cases, the Genetic Programming model has a lower prediction accuracy than other techniques, such as artificial neural networks and the moving least square method (Armani, 2014).

3. Several possible solutions could be found for a specific problem.

4. Regressed expression may not always be clear enough to read (Sims, 1993).

## 2.5 Summary

The study of the analysis of helical springs begins with the very basic theory of helix curves and curved beams. These theories manage to represent the geometry of helical springs and investigate their static response in an efficient way. As the helical springs and their applications develop over time, the elementary theory of the spring is continuously being engineered to meet the rising demands of spring designs in different applications. One essential application of helical springs is to act as valve springs in high-speed engines. After realising that the high-speed loadings generated significant dynamic responses, which the static spring theories could not explain, it attracted researchers to study the dynamic effects of these valve springs. Therefore, three types of dynamic spring models – distributed parameter model, lumped parameter model and finite element model are proposed based on different modelling strategies. These spring models and the elementary spring theories are widely applied in helical spring's design and analysis tasks. However, the helical springs used nowadays mostly contain nonlinear properties such as variable coil diameter, dead coils (coils cannot move either before or during compressions), and narrow pitch. The existing spring models and theories have faced great difficulties in addressing these nonlinear problems in analysing and designing nonlinear helical springs. A deep understanding of the significant dynamic response of valve springs under high-speed loadings is also

required. In addition, studies on implementing machine learning techniques on the analysis of mechanical components show a promising way to aid the analysis and design of helical springs, which will be discussed in the thesis.

# 3 High Speed Engine Head Test

## 3.1 Valve Train Mechanism

A car engine, which is usually an internal combustion (IC) engine, is a core component in normal cars and also other vehicles. It works by converting the heat energy from fuel combustion to the kinetic energy of cars. An essential system in an engine that controls gas intake and exhaust operations is the valve train mechanism. The types of valve train mechanisms are manifold, which basically depends on the location of the camshaft. Four different layouts of the valve train mechanism are shown in Figure 3-1. Both Figure 3-1(a) and Figure 3-1(b) are called double overhead camshaft (DOHC), while the difference is that in the first configuration, the cam directly acts on the valve head and in the second configuration, the cam acts on the valve head through a rocker arm. Figure 3-1(c) shows another valve train configuration, called single overhead camshaft (SOHC). Its cam will push the pushrod firstly, and then the pushrod actuates the rocker arm to act on the valve head, which is the reason why it is also called ‘pushrod camshaft’. Finally, the valve train configuration shown in Figure 3-1(d) is called the Desmodromic configuration, which closes the valve by a cam and leverage system instead of using a valve spring. Except in the last configuration, valve springs play an essential role to control the motion of valves.

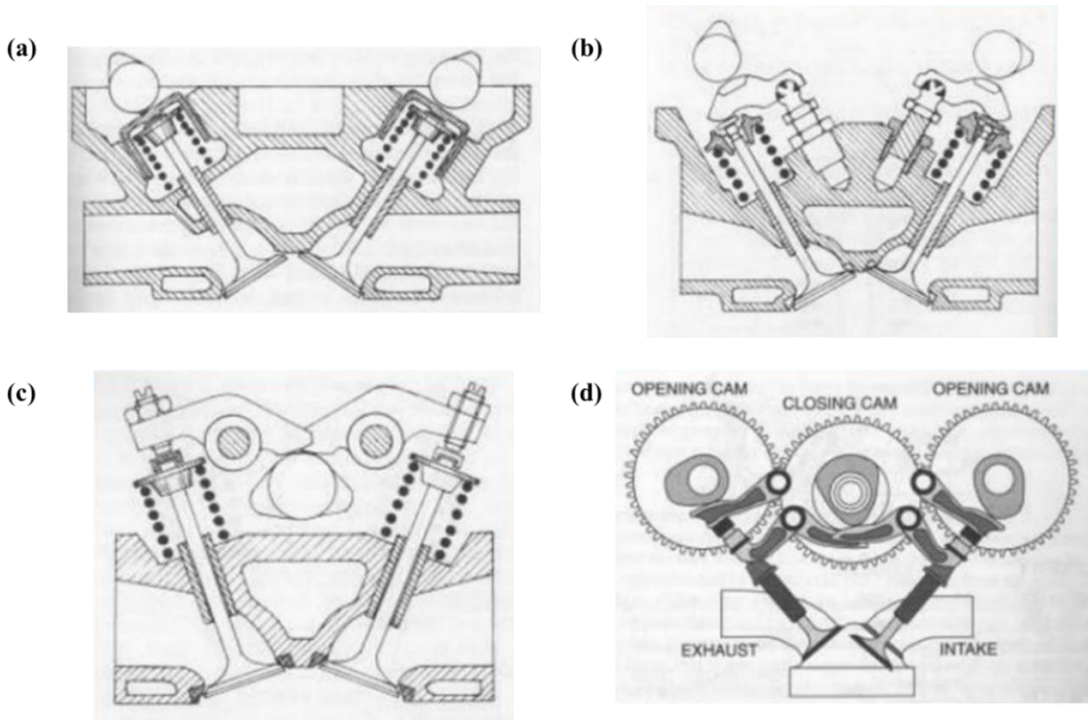


*Figure 3-1: Brief sketches of different types of valve train configurations: (a). Direct double overhead camshaft system. (b). Double overhead camshaft system with rocker arm. (c). Single overhead camshaft system with the pushrod. (d). Desmodromic camshaft system. (dos Reis Nogueira, 2014)*

## 3.2 Valve Spring and Engine Head

A valve spring is a special type of helical spring designated to undergo high-speed reciprocating motions in the valve train mechanism. As a result, it always needs to bear high-frequency strain and stress, which sometimes causes dynamic responses like spring surge and coil clash. The valve spring is not limited to one certain type; on the contrary, the types of it can be various, for instance, cylindrical asymmetric in Figure 3-2(a), conical Figure 3-2(b) and beehive springs Figure 3-2(c). Generally, the concepts of designer embodied in these various shapes of valve springs aim to ensure a stable working condition and high product life. Specifically, these unique designs contain their

own functionalities in reducing the dynamic response of the valve spring during operation.

In this thesis, the valve spring sample is a beehive spring (Figure 3-2(d)) which Force Technology Ltd manufactures. The detailed properties and dimensions of the beehive spring are demonstrated in the section of analytical and finite element models. The beehive spring serves for McLaren sports cars so that it works under high-speed loadings.

Figure 3-3 shows the engine head of the McLaren sports car, each of which covers four tops of cylinders. For the top of each cylinder, there are two exhaust valves and two inlet valves, and each valve is coupled with a beehive valve spring. In total, there are 16 valve springs in one engine head. The valve springs are seated on the main body of the engine head, and the upper end of each spring is covered by a spring retainer which can be compressed by the rocker arm. When the engine is in operation, the camshaft over the rocker arm will rotate and the cam profile press the valve springs and let them open and close periodically. The engine head test rig is set up in the factory of the Force Technology Ltd. The sensors of the spring forces are attached on the bottom surfaces of these beehive springs inside the engine head. All the tests are conducted by the author and also the professional experimenters of the Force Technology Ltd. In the end, the spring forces are recorded at various engine speeds.

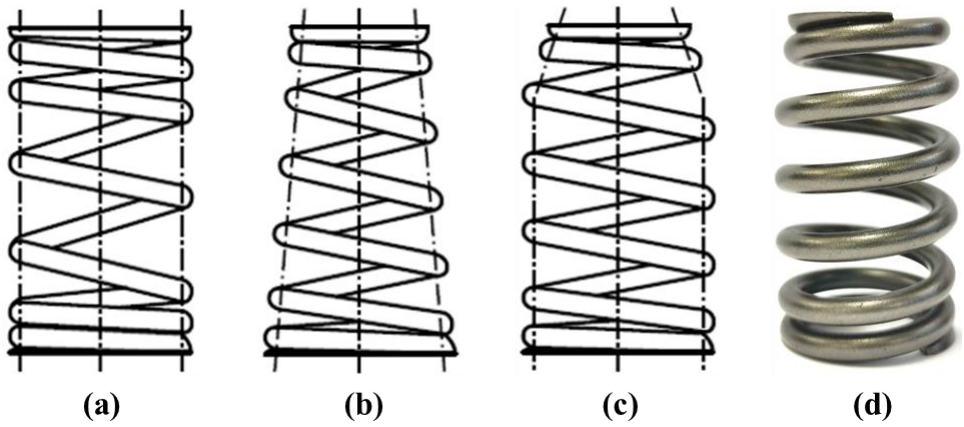


*Figure 3-2: Different types of valve springs: (a). cylindrical asymmetric, (b). Conical and (c). Beehive springs. And (d). the manufactured beehive spring sample.*

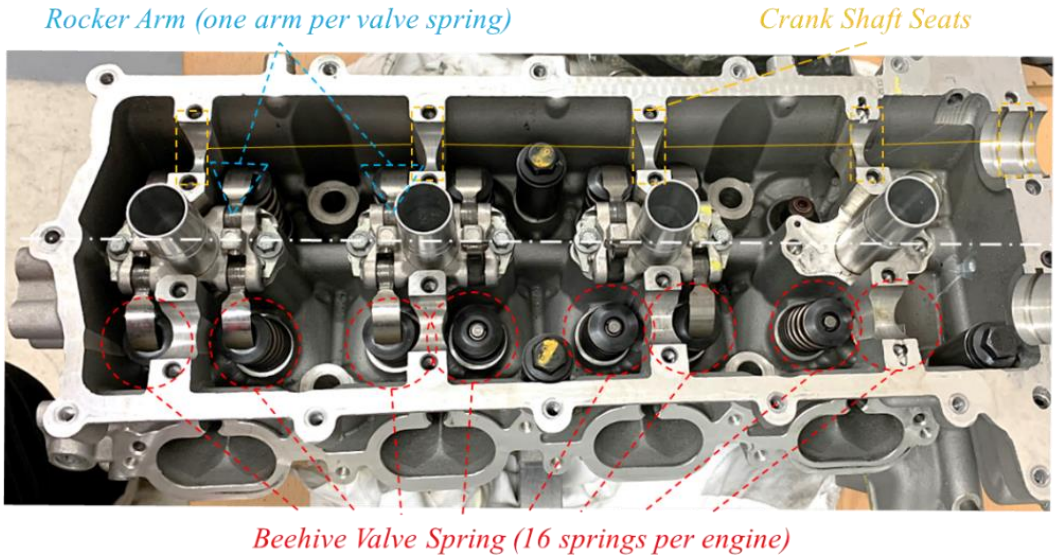


*Figure 3-3: Engine head of the McLaren sports car.*

## 3.3 Static and Dynamic Valve Spring Tests

### 3.3.1. Static Compression Test

The static compression test is one of the crucial tests for a real valve spring product. Firstly, it is because that the compression test can monitor the possible interference between coils which might be caused by the process of fabrication. More importantly,

a valve spring is often pre-compressed in the valve train mechanism. It will prevent undesired phenomena like valve jump and coil clash between spring ends and retainer. However, too much pre-compression would significantly reduce the engine's efficiency as it brings a larger spring force to resist the motion of the rocker arm. Therefore, the static compression test of a valve spring is essential to ensure the desired pre-compression is acceptable by engineers. In the present project, the beehive spring is always pre-compressed by 7mm in the engine head. Therefore, a static 7mm compression test is conducted in the lab of Force Technology Ltd, as shown in Figure 3-4(a). The beehive spring is compressed by a speed of 0.2mm/s which is a relatively slow speed compared to its usual working speeds in the car engine. The spring shapes and coils contact status at 1mm, 3mm and 7mm compressions are shown in Figure 3-4(b), Figure 3-4(c) and Figure 3-4(d). Together with the recorded spring force, these test results are discussed later and compared with static FE results in Section 4.3.

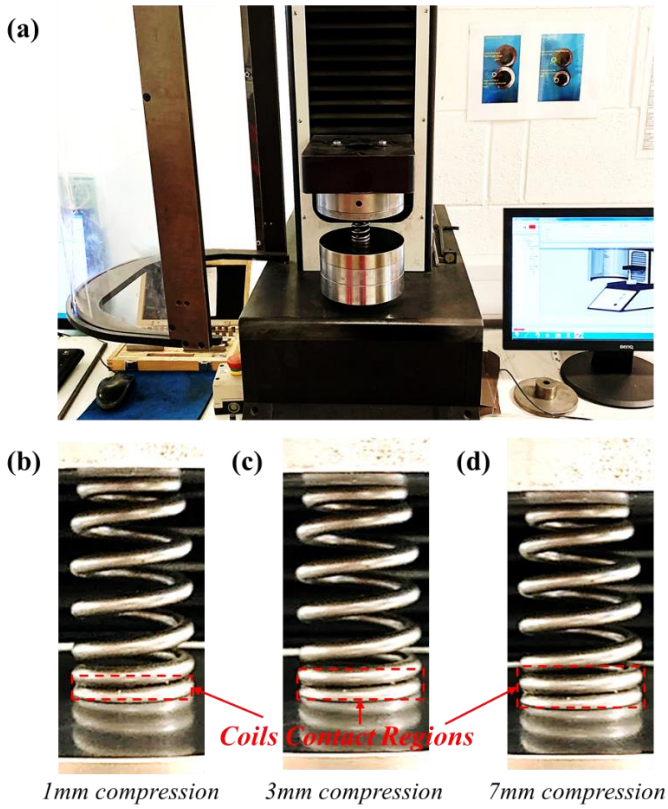


*Figure 3-4: (a). The 7mm compression test conducted on the beehive valve spring sample, and the contact status of spring coils at (b).1mm, (c).3mm and (d).7mm compression obtained from the testing result.*

### 3.3.2. Dynamic Engine Head Test

The real engine head and the installed beehive valve springs are mounted in an engine head test rig, as shown in Figure 3-5. The engine head is actuated by an electric motor by which the camshaft's speed can be controlled. In this test rig, the reaction force of the beehive spring to the spring seat is monitored. The forces are recorded every 1e-5 second, and averagely 10 cam cycles pass in around every 100 RPM. This resolution has been generally used by the Force Technology for ensuring a stable accuracy of recording dynamic spring forces.

Figure 3-6(a) shows the recorded spring force at engine speeds within the range of 4200 rpm to 9600 rpm. The first y-axis stands for the recorded spring forces (for blue lines), and the second y-axis shows the the engine speeds (for the red line). It is observed that slight vibrations of the spring force occur at lower engine speeds than (approximate) 6000 rpm. The existing spring theory can explain that the spring surge can increase the force amplitude. It is observed that significant spike forces appear at around 8000 rpm, which however, cannot be explained by the standard theory of spring surge. Besides, this phenomenon is also observed at engine speed around 9200 rpm, where the spring force approaches 2000N. In addition, high spike forces are not observed at engine speeds between 8200 rpm and 8800 rpm. These spike forces, which can be as large as double of static force, becomes a big potential risk of the car engine in practice. It is because that these significant forces can either directly damage the valve spring or shorten the actual fatigue life of the valve spring, which could result in the malfunction of the car engine. Hence, it is an urgent task to determine the reasons causing the spike forces and, therefore, determine a strategy to reduce or even eliminate them.

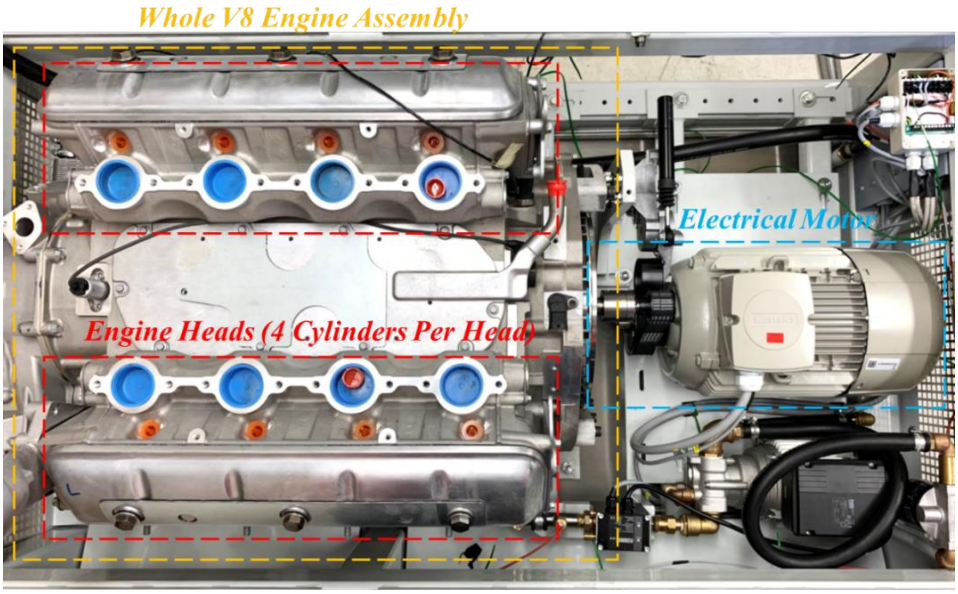


*Figure 3-5: Speed controlled engine head test rig for the engine of the McLaren sports car.*

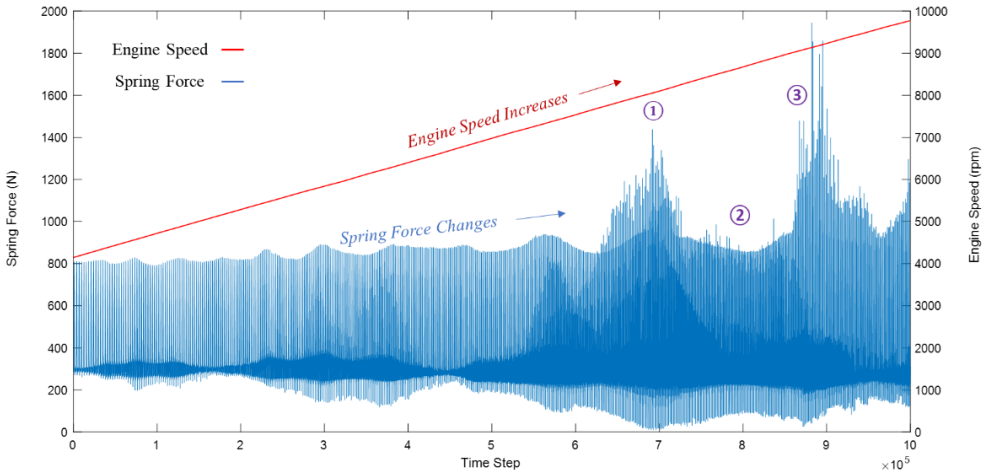


*Figure 3-6: The beehive valve spring forces measured in the high-speed engine head test ranging from 4200-rpm to 9600-rpm.*

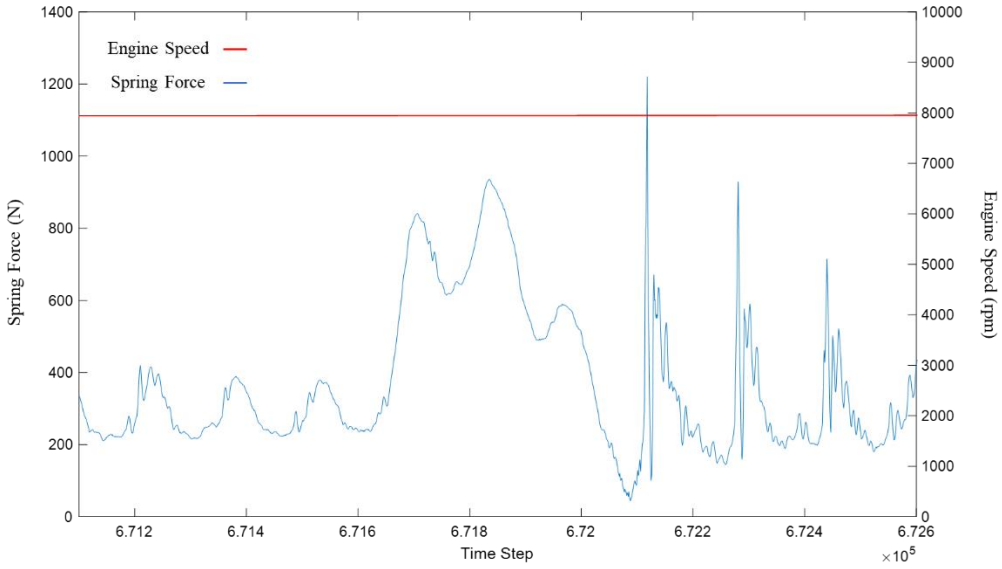


*Figure 3-7: Dynamic spring force of the beehive valve spring measured in the high-speed engine head test at 8000-rpm engine speed.*

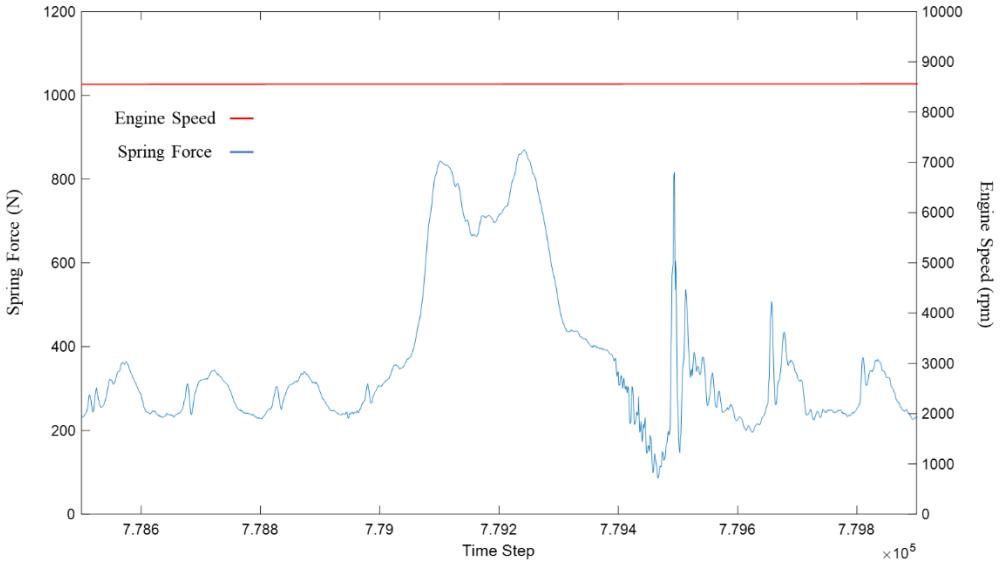


*Figure 3-8: Dynamic spring force of the beehive valve spring measured in the high-speed engine head test at 8600-rpm engine speed.*

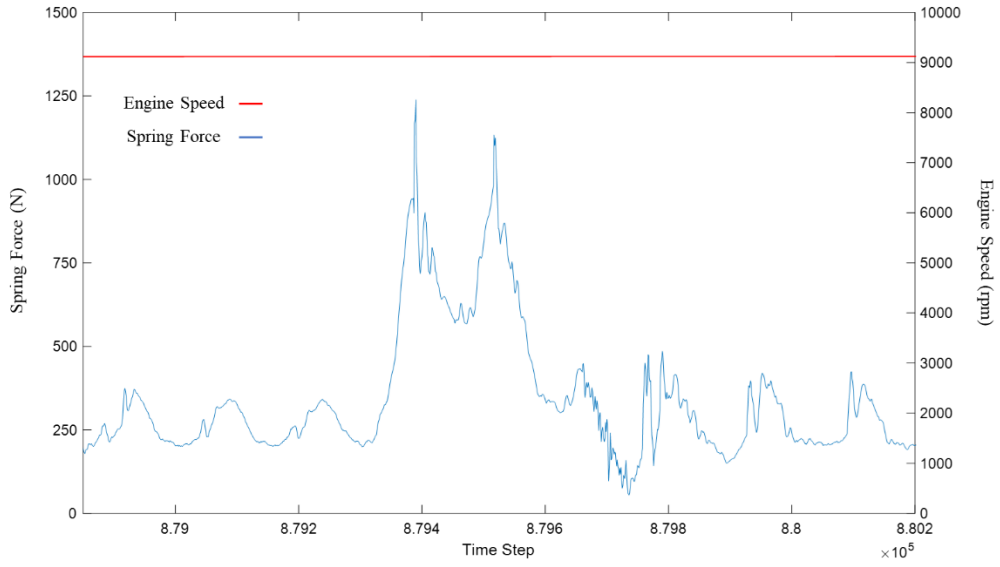


*Figure 3-9: Dynamic spring force of the beehive valve spring measured in the high-speed engine head test at 9100-rpm engine speed.*

In order to investigate the significant spike forces, the spring forces recorded at the positions ①, ② and ③ in Figure 3-6 are extracted. In the figure, x axis is each step to record the reaction forces. The spring forces of one entire cam cycle at around 8000 rpm (position ①), 8600 rpm (position ②) and 9100 rpm (position ③) are shown in Figure 3-7, Figure 3-8 and Figure 3-9, respectively. The force curves in these figures frequently vibrate, which demonstrate the dynamic effects of spring surge. It is noteworthy that the spring force shown in Figure 3-7 increases significantly in a very short period after the cam excitation, and in Figure 3-9, the force increases significantly around the maximum displacement of the cam excitation (around the middle position of one cam cycle). This is because the amplitudes of both the significant spike forces exceed the amplitudes of regular dynamic forces caused by spring surges. On the other hand, the spring force increases significantly after the cam excitation; however, its amplitude is slightly lower than the maximum value of dynamic force. Therefore, it can be considered that the unusual significant forces observed at engine speeds over 8000 rpm should be these significantly increased amplitudes, which appear in different cam excitation stages at various engine speeds.

In summary, the sports car's engine is mounted and tested in an engine head test rig. The reaction force of the beehive valve spring in this engine is monitored. It is shown that the dynamic effects of spring can be observed at low engine speeds. However, significant spike forces appear when the engine speed is higher than 8000 rpm, resulting in severe failures of the car engine. Therefore, it is an urgent task to develop a strategy to investigate this phenomenon and then redesign the valve spring to reduce or eliminate these significant spike forces.

# 4 Analytical Model of Helical Springs

## 4.1 Improved Spring Formulas

The traditional linear spring formulas proposed by Wahl (1944) are reviewed in detail in chapter 2. Among these formulas, Eq.(2.32) and (2.40) are widely used by the following researchers for calculating spring stiffness and fundamental natural frequency. However, only linear assumptions of the spring geometries can be made in this research since these formulas neglect the nonlinearities in the spring design. As a result, errors could be introduced by using these linear formulas to estimate the properties of nonlinear helical springs. The beehive spring used in this thesis contains obvious nonlinear properties, such as varied coil diameter and asymmetric spring pitch. Therefore, advanced spring formulas based on Wahl's theory are developed in this chapter to consider the nonlinearities of the beehive spring. In addition, a distributed parameter spring model coupled with the developed nonlinear spring formulas is developed to simulate the dynamic responses of the beehive spring at various engine speeds. Finally, both static and dynamic results of the analytical model are compared with the results of the compression test and the engine head test.

### 4.1.1. Stiffness Formula Considering Varied Coil Diameter

Firstly, the nonlinear effects of varied coil diameter into the stiffness formula are included. Based on Wahl's theory, the helical spring is assumed as a simplified curved beam. Each infinitesimal beam element is assumed having a length *dl* and going by $d\alpha$ helix angle, as shown in Figure 4-1. When the helical spring is subjected to axial

compression *F*, each infinitesimal beam element is assumed subjected to an axial deformation $d\delta$. The axial deformation of $d\delta$ can be calculated by:

$$d\delta = \frac{D(\alpha)}{2} \cdot d\theta \tag{4.1}$$

where $\alpha$ denotes the coil rotating angle, $\theta$ is the angle of twist of the spring element caused by the compressive force *F*, and $D(\alpha)$ is a function of $\alpha$, which denotes the varied coil diameter. Thus, the length of the spring element can be defined by:

$$dl = \frac{D(\alpha)}{2} \cdot d\alpha \tag{4.2}$$

According to the commonly used formula of beam torsion, the beam element contains the relation that:

$$\frac{T}{J} = \frac{G \cdot d\delta}{dl} \tag{4.3}$$

where the torsion moment is:

$$T = F\frac{D(\alpha)}{2} \tag{4.4}$$

and the polar moment of the circular cross-section is:

$$J = \frac{\pi d^4}{32} \tag{4.5}$$

where *d* denotes the diameter of the wire cross-section. By substituting Eq.(4.1) Eq.(4.2), Eq.(4.4) and Eq.(4.5) into Eq.(4.3), we obtained the expression for the displacement of each infinitesimal spring element as:

$$d\delta = \frac{4FD(\alpha)^3 \cdot d\alpha}{G\pi d^4} \tag{4.6}$$

In order to calculate the overall displacement of the moving end of the spring, the integral of *dx* in the interval [0, *X*] is calculated by:

$$X = \int_0^X d\delta = \frac{4F}{G\pi d^4}\int_0^{\alpha_0} D(\alpha)^3 d\alpha \tag{4.7}$$

And according to Hook's law, the stiffness of the spring can be written as:

$$k = \frac{F}{X} = \frac{G\pi d^4}{4} \cdot \frac{1}{\int_0^{\alpha_0} D(\alpha)^3 d\alpha} \tag{4.8}$$

In these equations, $\alpha_0$ represent the total coil rotating radius of a specific helical spring which will differ with different spring designs. In addition, it has a relationship with the number of active coils $N_a$ that:

$$\alpha_0 = 2\pi N_a \tag{4.9}$$

Therefore, Eq.(4.8) can also be written as a function considering the number of active coils $N_a$ by:

$$k = \frac{F}{X} = \frac{G\pi d^4}{4} \cdot \frac{1}{\int_0^{2\pi N_a} D(\alpha)^3 d\alpha} \tag{4.10}$$

It can be seen that the proposed stiffness formula includes the effect of varied coil diameter by adding the coil diameter function *D(α)*. Same as Wahl's theory, the formula assumes that torsional effects play an essential role so that the bending and shear effects of the spring are neglected. In addition, the formula assumes the helix angle or saying the number of active coils $N_a$ as a constant. Hence, it could be better suitable for springs with symmetric spring pitch of which coils usually do not contact each other. The proposed stiffness formula for considering both varied coil diameter and varied spring pitch is presented in the next section.

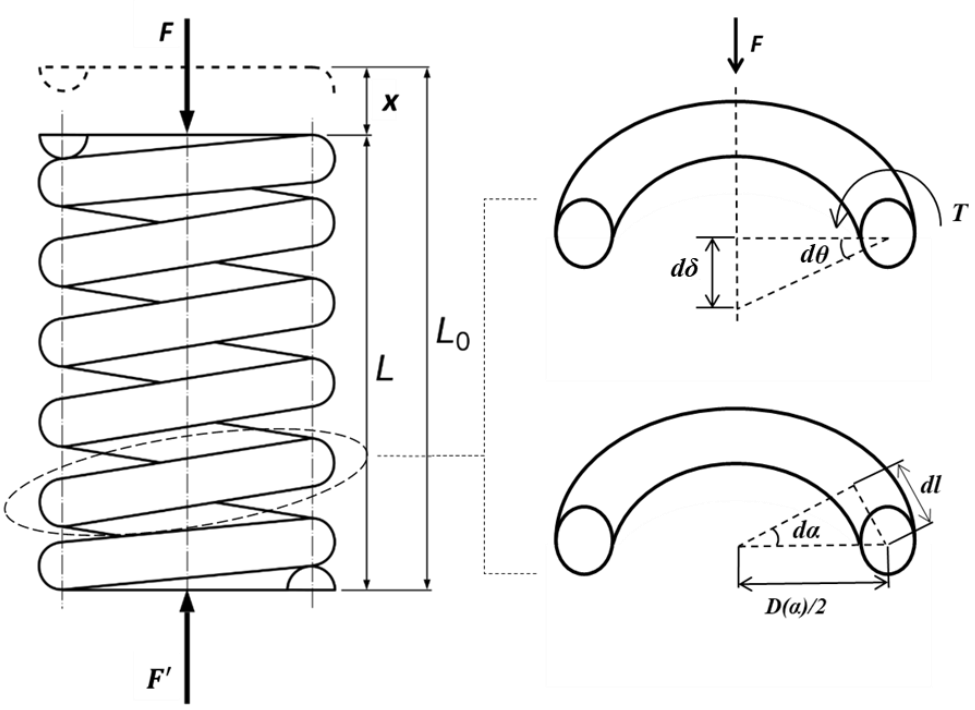


*Figure 4-1: Sketch of a normal helical spring and the load conditions of spring coils.*

### 4.1.2. Stiffness Formula Considering Varied Spring Pitch

Traditional helical springs usually have constant spring pitches in many engineering applications. However, with the development of the spring design techniques, asymmetric pitch appears in the design of helical springs. These springs are found to have many benefits in various applications; for instance, in suspension systems, the narrow pitch makes the spring stiffer after a certain compression and in valve train mechanism, the closing coils can increase the natural frequency of the valve spring and, therefore, reduce the maximum dynamic forces. The stiffness formula in the last section is then improved here to consider the effect of the narrow pitch. At first, Eq.(4.7) is rewritten as:

$$X(t) = S_f \cdot F(t) \cdot \int_0^{\alpha_0} D(\alpha)^3 d\alpha \tag{4.11}$$

where the $S_f$ is a constant and can be written as:

$$S_f = \frac{4}{G\pi d^4} \tag{4.12}$$

As the effect of the narrow pitch changes with loading time, the force *F* is replaced *F(t),* which is a function of the loading time *t*. Besides, it should be noted that in Eq.(4.11), the lower limit of integral is zero, which indicates that the integral of the displacement starts from the first spring element of the fixed spring end. The upper limit of integral is $\alpha_0$ which means the last spring element of the spring moving end. However, the integral should start from the first untouched spring element from the fixed spring end when the coils contact is considered. And the upper limit should be the last untouched spring element from the moving end. Hence, Eq.(4.11) is rewritten as:

$$X(t) = S_f \cdot F(t) \cdot \int_{\alpha_i(t)}^{\alpha_e(t)} D(\alpha)^3 d\alpha \tag{4.13}$$

where $\alpha_{e(t)}$ and $\alpha_{i(t)}$ represent the helix angles of the first untouched spring element and the last untouched spring element, respectively. To determine $\alpha_e$ and $\alpha_i$, the function of spring pitch $P_t(\alpha)$ with respect to the helix angle α should be introduced. This function represents the value of the spring pitch of the infinitesimal spring element at helix angle $\alpha$. The theory is that the closed coils of both lower and upper ends of the spring are treated as isolated helical springs. Then the displacements of these isolated helical springs are calculated by:

$$X_i(t) = S_f \cdot F(t) \cdot \int_{0}^{\alpha_i(t)} D(\alpha)^3 d\alpha \tag{4.14}$$

$$X_e(t) = S_f \cdot F(t) \cdot \int_{\alpha_e(t)}^{\alpha_0} D(\alpha)^3 d\alpha \tag{4.15}$$

In Eq.(4.14) and Eq.(4.15), $X_i(t)$ and $X_e(t)$ denote the displacements of the isolated springs at the fixed end and the moving end, respectively.

Figure 4-2 shows a helical spring that is subjected to a time-dependent loading *F(t)*. The loading *F(t)* results in a displacement at the upper end of the helical spring *X(t)*. Under this loading, several coils begin to contact other coils. Then, these contacted coils at the upper and lower ends are considered isolated springs 1 and 2, respectively, in Figure 16, where *Pt_i* and *Pt_e* represent the sum of the pitches of the contacted coils at the same time vertical position of the last untouched spring elements. Therefore, they are calculated, respectively, by:

$$P_{t\_i}(\alpha_i(t)) = \sum_{n=0}^{\left[\frac{\alpha_i}{2\pi}\right]} P_t(\alpha_i(t) - 2\pi \cdot n) \tag{4.16}$$

$$P_{t\_e}(\alpha_e(t)) = \sum_{n=0}^{\left[\frac{\alpha_0 - \alpha_i}{2\pi}\right]} P_t(\alpha_e(t) + 2\pi \cdot n) \tag{4.17}$$

where $P_t(\alpha)$ is the function of the spring pitch with respect to helix angle $\alpha$. $[\cdot]$ is the signal of rounding down.

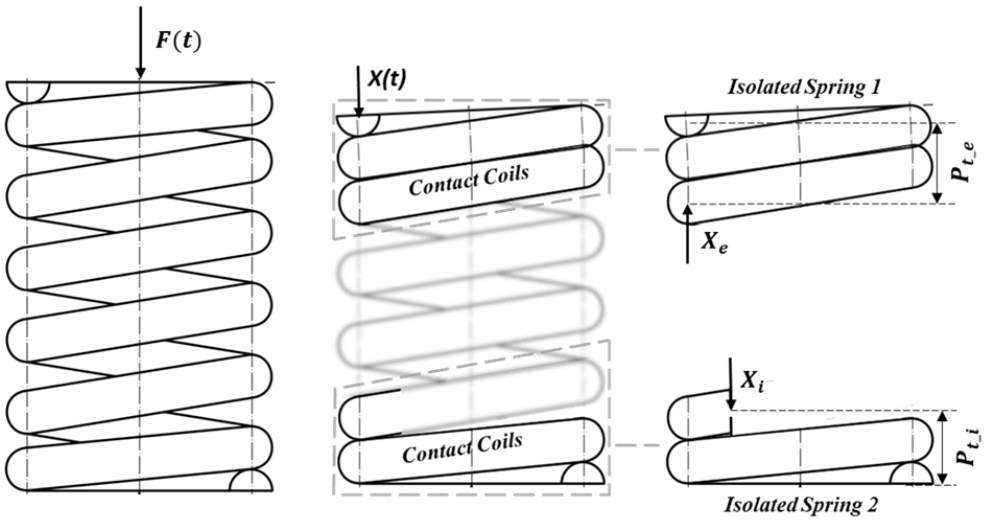


*Figure 4-2: Sketch of the closed spring coils under compressions which are treated as isolated springs.*

The displacements $X_i$ and $X_e$ of the isolated springs 1 and 2 should equal the total pitch values $P_{t\_i}$ and $P_{t\_e}$, respectively. In other words, coils are closed when they satisfy that:

$$X_i(t) = P_{t\_i}(\alpha_i(t)) \tag{4.18}$$

and

$$X_e(t) = P_{t\_e}(\alpha_e(t)) \tag{4.19}$$

Then, $\alpha_e$ and $\alpha_i$ can be solved from the equations above. By substituting $\alpha_{e(t)}$ and $\alpha_{i(t)}$ into Eq.(4.13) , the function of displacement $X(t)$ considering closed coils can be obtained. Finally, the stiffness function can be achieved by applying Hook's Law as:

$$k(t) = \frac{F(t)}{X(t)} = \frac{1}{S_f \cdot \int_{\alpha_i(t)}^{\alpha_e(t)} D(\alpha)^3 d\alpha} \tag{4.20}$$

It can be seen that the stiffness $k(t)$ becomes a function of time $t$ instead of a constant by considering the effects of closing coils. It is because at each loading time step, the number of closed coils, or saying the number of non-active coils, could be different so that the stiffness changes accordingly.

## 4.2 Dynamic Analytical Model

The analytical model presented in this section is a distributed parameter model that Wahl (1944) proposed. Later in the article of Phlips et al. (1989), the detailed process of solving the dynamic spring model was presented. According to Eq.(2.34), it is found that when the motions of the spring element can be described as a partial differential equation which is in the same form as the one-dimensional wave equation. Therefore, it can be simply rewritten by:

$$\frac{\partial^2 y(x,t)}{\partial t^2} = c^2 \frac{\partial^2 y(x,t)}{\partial x^2} \tag{4.21}$$

where $c = l\sqrt{k/m}$ is the speed of wave propagation in the spring. *y(x, t)* is the displacement of the spring element with respect to the position of the element *x* and the time *t*. *k*, *l* and *m* are the stiffness, length and active mass of the spring, respectively. As mentioned in chapter 2, it was stated that the dynamic motion of the spring element has a relationship with its eigenmodes. Therefore, the idea in this section is that the overall dynamic response of a helical spring is assumed as a superposition of the dynamic motions of spring elements at every eigenmode (every order of natural frequency).

In this study, the eigenmodes of the beehive spring are directly simulated in the developed finite element spring mdoel for convienience. Besides, in practice, one end of the valve spring is mounted on the valve seat when the other end is subjected to the motion of the cam. Hence, in this analytical model, one end of the spring is assumed fixed, and the other end moves exited by the cam profile. As a result of this boundary condition, one can easily know that the displacement of the spring element at the fixed end is zero and that of the spring element at the moving end is equal to the valve displacement:

$$y(0,t) = z(t), and\ y(l_0,t) = 0 \tag{4.22}$$

where $l_0$ is the element's position at the moving end, which is also the free length of the spring.

If we assume that the motion of the spring is formed of a static response and a dynamic response, the displacement of the spring element can be therefore written as:

$$y(x,t) = s_s(x) + s_d(x,t) \tag{4.23}$$

where $s_s(x)$ denotes the static contribution, so it is a function of *x* only. $s_d(x, t)$ denotes the dynamic contribution, so it is a function of both *x* and *t*. In the static term, it is generally assumed that the static displacement of the spring element at positions is

proportional to the displacement of the moving end or saying the cam excitation. Hence, it should have a relationship as:

$$s_s(x) = \frac{l_0 - x}{l_0} \cdot z(t) \tag{4.24}$$

By substituting Eq.(4.23) and Eq.(4.24) into Eq.(4.21) , it is obtained that:

$$\frac{\partial^2 s_d(x,t)}{\partial t^2} = c^2 \frac{\partial^2 s_d(x,t)}{\partial x^2} - \frac{l_0 - x}{l_0} \cdot \frac{d^2 z(t)}{dt^2} \tag{4.25}$$

As the dynamic term $s_d(x, t)$ is always treated as a harmonic in time (Chen and Zhou, 1993), its free solution is looking for a separable form as:

$$s_d(x,t) = f(x)e^{iwt} \tag{4.26}$$

By substituting Eq.(4.26) into Eq.(4.25), the free solution can be found from:

$$\frac{d^2 f(x)}{dx^2} + \frac{\omega^2}{c^2} f(x) = 0 \tag{4.27}$$

when $f(0) = f(l_0) = 0$ is the boundary condition. The ordinary differential equation can be simply solved, and it is obtained that:

$$f(x) = \sin\left(\frac{\omega x}{c}\right) \; when \; n = 1, 2, 3, \ldots \tag{4.28}$$

We know

$$f(l_0) = \sin\left(\frac{\omega l_0}{c}\right) = 0 \tag{4.29}$$

Hence, one can find the relationship that

$$\frac{\omega}{c} = \frac{n\pi}{l_0} \tag{4.30}$$

Eventually, the *n*'th mode of frequency can be obtained by:

$$\omega_n = n\pi \sqrt{\frac{k}{m}} \; where \; n = 1, 2, 3, \ldots \tag{4.31}$$

An efficient way to solve the dynamic equation is firstly to express the solution of these as the superposition of the modes (Schamel et al., 1993, Schamel, 1993, Phlips et al., 1989). Therefore, the dynamic term can be written as:

$$s_d(x,t) = \sum_n S_n(t)\sin(\frac{n\pi x}{l_0}) \tag{4.32}$$

In this equation, $S_n(t)$ is the term used to assume the dynamic response of the spring at each frequency mode $n$. In addition, the coefficient of the cam excitation can also be expressed as components in the $n$'th mode shapes:

$$\frac{l_0 - x}{l_0} = \sum_n \frac{2}{n\pi}\sin\left(\frac{n\pi x}{l_0}\right),\ where\ 0 < x < l_0 \tag{4.33}$$

Substituting Eq.(4.32) and Eq.(4.33) into Eq.(4.25) it gives that:

$$\frac{d^2S_n(t)}{dt^2} + \omega_n^2 S_n(t) = -\frac{2}{n\pi} \cdot \frac{d^2z(t)}{dt^2} \tag{4.34}$$

It is seen that the dynamic equation is transformed from a partial differential equation to a set of ordinary differential equations. It should also be noted that the valve spring's internal damping has not been considered in the equations. However, it has been widely proved that damping played an essential role in accurately estimating the magnitude of the spring surge (Schamel et al., 1993, Schamel, 1993). Therefore, in order to include the damping effects, a viscous damping term is added into the equation above as:

$$\frac{d^2S_n(t)}{dt^2} + 2\xi\omega_n\frac{dS_n(t)}{dt} + \omega_n^2 S_n(t) = -\frac{2}{n\pi} \cdot \frac{d^2z(t)}{dt^2} \tag{4.35}$$

where $\xi$ is the viscous damping ratio. Then, by solving the dynamic response $S_n$ from the equation, the dynamic force exerted on the valve spring can be calculated by:

$$F_d = \pi k \sum_n n S_n(t) \tag{4.36}$$

Eventually, the total force that is formed of the dynamic force and the static force can be obtained by:

$$F = k\left(x_p + z(t)\right) + \pi k \sum_n n S_n(t) \tag{4.37}$$

where $x_p$ denotes the displacement caused by the install height in the valve train. Usually, it is not subjected to one method to solve the dynamic equations. Among these methods is the Fourier method, which is used in this thesis. The detail of the solution method can also be found in the studies of Schamel et al. (1993) and Schamel (1993). At first, unit time $t$ is replaced by the cam speed $\omega_{cs}$ and the cam angle $\varphi$, which has the relation that $dt = d\varphi/\omega_{cs}$. Hence, Eq.(4.35) can be rewritten as:

$$\frac{d^2 S_n(\varphi)}{d\varphi^2} + 2\xi \frac{\omega_n}{\omega_{cs}} \cdot \frac{dS_n(\varphi)}{d\varphi} + \frac{\omega_n^2}{\omega_{cs}^2} S_n(\varphi) = -\frac{2}{n\pi} \cdot \frac{d^2 z(\varphi)}{d\varphi^2} \tag{4.38}$$

Then, the differential terms in the equation can be expressed by Fourier series:

$$S_n(\varphi) = \sum_{k=0}^{\infty} (p_k \cos(k\varphi) + q_k \sin(k\varphi)) \tag{4.39}$$

$$\frac{d^2 z(\varphi)}{d\varphi^2} = \sum_{k=0}^{\infty} (a_k \cos(k\varphi) + b_k \sin(k\varphi)) \tag{4.40}$$

where $a_k$, $b_k$, $p_k$, $q_k$ are all the coefficients of the Fourier series. By substituting Eq.(4.39) and Eq.(4.40) into Eq.(4.38) , it is easy to find the solution of $p_k$ and $q_k$ by:

$$p_k = \frac{-2a_k/n\pi - 2q_k \xi \omega_n k/\omega_{cs}}{\omega_n^2/\omega_{cs}^2 - k^2} \tag{4.41}$$

$$q_k = \frac{-2b_k/n\pi - 2p_k \xi \omega_n k/\omega_{cs}}{\omega_n^2/\omega_{cs}^2 - k^2} \tag{4.42}$$

Eventually, the total spring force $F_d$ can be calculated after the dynamic term $S_n(t)$ is solved by the values of $p_k$ and $q_k$.

## 4.3 Numerical Example of Beehive Spring

### 4.3.1. Geometry and Material

The same beehive spring used in the tests is used as in this section to validate the efficiency of the developed nonlinear spring formulas. The beehive spring (Figure 4-3a) is manufactured by Force Technology Ltd. and serves in the high-speed engine of sports cars, which is the same beehive spring as used in the static and dynamic tests. Figure 4-3b, Figure 4-3c, Figure 4-3d and Figure 4-3e depict the wire diameters, coil diameters, spring heights and spring pitches based on the design specifications and 3D scanning measurement, respectively. The scan data is obtained from a 3D laser scanner in Force Technology specially designed for vavle springs. The beehive spring rotates 360 degrees in the scanner to achieve the full 3D geometric dimensions. Apart from the wire diameter, small discrepancies in the spring height and the coil diameter are observed between the design specification and the actual geometry from 3D scanning. It is because, usually, a helical spring is designed to have a linear geometry, as described by the traditional spring formulas. However, errors can be introduced in the process of manufacturing, which may result in geometrical nonlinearities. Hence, any analysis based on design specifications could lead to unrealistic predictions of the spring performance. An analysis based on the scanned geometry should provide more accurate results.

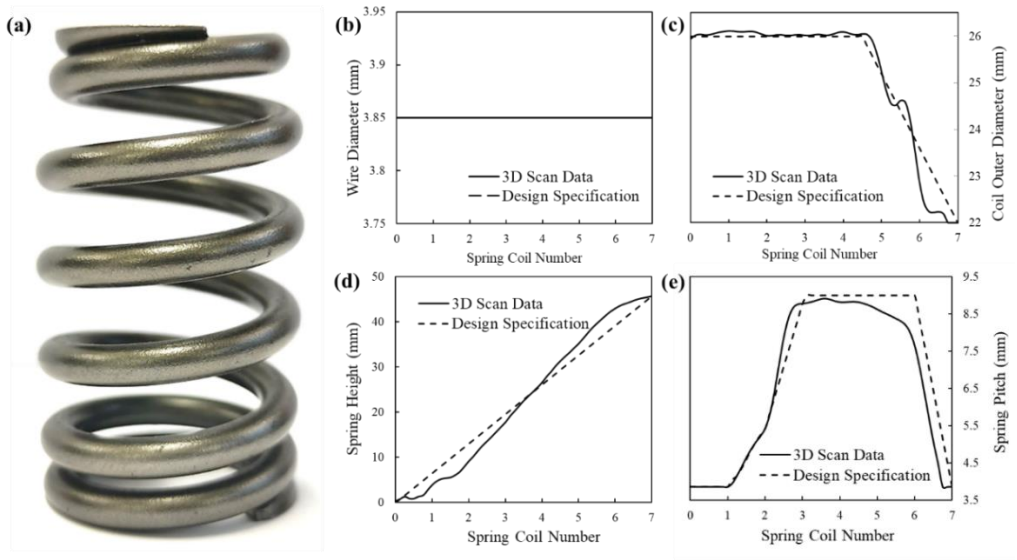


*Figure 4-3: (a). Beehive spring product and its geometry based on 3D scan technique and design specifications of (b). wire diameter, (c). coil diameter, (d). spring height and (e). spring pitch.*

The material used to fabricate the beehive spring is super clean spring steel with the type code of Oteva 90. It is a widely used steel for manufacturing springs with high fatigue properties and excellent relaxation properties. The beehive spring sample used in this study shot peened, and both ends are grounded. The spring coils are twisted on the coiling machine from a straight steel rod, where the end is cut on the same machine. Table 4-1 shows the mechanical properties of the material.

*Table 4-1: Mechanical properties of super clean spring steel Oteva 90.*

**Physical properties**

| Wire (mm) | Tensile strength ($N/mm^2$) | Modulus of elasticity (GPa) | Modulus of shear (GPa) | Posion's ratio |
|---|---|---|---|---|
| 3.85 | 2080-2180 | 206 | 79.5 | 0.29 |

### 4.3.2. Static Analytical Results and Validation

The spring formula developed in Section 4.1 is applied to analyse the mechanical properties of the beehive spring. As stated in the previous sections, the beehive spring

has geometrical nonlinearities (varying coil diameter and changing spring pitch). In order to consider these factors, firstly, an expression that can fit the 3D scan data of the coil diameter and spring pitch should be found. In this study, the least-squares polynomial fit method achieved by the Python package 'NumPy' is employed to regress the fitting functions. This method aims to find the minimum variance between the values from the regression function and the scan data values. A fit degree is usually introduced to regulate the length and the dimension of the regression polynomial expression. In other words, the value of the fit degree represents the maximum order and the number of terms of the regression polynomial expression. A low fit degree may fail to fit the data points, while a high fit degree always results in higher computational efforts. The complete Python codes for fitting 3D scan data is presented in Appendix A.

Figure 4-4a and Figure 4-4b show the varying coil diameter regression functions and the changing spring pitch by using the least square polynomial method. When the orders of fit degree are below 10, the fitting curves of both the coil diameter and the spring pitch show a notable mismatch with the 3D scan data. When the order of fit degree is raised to 15, it appears that the regression polynomials functions can fit the scanned coil diameter and spring pitch curves very well. Therefore, the order of fit degree for fitting both the coil diameter and the spring pitch curves are chosen to be 15 in this study.

Next, the regression function of spring pitch $P_t$ is used to construct the function of pitch summation $P_{t\_i}$ and $P_{t\_e}$ in Eq.(4.16) and Eq.(4.17). The fitting quality of the constructed $P_{t\_i}$ and $P_{t\_e}$ is shown in Figure 4-4c by comparing with the summation of the 3D scan spring pitch data. It can be seen that an order of fit degree 15 is sufficiently high for fitting the scan data. In the beehive spring of this study, only the lower portion of the spring has damping coils (have narrow pitches). Therefore, it is assumed that

during the 7mm compression, only the coils at the lower portion will be closed progressively. Thus, the solutions of the Eq.(4.18) should be determined at different loadings steps. Figure 4-4d depicts the relationships between the curves of $X_i$ and $P_{t\_i}(\alpha_i)$ under various loading steps. The $X_i$ curve has no intersections with the $P_{t\_i}(\alpha_i)$ curve at a spring force of 100N, making Eq.(4.18) have no solution. It means that the spring coils have not contacted each other at this loading step. When the spring force increases to 220N, the $X_i$ curve has one intersection with the $P_{t\_i}(\alpha_i)$ curve at around 1rad helix angle. Therefore, the contacting helix angle αi can be solved from Eq.(4.18), which is used to determine the current number of active coils $N_a$. When the spring force reaches 320N, the $X_i$ curve has more than one intersection with the $P_{t\_i}(\alpha_i)$ curve. The intersections at the largest helix angle (around 5.5rad) are the last contact spring element, and all the spring elements at the helix angle are smaller than they are assumed to be in full contact. The proposed analytical spring model was implemented and solved in the open-source integrated development environment (IDE) Spyder coding in Python.

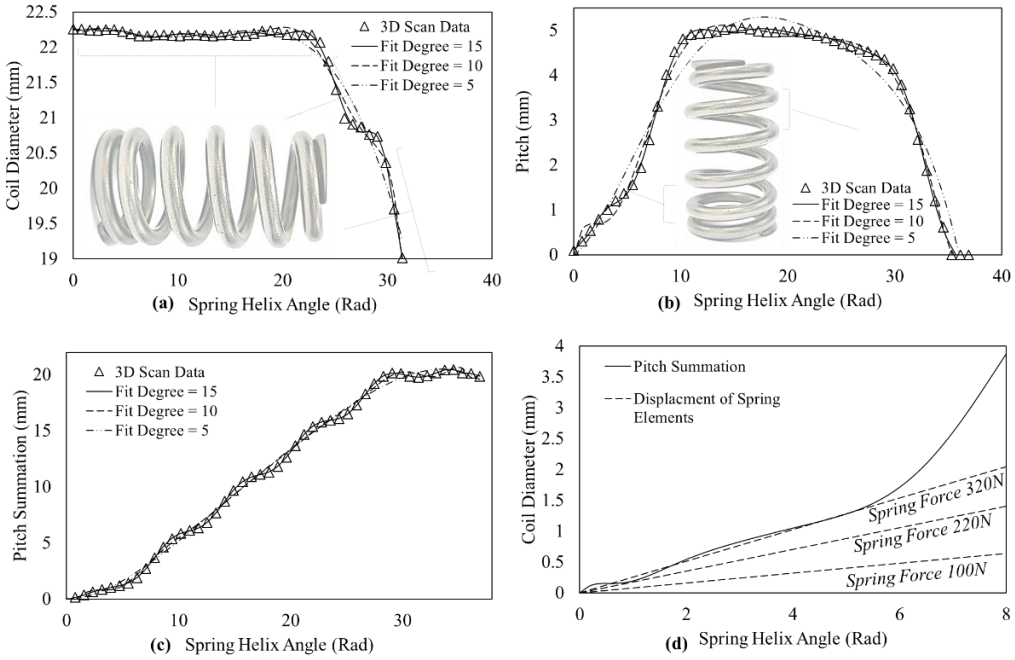


*Figure 4-4: Polynomials functions with 5, 10 and 15 fit degrees for fitting the 3D scan data of (a). coil diameter, (b). spring pitch and (c). summation of the pitch. And (d). position of contact coils at different loading steps.*

Then, the function $D(\alpha)$ for fitting the coil diameter curve and the helix angle of the last untouched spring element $\alpha_i$ can be substituted into the proposed spring formula, and the spring stiffness can be calculated by considering the effects of the variable coil diameter and changing spring pitch. The compression force of the beehive spring estimated by the traditional analytical formula, by the proposed analytical formulas considering only variable spring pitch, only variable coil diameter and considering both variable pitch and variable coil diameter are presented in Figure 4-5. In addition, the experimental results are also plotted to validate the analytical results. A significant discrepancy can be observed between the results based on the traditional spring formula and others. At 7mm compression, the force can only reach approximate 210N according to the traditional spring formula, while it is around 312N based on the experimental results. It is mainly because that the reduced size of the spring coils at the upper portion and the narrowed pitch at the lower portion of the beehive make the spring stiffer, which the traditional formula cannot consider. As a result, the traditional formula that assumes a constant coil diameter and pitch underestimates the spring force significantly compared with the experimental results.

For the analytical model that considers only variable pitch, the calculated spring force is around 270N at 7mm compression, slightly lower than the experimental results. However, the result is closer to the experimental results than the ones obtained from the traditional formula. It is because that the spring stiffness becomes higher during compression when considering the closed spring coils. The relatively higher stiffness results in a higher spring force. Similarly, the proposed spring formula considering only the variable coil diameter estimates the spring force around 280N at 7mm compression, which is slightly higher than the results obtained by the formula considering only variable pitch. It is noted that this curve has a good agreement with the experimental

results before 5mm compression. However, the deflection is much bigger when the compression is between 5mm and 7mm. as shown in Figure 4-6, which is a zoomed view of the compression between 5mm and 7mm. This phenomenon is due to the contacts between the coils with narrow pitch, i.e., when the compression exceeds 5mm, these coils become closed coils. Consequently, the actual number of active coils is reduced, which increases the overall stiffness of the spring.

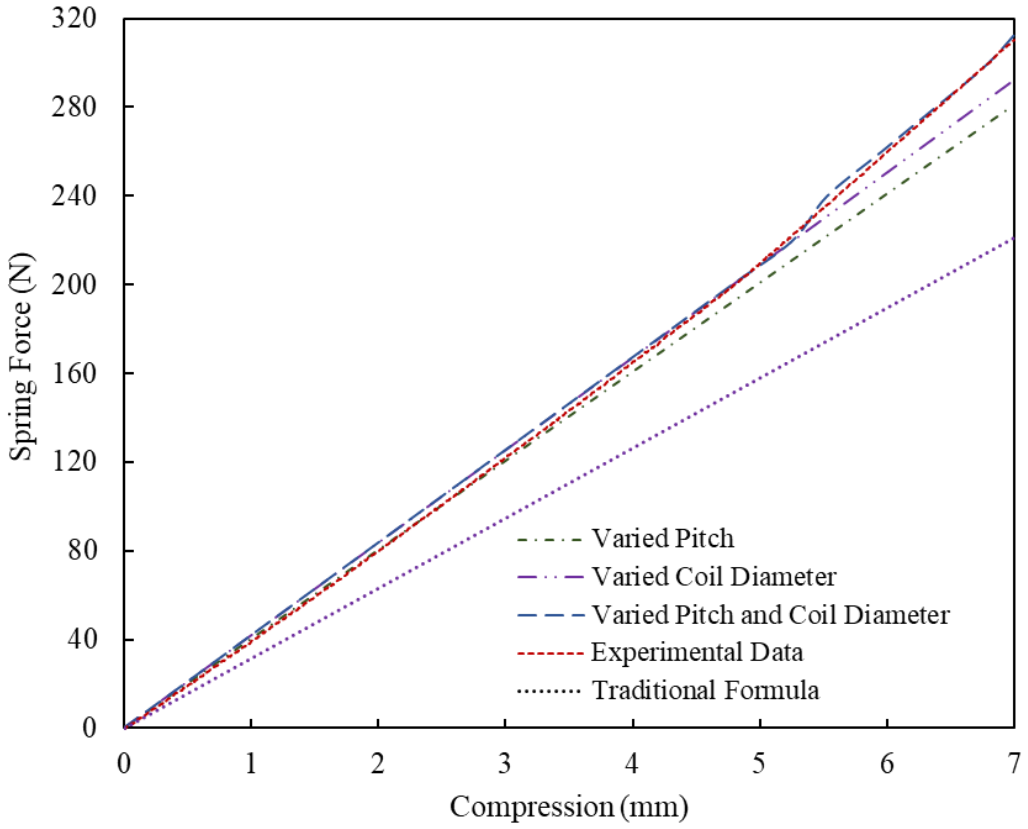


*Figure 4-5: Spring force curves under a 7mm compression based on experimental data, traditional spring formula and proposed analytical models considering varied pitch and varied coil diameter.*

The proposed spring formula, which considers the effects of both variable coil diameter and coil contact, shows its strong ability to estimate the force of nonlinear spring during compression. At 7mm compression, the calculated spring force is approximate 314N, which is very close to the experiment results (312N). In addition,

the curve of force fits very well with the experimental curves during the entire compression process (from 0mm to 7mm). It demonstrates that the proposed spring formula has the ability to estimate the mechanical properties of a helical spring accurately. Especially when the helical spring has high nonlinear geometries, such as variable coil diameter and narrow pitches, the proposed formula can still accurately predict when the traditional spring formula fails.

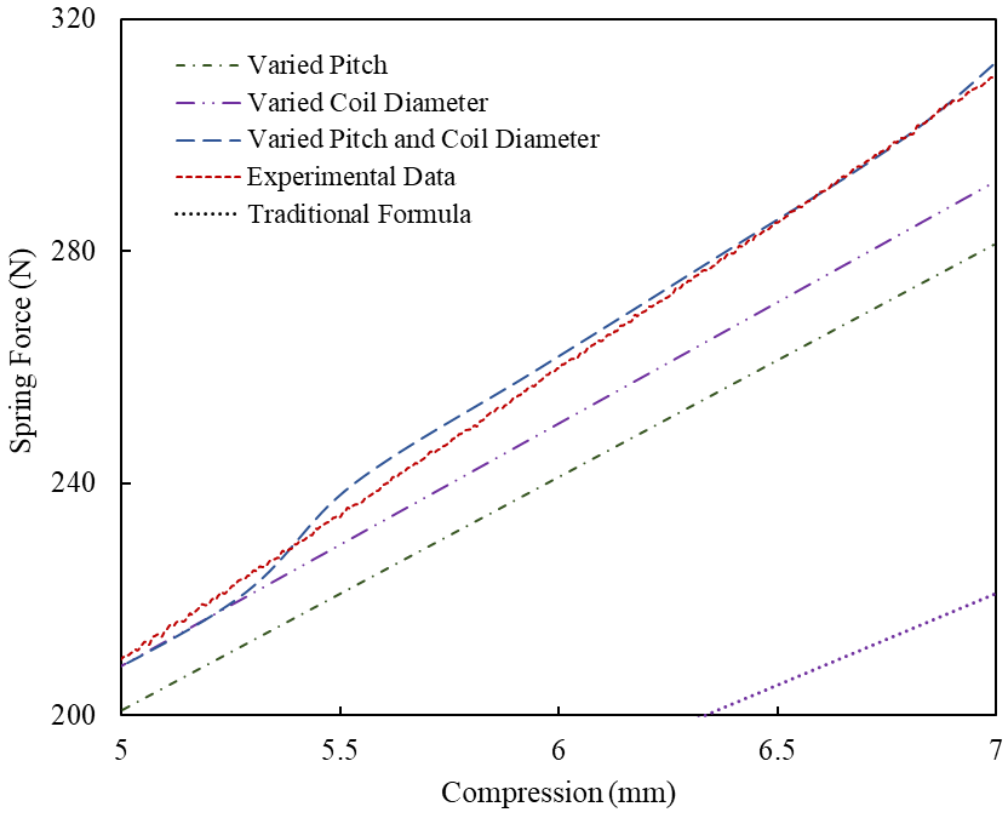


*Figure 4-6: Spring force curves under a 7mm compression based on experimental data, traditional spring formula and proposed analytical models considering varied pitch and varied coil diameter. (Zoom in the area between 5mm and 7mm compression)*

### 4.3.3. High-speed dynamic Analytical Results and Validation

In addition to the nonlinear performances of helical springs under static loading conditions, the dynamic properties of the beehive spring are also of great importance in practice. However, the existing analytical dynamic models are mainly based on the springs with linear geometries, which are not capable of predicting the dynamic force of a nonlinear spring. This section shows the dynamic results of the beehive spring by coupling the developed spring formulas with the distribute parameter spring model.

As per the development of the analytical model for predicting the dynamic performances of springs with nonlinear geometries, the dynamic effects of a helical spring are composed of a static term and a dynamic term. The developed analytical model is coded using the scientific packages 'Symfit' and 'Numpy' in the open-source software Python. In the analysis, the beehive spring is pre-compressed by 7mm to simulate the assembly in a real valve train system, providing enough force to close the valve. So, a 7mm preloading is firstly added into the model. Then, the dynamic input is derived from the profile of the cam over the spring. The cam rotates when the engine works, and it executes displacement on the top of the spring. The dynamic loading applied in the analytical model is shown in Figure 4-7a, which shows the displacement of one cycle of cam rotation. As a result of the displacement, the varying stiffness of the beehive spring $k(\varphi)$ during the cam cycle is shown in Figure 4-7b, calculated using Eq.(4.20) . Finally, these results are imported to the developed dynamic analytical model in Eq.(4.37) to calculate the dynamic spring force.

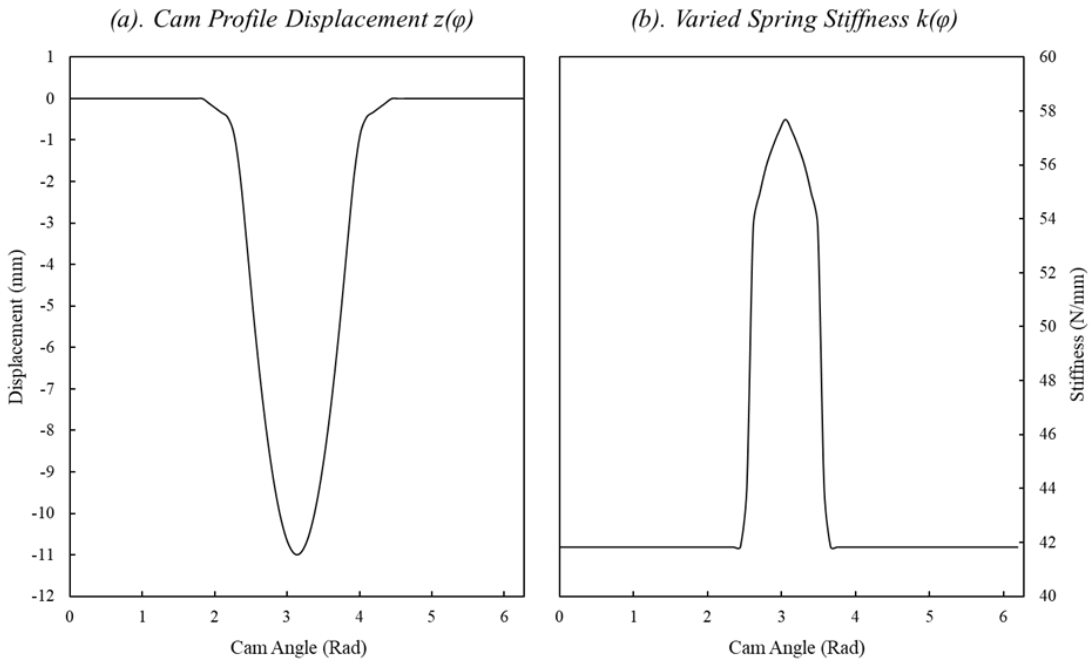


*Figure 4-7: (a). The cam profile of the valve train mechanism. (b). The varied spring stiffness of the beehive spring respects the angle of the cam.*

As demonstrated in previous chapters, the first step for calculating the dynamic spring force is to find the dynamic amplitude, *Sn(φ),* of each vibration mode *n*. The first simulated engine speed is 4200-rpm, which equals 2100-rpm cam speed. Firstly, the external loading *z(φ)* is input to Eq.(4.40) to calculate the Fourier coefficients $a_i$ and $b_i$. The damping ratio $\zeta$ is 0.016, and the first-order natural frequency $\omega_1$ is 631Hz, the same as in the finite element model. The dynamic amplitude *Sn(φ)* can be obtained by substituting the inputs *ai, bi,* $\zeta$ and $\omega_1$ into Eq.(4.41) and Eq.(4.42) to solve $q_k$ and $p_k$. Figure 4-8a - Figure 4-8e display the modal vibrations of the first five vibration modes *n·Sn(φ),* respectively.

The cam profile displacement *z(φ)* in Figure 4-7a demonstrates that no external loading is applied to the spring at 0-2 rad and 4.5-6.28 rad. However, the spring still has modal vibrations at each mode, especially at the first mode *n*=1, as shown in Figure 4-8. It is because that the spring experience free vibration for dissipating the residual

dynamic energy at 4200-rpm engine speed. At approx. 2.5 rad and 4.2 rad, the cam starts to compress the spring, the vibration status experience a sudden change, and short pulses are generated at each mode, as shown in Figure 4-8. In addition, it is observed that the vibrations between 2.5 rad and 4.2 rad have larger amplitudes than free vibrations as the spring under an external loading from the cam. Therefore, according to Eq.(4.37), the effects of the dynamic responses of all the vibration modes will be added to the static response of the spring (Figure 4-8f). In addition, it is noted that the vibration contributes less to the overall dynamic response when the vibration mode is higher. Therefore, only the vibrations of the first five modes are considered in the analytical model in this study.

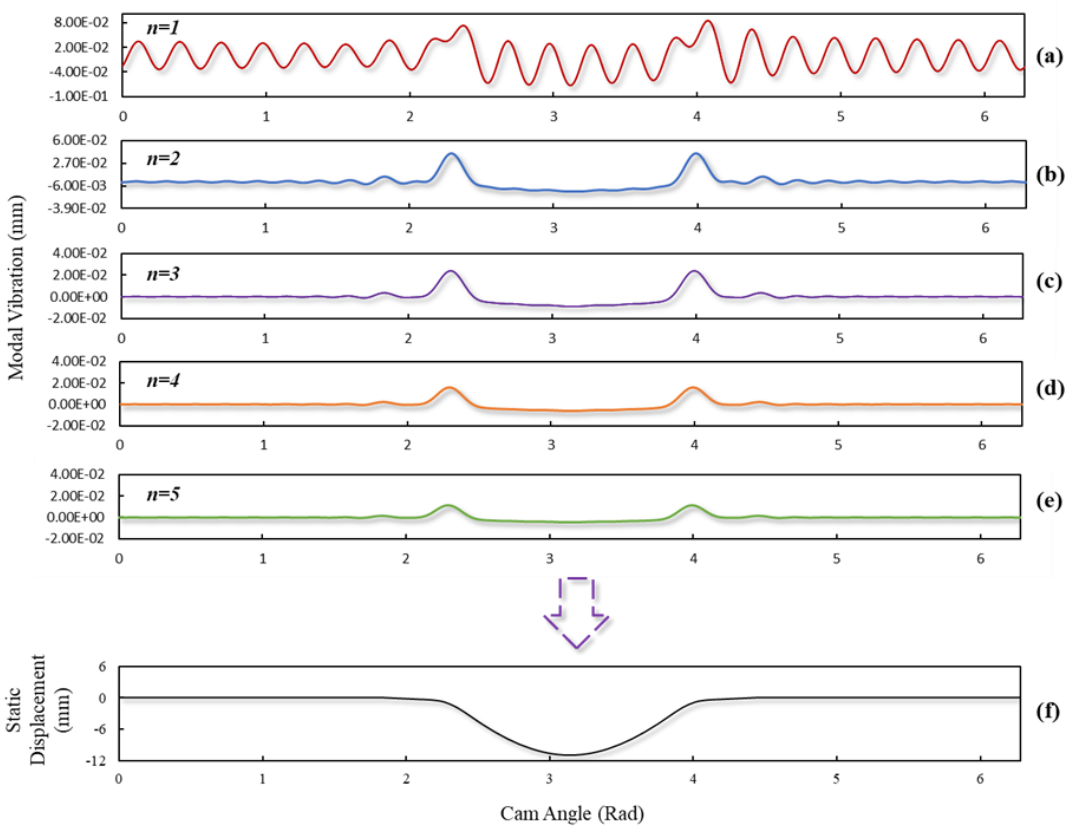


*Figure 4-8: The modal vibrations of the beehive spring of modal modes (a). n = 1, (b). n = 2, (c). n = 3, (d). n = 4 and (e). n = 5 at 4200-rpm engine speed, respectively. And the static displacement of the upper end of the spring caused by cam rotation.*

The overall dynamic force of one cam cycle at 4200-rpm engine speed is shown in Figure 4-9, which can be calculated using Eq.(4.37). The result of the engine head test is also plotted to validate the developed analytical model. Throughout the entire cam cycle, the analytical has a good agreement with the test data. The spring force starts with approx. 312N, which is the result of the 7mm pre-load. The tested spring force slightly fluctuates between 0 rad and 2 rad, indicating that the energy from the last cam cycle has not been completely dissipated, and the spring is under free vibration. In addition, the spring force shows similar vibrations between 4rad and 6.28 rad. This is caused by the cease of the external loading at 4 rad, and the spring experience free vibration again. The analytical model can simulate the free vibrations of the spring well at the two stages. From 2rad to 3.14rad, the tested force increases gradually, and it drops after the peak force around 851N at 3.14 rad to around 310N again at 4 rad. This process is caused by the cam profile, which reaches its largest displacement (11mm) at 3.14 rad. During this stage, the analytical model can fit the test result well. The comparisons between the forces based on the analytical model and the engine head test illustrate that the spring already has noticeable vibrations when working under cycling loadings at around 4200-rpm engine speed. More importantly, the analytical model proves its ability to accurately and quickly predict the magnitude of dynamic force and the existence of spring vibrations by comparing it with test results.

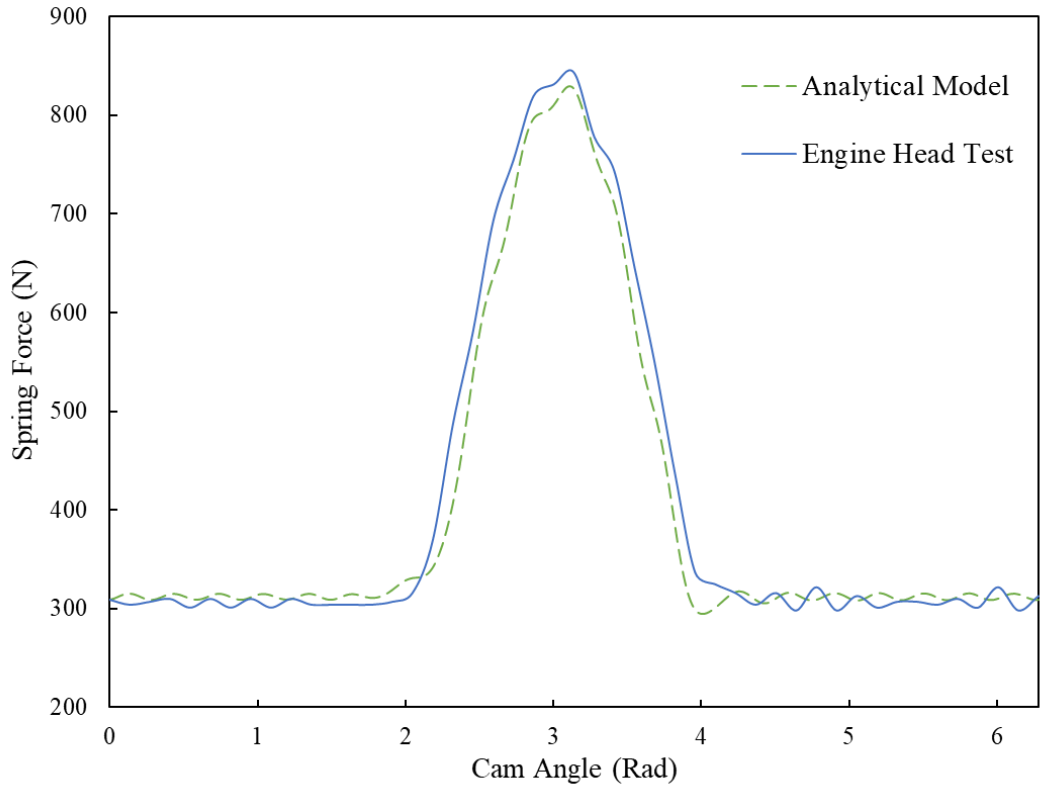


*Figure 4-9: The comparison between the dynamic forces of the beehive spring within one cam cycle at 4200-rpm engine speed based on the analytical model and engine head test results.*

The analytical model is also used to simulate the dynamic spring force of the spring at a higher engine speed 5600-rpm. It is easy to calculate that 5600-rpm is 1400-rpm higher than 4200-rpm in terms of engine speed and 700-rpm higher in terms of cam speed. Hence, the analytical model parameters are unchanged despite that the cam speed is increased to 2700-rpm. The modal vibrations of the first five modes at 5600-rpm are shown in Figure 4-10(a) - Figure 4-10(e), respectively. At the first mode n=1, the largest amplitude of the vibration can reach around 0.5mm, which is significantly larger than 0.08mm at 4200-rpm. It is reasonable as the higher engine speed actually results in higher vibrational energy. In addition, it is observed that the period of one vibration cycle at 5600-rpm is shorter than that at 4200-rpm. It is because the higher engine speed decreases the time for every cam cycle. It is also noteworthy that 5600-rpm is, when

compared with 4200-rpm, closer to the second-order natural frequency, which is around 1262Hz. It explains the phenomenon that the second mode, n=2 at 5600-rpm, shows more obvious vibration (Figure 4-10b) than that at 4200-rpm does (Figure 4-8b). Besides, the fifth mode vibration contributes very little to the overall dynamic response at 5600-rpm, similar to the phenomenon at 4200-rpm engine speed. (Figure 4-10e). Eventually, the dynamic vibration of each mode can be accumulated and added to the static displacement (Figure 4-10f).

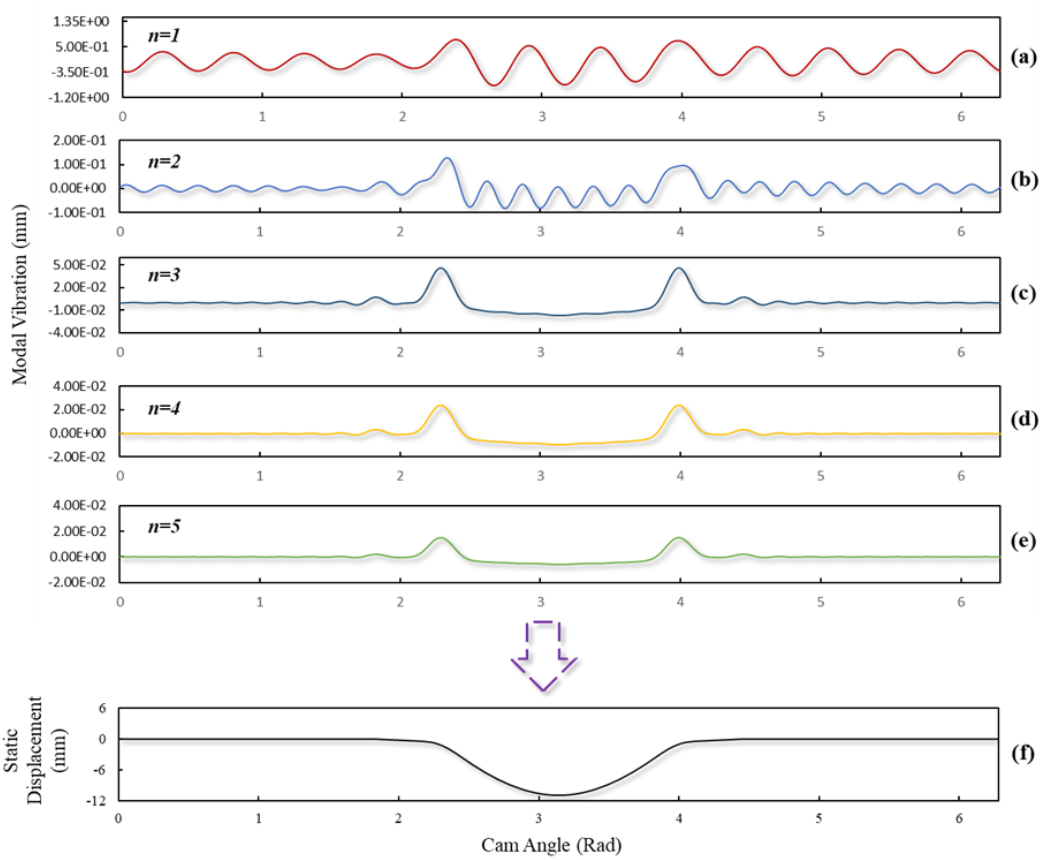


*Figure 4-10: The modal vibrations of the beehive spring of modal modes (a). n = 1, (b). n = 2, (c). n = 3, (d). n = 4 and (e). n = 5 at 5600-rpm engine speed, respectively. And the static displacement of the upper end of the spring caused by cam rotation.*

The overall dynamic force of the beehive spring at 5600-rpm is plotted in Figure 4-11 together with the results of the engine head test. When the engine speed reaches 5600-rpm, the internal vibration of the spring becomes more significant no matter at either the stage of free vibration (0 rad – 2 rad and 4 rad – 6.28 rad) or the stage of

forced vibration (between 2 rad and 4 rad). To be specific, the largest vibration amplitude at the free vibration stage can reach approx. 100N (from 250N to 350N) compared to approx. 10N at 4200-rpm engine speed. After 2 rad, when the spring is under external cam compression, the spring force starts to increase gradually. Then, however, the force suddenly drops at around 2.9 rad and then increases again until reaching the peak force 849N from the test, 841N from the analytical results and 890N for the test results at 3.14 rad. A similar phenomenon can also be observed at approx. 3.4 rad, when the spring force reverses to increase during the process of decreasing. In addition, it is noted that there is a rapid change of the spring force at around 4.2 rad. This phenomenon is caused by the impacts between the narrow coils at the fixed end. The reasons and details of the phenomenon will be explained and discussed in the later Chapter 6. After the forced vibration, the spring comes into the second free vibration stage after 4.2 rad. Therefore, it can be concluded that the analytical model has successfully predicted the dynamic force of the beehive spring by comparing it with the results of the engine head test even when the engine speed is increased to a higher speed of 5600-rpm.

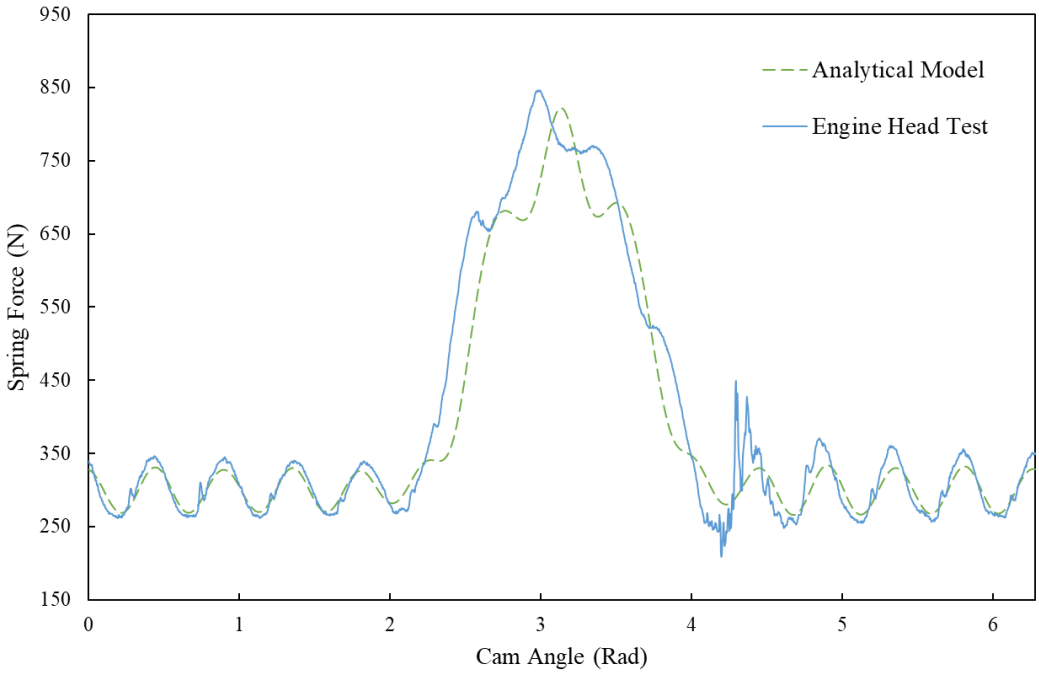


*Figure 4-11: The comparison between the dynamic forces of the beehive spring within one cam cycle at 5600-rpm engine speed based on the analytical model and engine head test results.*

## 4.4 Summary

This chapter presents an analytical spring model for predicting helical springs' static and dynamic mechanical properties with nonlinear geometries. Unlike the conventional cylindrical helical springs, these springs contain highly nonlinear geometries: variable coil diameter and pitches. The proposed model shows a robust ability to deal with these nonlinearities while the traditional spring formulas fail.

It is found that a practical beehive spring usually has highly irregular geometries, such as variable coil diameters and pitches. 3D scanning data of the helical spring can better describe the nonlinear geometry of a real beehive spring as it includes the tolerance from the manufacturing process. In this section, the nonlinear geometry is represented by two 15 order polynomial functions. The good representation of the

helical geometries provides a solid foundation for accurately predicting the mechanical properties of nonlinear helical springs under both static and dynamic loadings.

The static performances of the spring are analysed by comparing the results of the traditional spring model, the developed analytical model and the experimental data. In static analysis, it is found that the traditional spring model is unable to analyse the helical springs with nonlinear geometric properties (varied coil diameter, narrow pitch and coil contacts). It is due to its linear assumption that helical springs always have a constant coil diameter and number of active coils. So, it assumes the spring stiffness is linear during compression. On the contrary, the developed spring formulas can accurately estimate the mechanical properties of nonlinear helical springs, which are validated by the experimental result. More importantly, the developed analytical model significantly expands applicable parameters of spring geometries to a larger design domain for helical springs, in addition to its capability of analysing the nonlinearity. Based on the developed model, it is possible to include variable pitch and diameters of individual coils as tuneable parameters, which cannot be considered in the current design methods.

In dynamic analysis, the developed spring model is coupled with the analytical modal spring model to simulate the dynamic response of the nonlinear beehive spring. In addition, it is noted that the developed spring formulas are efficient to couple with the distributed parameter model to predict the dynamic response of the spring at 4200- and 5600-rpm engine speeds. The results show that the developed dynamic spring model can well predict the spring's dynamic force by considering the spring's nonlinear properties. Furthermore, at both 4200-rpm and 5600-rpm engine speeds, the calculated dynamic forces fit perfectly with the experimental data at both free and forced vibrations stages. It is because that the developed spring model could include the effects of coil

clash and variable spring diameter. They are essential for accurately predicting spring forces, especially at the stage of forced vibration, when the compression alters the stiffness of the spring and, thus, the peak spring forces.

# 5 Static FE Models of Helical Springs

The wide usage of the finite element method in analysing both static and dynamic performances of helical springs has been reviewed in chapter 2. It is found that these finite element models have the ability to estimate the static behaviours of the helical springs. However, the existing FE spring models are usually based on normal helical springs with linear geometries. More importantly, these FE models are mostly used to simulate the static response of these normal helical springs. Though these FE models show good results compared with the results of static experiments, they are unable to represent the helical springs with complex nonlinear geometries and are unable to simulate helical springs under high-speed dynamic loadings. In this section, a finite element model is proposed for simulating both the beehive spring's static and dynamic behaviours, which has highly nonlinear geometry. Firstly, a 3D geometry model is developed to describe the nonlinear shape of the beehive valve spring. Then, the geometry model has meshed, and static compression loadings are applied to simulate the working conditions in the valve-train mechanism.

## 5.1 Representation of Spring Geometry

It is a common practice to represent the geometry of linear helical springs by the spring generation toolkit embedded in 3-dimensional computer-aided design (CAD) software like CATIA, SolidWorks and Ansys (Stephen et al., 2019, Pawar and Desale, 2018, Kanimozhi et al., 2018). These toolkits are usually very efficient in generating linear spring geometries as they have constant spring diameter and pitch. However, the beehive spring in this study contains nonlinear geometry features, for instance, varied

spring diameter and a two-step pitch curve. Therefore, a new method is used in this study to represent the geometry of the nonlinear helical spring.

The terminology and the 3D scan data of the geometry of the beehive spring are already shown in Figure 4-3 in the previous chapter. It can be seen in Figure 4-3a–d that the scanned profile of the manufactured spring sample is of great difference when it is compared with its design specification. In Figure 4-3c, a significant misalignment between the coil diameters of design specification and scan data can be observed after coil 04. The diameter based on design specification decreases linearly between coil 04 and coil 07, while the diameter based on scan data decreases in steps. For the spring height shown in Figure 4-3d, the curve of design specification increases linearly across the whole spring while that of scan data experiences several fluctuations. In Figure 4-3e, it is shown that the beehive pitch increases gradually from coil 01 to coil 03 and then keeps constant between coil 03 and coil 06. However, due to the existence of manufacturing tolerance and residual stresses, certain deviations occurred on the curve of scan data. Especially at coil 05, there is a significant drop in the pitch. In short, although a helical spring is designed to have linear geometries, deviations in geometric features could result from manufacturing and heat treatment. These deviations may significantly affect the simulation results of natural frequency, spring stiffness and coil clash. As a result, the 3D scan data is used in this study to represent the spring geometries and therefore include these effects.

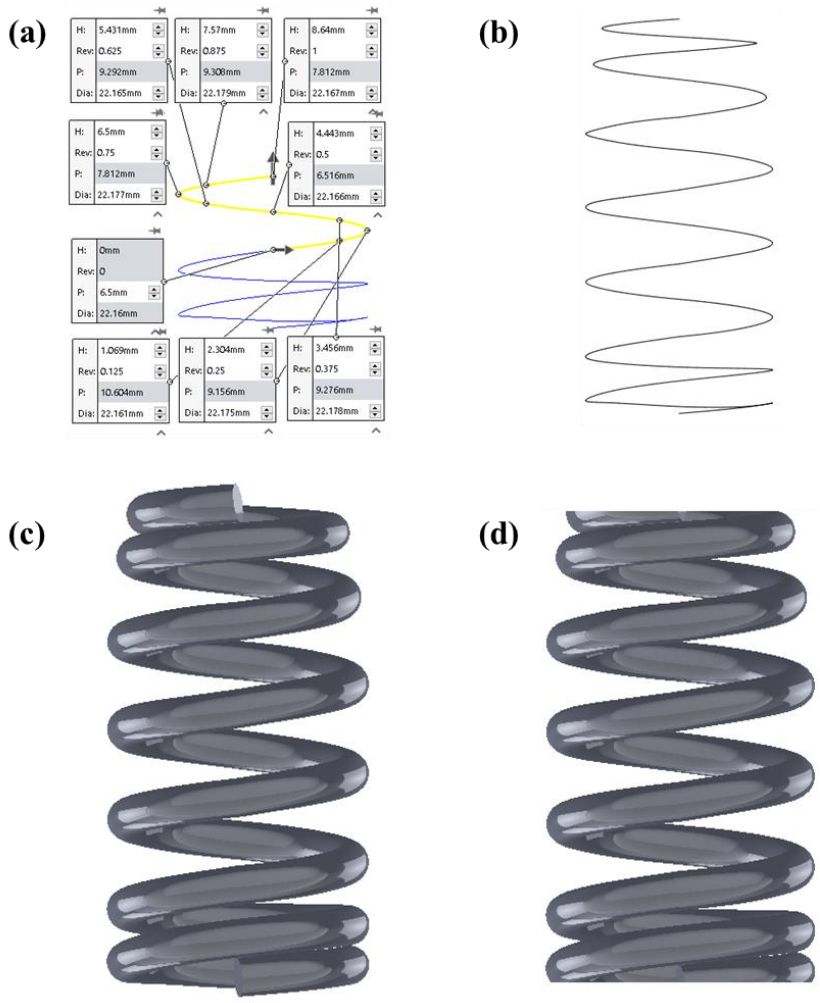


*Figure 5-1: (a). 3D helix curve based on defining coil diameter and spring height. (b). The generated 3D helix curve for describing the centreline of the coil rod of the beehive spring. (c). 3D geometry model of the beehive spring with round ends. (d). 3D geometry model of the beehive spring with grounded ends.*

The geometric spring model is generated in the commercial software Solidworks. Unlike linear helical springs usually generated by using the spring toolkit directly, the geometry model of the beehive spring is developed by describing the spring centre curve as a 3D helix curve. Specifically, the coil diameter and the spring height with respect to coil number based on scan data are first defined, and the spring pitch is self-adaptive, as shown in Figure 5-1a. The whole spring curve is then obtained based on the defined 3D helix curve as shown in Figure 5-1b. Following that, the solid geometry with the same diameter as the coil diameter is swept along the helix curve (Figure 5-1c). Until

this step, the spring geometry is successfully represented based on the scan data. However, in practice, both the ends of the beehive spring should be grounded for the purpose of being mounted in the valve train system. Therefore, both the ends are grounded by the height of 0.25 mm, which makes the overall height of the spring 45.75 mm. Compared with the spring height of the real spring product, which is 45.73 mm, the geometric model can well represent the nonlinear properties of the beehive spring. The geometric model of the beehive spring (Figure 5-1d) is then exported to the commercial software Ansys to build up the finite element model for both static and dynamic simulations.

## 5.2 Materials of the Beehive Valve spring

The beehive valve spring sample is manufactured by Force Technology Ltd and serves for the engines of McLaren sports cars. The material used to fabricate the spring is super clear (SC) spring steel OTEVA 90, of which full name is Oil tempered SiCrVNi-alloyed ultra-high tensile valve spring wire with surface nitriding. This material is specially intended to manufacture helical springs with extremely high fatigue properties and good relaxation properties at increased working temperatures. The chemical composition of the spring steel is shown in Table 5-1. The physical properties of the material are already listed in Table 4-1 of Chapter4. In this study, the beehive spring has a 3.85 mm wire diameter. The Young's modulus $E$ of the material is defined as 206 kN/mm$^{2,}$ and the shear modulus $G$ is 79.5 kN/mm$^2$.

*Table 5-1: Material properties of Oteva 90 Spring Steel*

| C % | Si % | Mn % | P max. % | S max % | Cr % | V % | Ni % |
|---|---|---|---|---|---|---|---|
| 0.5–0.7 | 1.8–2.2 | 0.7-1.0 | 0.02 | 0.02 | 0.85-1.05 | 0.05-0.15 | 0.20-0.40 |

## 5.3 Static Finite Element Analysis

It is widely known that spring stiffness is always one of the most essential features of a helical spring when analysing its static behaviours. It is usually used to describe the relationship between the spring displacement and the spring force of a certain helical spring. In this section, a static finite element model of the beehive spring is developed in Ansys to estimate the spring force generated during static longitudinal compression accurately. The geometric model, which is illustrated in the last section, is imported in Ansys. Figure 5-2 shows the meshed finite element spring model and its constraints. It is seen that the coil 02-06 are meshed by hexahedron elements which can significantly reduce the number of nodes involved in the calculation. On the contrary, coil 01 and 07 are meshed by tetrahedron elements and higher mesh density, which will increase the computational efforts. It is because both the ends of the spring are grounded so that the tetrahedron element can better represent the irregular shapes of the end coils. As a result, the finite element spring model contains in total 70475 elements and 160500 nodes correspondingly.

Constraints are also defined in this finite element model. As the manufactured spring sample is grounded, there is a flat surface A on the upper-end coil and a flat surface B on the lower end coil. In practice, surface B is mounted on the valve seat, and they keep contacting with each other all the time due to the existence of the installing force. Therefore, surface B is assumed as being under the condition of 'fixed' in the finite element model. In practice, surface A is connected with the valve head, which is actuated by the cam rotation. As a result, surface A, together with the valve head, will move along the axis of the helix curve. Hence, surface A is subject to a longitudinal input of displacement. Besides these, every coil in practice may collide with each other during the process of compression, which should also be included in the finite element

model. Therefore, the condition of 'frictionless contact' is defined across all the surfaces of the spring coils. In ANSYS, this nonlinear contacting constraint assumes zero pressure between contacting faces if separation occurs, and forces are applied when the surfaces of coils contact. Besides, the 'large deformation' is on in the analysis settings as the deformation of the spring coil is relatively large.

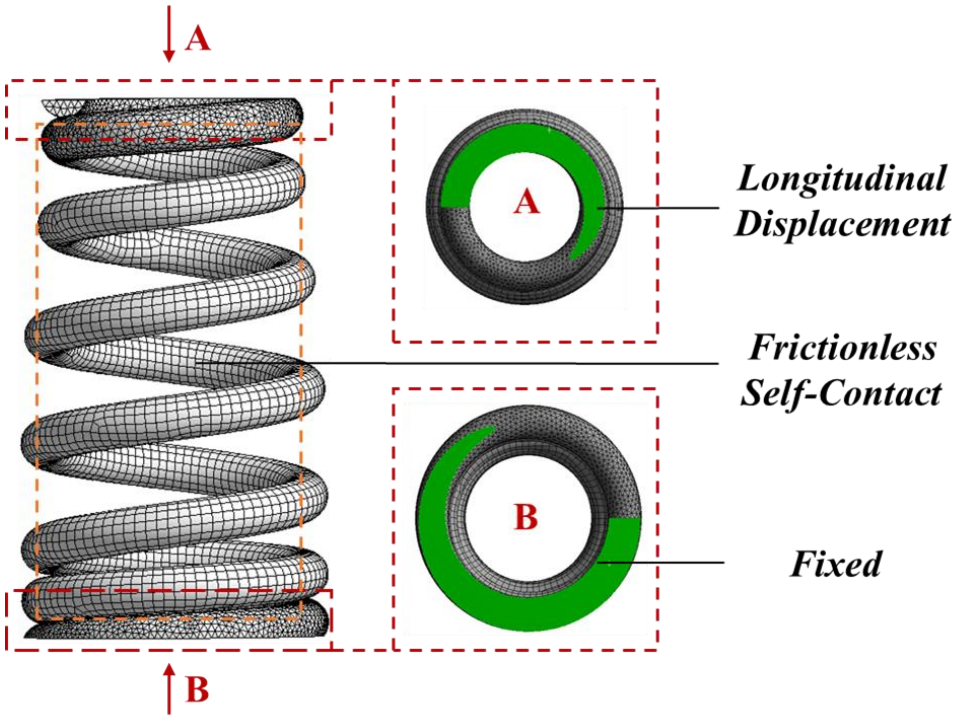


*Figure 5-2: Meshed FE spring model of the beehive spring and the boundary conditions defined on both the upper and lower ends.*

In this case, the beehive valve spring is installed in the valve train with a 7mm install height. Setting an install height for valve springs is usually a common practice in a valve-train system to prevent the so-called 'valve jump' phenomenon. A 7mm install height means the reserved height between the cam and the spring seat is 7mm smaller than the free length of the beehive speed. In other words, the beehive spring is always returned to a 7mm pre-compression status at the end of each cam cycle. Hence, in the static finite element simulation, a 7mm longitudinal displacement (Figure 5-3a) is

exerted on surface A. The finite element model is simulated under these conditions, and the spring force generated on the lower end face (surface B) is obtained. Besides, the spring forces at 7mm compression obtained from the spring compression test and calculated by the existing analytical model based on Eq.(2.23) are plotted and compared with the finite element results in Figure 5-3b. It shows that the finite element result has an excellent agreement with the experimental data, and they all reach around 300N at 7mm compression.

On the contrary, the analytical result keeps an acceptable agreement with the finite element result and the experimental data before 2mm compression. However, a significant departure of the analytical result is observed, and it reaches approximate 220N at 7mm compression. The spring coils can explain the discrepancy by progressively closing the narrow pitch during compression, leading to a higher spring stiffness. Hence, the slope of the force curve should become larger like those of the finite element result and the experimental data instead of that of the analytical result, which keeps constant in the whole process.

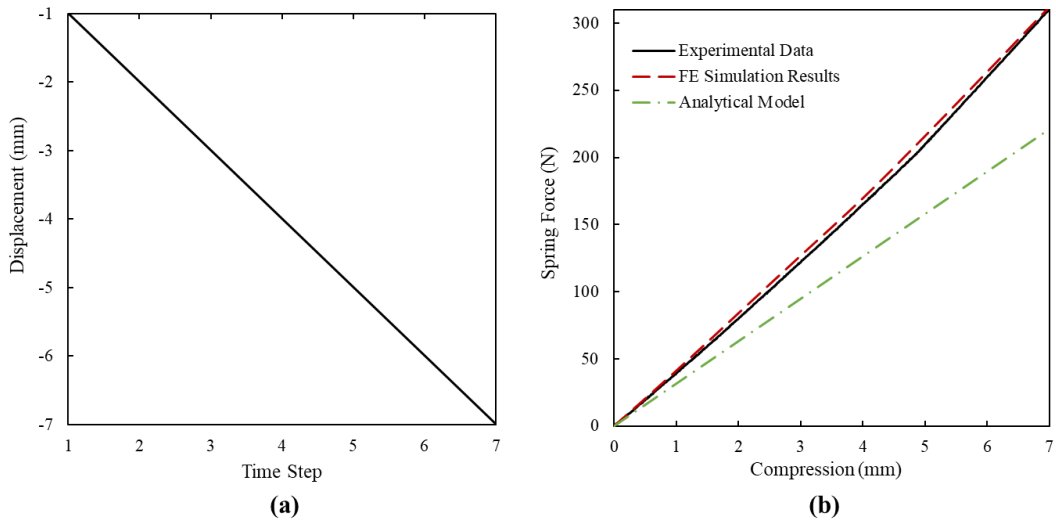


*Figure 5-3: (a). The input of a 7mm longitudinal displacement exerted on the face of the upper end of the beehive spring model. (b). Comparisons of spring forces were obtained from the experimental data, the FE spring model and the traditional analytical spring model.*

The difference between the analytical model and the FE model can also be explained by Figure 5-4 shows the spring status of the finite element simulation at 1mm, 3mm and 7mm compressions. The lowest two coils are initially separated at free length and then starts to contact each other at 1mm compression. As a result, the gradients of the force curves in Figure 5-3b are very close to each other. Then, the contact region begins growing under further compression, and the contact region at 3mm compression is shown in Figure 5-4b. This process leads to the FE simulation's spring forces increasing more sharply than that of the analytical model in Figure 5-3b. The contact region keeps growing as the spring compressed, and finally, nearly the whole surfaces of the lowest two coils are contacting each other at 7mm compression (Figure 5-4c). It makes the force curve of the FE model after 3mm compression grows farther away from that of the analytical model, as shown in Figure 5-3. More importantly, when comparing the simulated spring status in Figure 5-4a-c with the compressed springs in Figure 3-4b-d, it is found that the FE model precisely predicts the contact areas between the lowest two coils at different compressions. Hence, the FE model can precisely show the whole increasing process of the contact areas during the whole 7mm compression process.

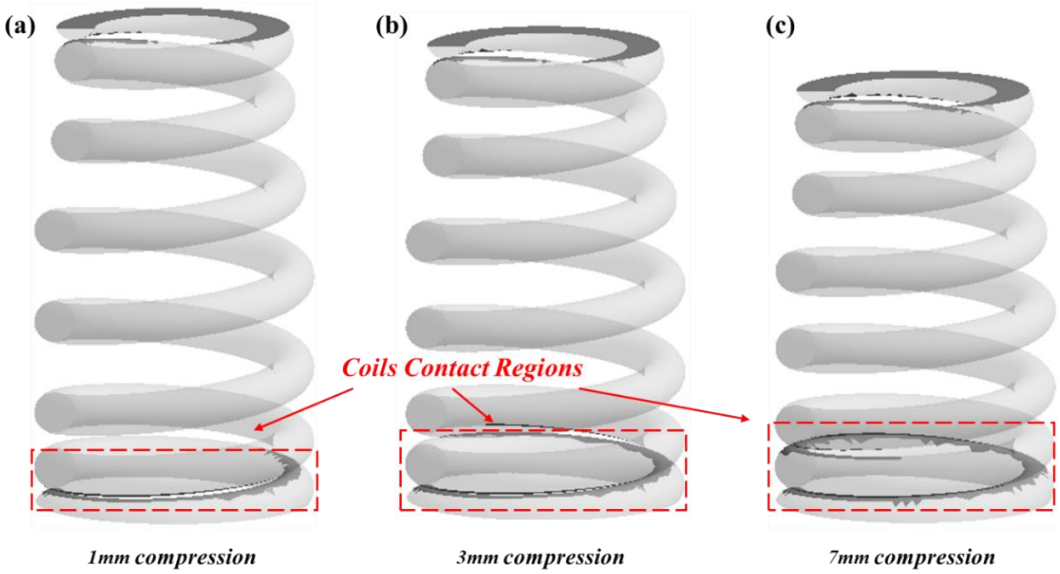


*Figure 5-4: The coil contact status of the beehive spring at (a). 1mm compression, (b). 3mm compression and (c). 7mm compression simulated by the FE model.*

In conclusion, the increase of contact region results in the reduction of the number of active coils *Na*, which then increases the stiffness of the spring. In other words, the results of the FE model, which involves the effects of coils contact, is closer to the experimental data. On the contrary, the traditional analytical model that neglects coil contact effects fails to simulate the spring when the spring pitch is narrow and coils contact with others.

## 5.4 Modal Finite Element Simulations

It has been widely known that the natural frequency of a helical spring is of extreme importance in analysing dynamic behaviours. It is because the magnitude of the spring surge is usually directly related to the spring's natural frequency. In addition, accurate estimation of the natural frequency can also contribute to estimating the internal damping of a helical spring (Liu and Kim, 2011). Traditional analytical models for

estimating natural frequency are commonly derived from Eq.(2.40), which relies on an accurate estimation of spring stiffness. However, as stated in the previous section, the traditional formula for estimating spring stiffness performs badly when the studied spring contains nonlinear properties, for instance, narrow pitch and varied coil diameter. Therefore, a modal spring model based on the finite element method is developed in this study. The same geometric model and meshing strategy as shown in Figure 5-2 are adopted in this section. Differently, both surface A and surface B are defined as 'fixed' at every loading step. The 'frictionless self-contact' condition is still applied on the surfaces of all the spring coils. Then, the modal finite element simulation is implemented in Ansys. Figure 5-5a displays the sensitivity study of the element size to the simuated first order natural frequency. It shows the results have converged when the element size is smaller than 1mm. In addition, the simulated first order natural frequency result (at 1mm) is also compared with 13 beehive spring samples as shown in Figure 5-5b. It can be seen that the FE result is around the average experimental results, and especially very close to the experimental results of the beehive spring sample used in this study.

The results of the first three modal modes of the beehive spring are shown in Figure 5-6a-c, respectively, together with the theoretical first three modal modes of a normal helical spring (Schamel et al., 1993, Schamel, 1993, Phlips et al., 1989) in Figure 5-6d. It shows at the first mode (Figure 5-6a) that the phase motion of the entire spring is towards the same spring end, and the central part has the largest amplitude. In the second mode (Figure 5-6b), the spring's upper and lower portion of the spring move in antiphase and squeeze the central portions. In the third mode (Figure 5-6c), the central portion and the upper portion move towards each other when the lower portion moves towards the lower end of the spring. It can be seen that the simulated motions of spring coils in

all three modal modes agree well with those of the theoretical description. The simulated natural fruencies for the first, second and third modes are 630 Hz, 1120 Hz and 1639 Hz respectively.

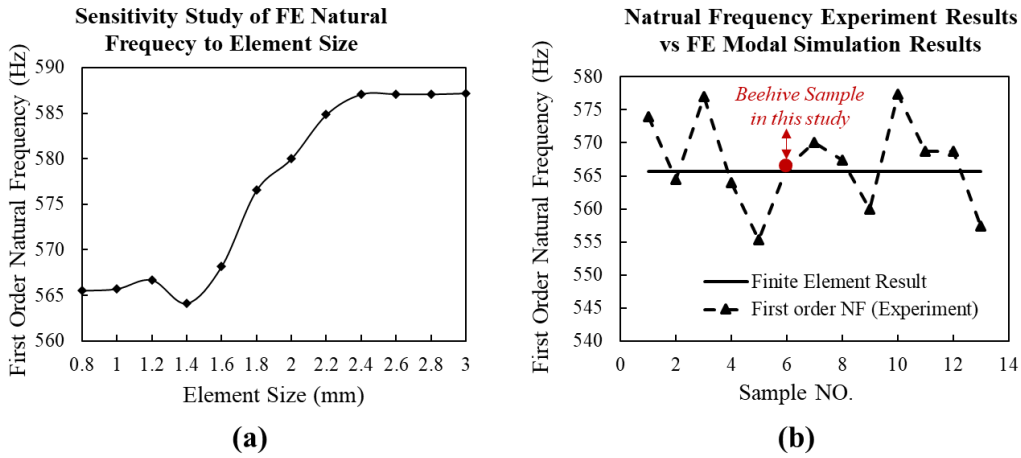


*Figure 5-5: (a). Sensitiviy sudy of element sizes to the FE natural frequency results. (b). Comparison between natural frequency experimental results and the FE simulation results.*

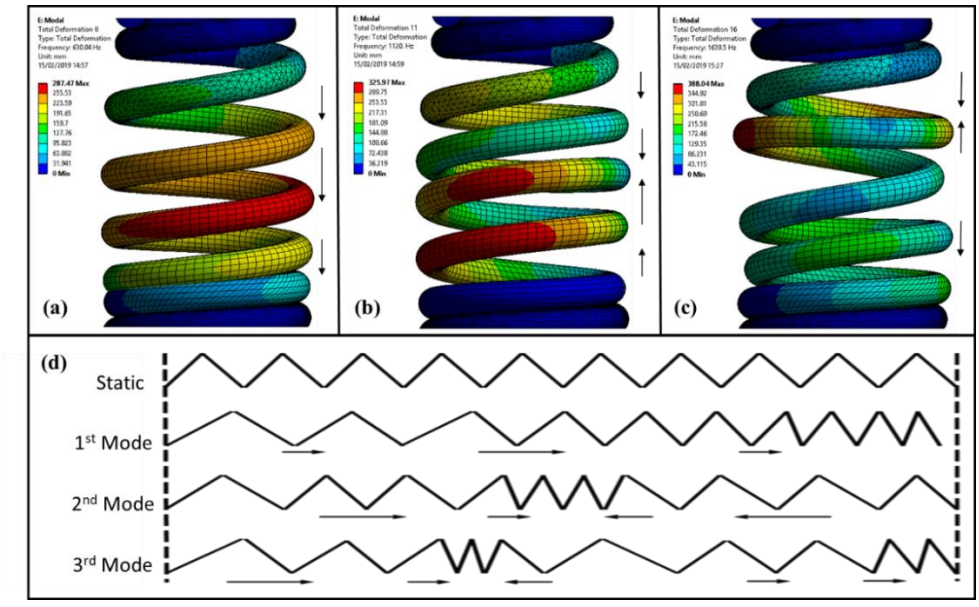


*Figure 5-6: The simulated (a). First. (b). Second, and (c). Third modal modes in Ansys FE Modal Analysis. (d). the theoretical first three modal modes described in (Schamel et al., 1993, Schamel, 1993, Phlips et al., 1989).*

## 5.5 Results comparison between the analytical model, the developed analytical model and the FE model

The results of the static FE model, the compression test and the traditional spring formulas are compared in Figure 5-3. In this section, the analytical results for estimating the compression force of the beehive spring by the traditional formula and the proposed formulas considering varied spring pitch only, of the varied coil diameter and both varied pitch and coil diameter are added in Figure 5-7. There is a significant departure between the result based on the traditional spring formula, the FE model results, and the developed spring formulas. Specifically, the traditional spring formula estimates around 210N spring forces at 7mm compression, while the FE and testing results are around 312N at the same compression. In addition, the FE results confirm the previous finding that the nonlinear geometries, or the variable coil diameter and varied pitch, shrink the contact areas of coils, and therefore these closed coils make the spring stiffer. As a result, the developed FE model can accurately estimate the spring force at each loading step, while the traditional formulas always estimate a smaller spring force of the beehive spring.

The developed spring formulas that consider the varied pitch estimate the spring force is only around 270N at 7mm compression. It is slightly smaller than the experimental and FE results but is significantly larger than the results of the traditional spring formula. Similarly, the developed spring formula considering only the varied coil diameter estimates an around 280N spring force at 7mm compression, which is slightly larger than the results by only considering varied pitches. It is noted that this curve has a good agreement with the experimental and FE results before 5mm compression, but a worse agreement at between 5mm and 7mm compression. Therefore, it can be concluded that the spring formulas by considering only a single nonlinear parameter

cannot perform as well as the FE model does. This phenomenon can be explained by Figure 5-8, which is the zoom-in area of Figure 5-7 between 5mm and 7mm compression. A big portion of coils with narrow pitch collapses into each other after 5mm compression, and then these coils turn into closed coils. This change reduces the actual number of active coils, which eventually makes the spring stiffer and the experimental and FE curve slope larger. However, the spring formulas cannot predict this effect by only considering a single nonlinear parameter, either varied coil diameter or coil contact.

On the contrary, the FE model shows a good agreement with the results of the developed spring formula, which considers the effects of both varied coil diameter and coil contact. They both estimate an approximate 314N spring force at 7mm compression, which fits well with the experimental data. Besides, the FE model shows an excellent agreement with the developed spring formula that considers both nonlinear parameters in the whole compression process. Therefore, it is proved that the FE model can accurately predict the spring force within the whole compression process. Besides, by comparing with the developed spring formulas and experimental data, it is found that the effects of both the varied coil diameter and coil contact should be considered for an accurate prediction of spring forces of the nonlinear beehive spring. Thus, the FE model can handle the nonlinear geometry of a helical spring by representing it into a 3D geometry and then meshed to simulate the spring force, which is of excellent efficiency.

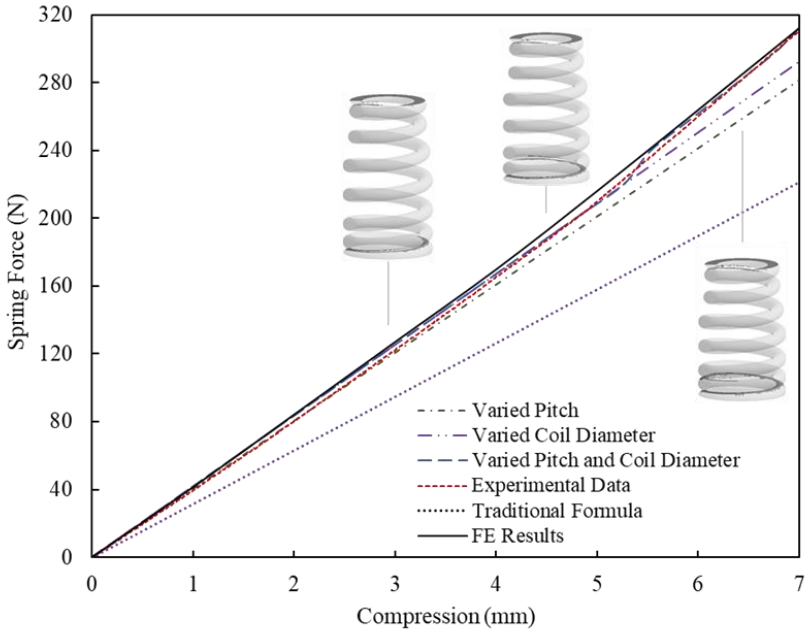


*Figure 5-7: Spring force curves under a 7mm compression based on experimental data, FE analysis, traditional spring formula and proposed analytical models considering varied pitch and varied coil diameter.*

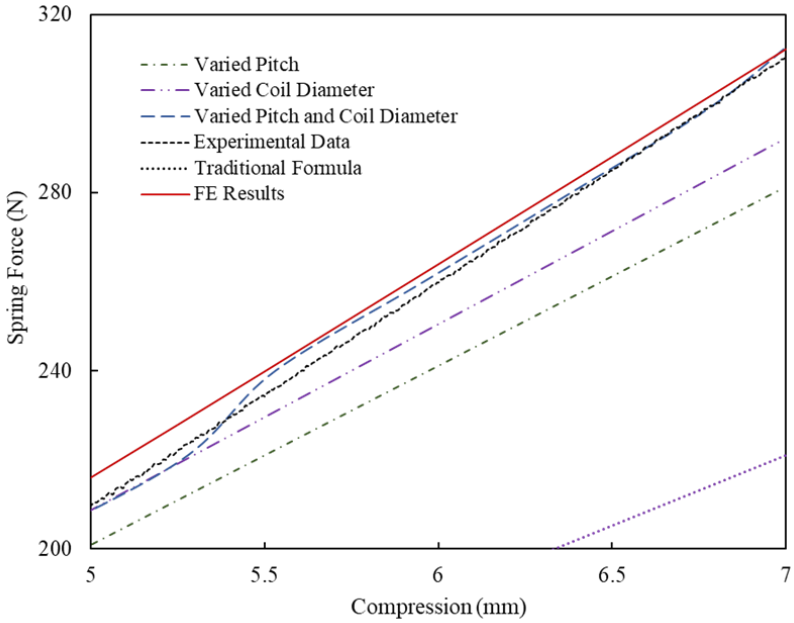


*Figure 5-8: Spring force curves under a 7mm compression based on experimental data, FE analysis, traditional spring formula and proposed analytical models considering varied pitch and varied coil diameter. (Zoom in the area between 5mm and 7mm compression)*

## 5.6 Summary

In this chapter, a static FE spring model is developed for the beehive valve spring by using a geometry model based on the 3D scan data. The boundary conditions are defined according to the real working conditions of the beehive spring in the valve-train mechanism. The loading applied on the FE model is a 7mm longitudinal compression which provides an install height of the spring in the engine. The simulated result is compared with the results of the traditional spring formula and the compression test. The comparison shows that the FE results have a good agreement with the experimental data, while the result of the traditional spring formula fails to. Furthermore, all the results are compared with the results of the developed spring formulas in the previous chapter. It can be concluded that the FE model can very well fit the experimental data as it considers all the geometric nonlinearities. On the other hand, when considering only a single nonlinear parameter in the spring geometry (only varied pitch or only varied coil diameter), the developed spring formula cannot accurately predict the spring force. However, the developed spring formula can accurately predict the compressive spring force at each loading step by considering the effects of both varied coil diameter and coil contact for the beehive spring. Thus, the FE model and the developed spring formula together explain how the varied coil and the coil contact affect the stiffness of the beehive spring during compression.

Besides predicting the spring force, the developed FE model is also used as a modal FE model to simulate the natural frequencies of the beehive spring. The simulated natural frequencies are essential parameters for the dynamic analytical model of helical spring developed in Section 4.2, and also build up the dynamic FE spring model developed in the following chapter.

# 6 Dynamic FE Analysis of Helical Springs

The FE spring model and static FE analysis are developed in the last chapter. The static FE model is simulated by applying 7mm compression, and the results are compared with experimental data and analytical results. However, as demonstrated in the literature, the static spring models are not applicable for simulating the dynamic spring response under high-speed loadings. Also, the significant dynamic spring force can be observed in the results of the engine head test, as shown in Chapter 3. In this chapter, a dynamic FE spring model is developed based on the same spring geometry as in the last chapter. Various high-speed loadings are applied to the FE model, and the results are compared with the experimental results and the dynamic analytical results. Based on the results of the simulations, the significant dynamic spring forces are explained.

## 6.1 Analysis Settings

For helical springs running in high-speed operations, for instance, valve springs, the static finite element analysis and modal finite element analysis cannot describe phenomena like spring surge and coil clash. Therefore, a dynamic finite element spring model is proposed in this study to describe the dynamic response of the beehive spring. The geometric model of the spring is used as the same as the one used for generating the static finite element model in section 5.3. In the real engine, the valve spring is mounted on the valve seat by one end, and the other end is covered by a spring retainer actuated by the cam. Hence, two solid bodies are added to the spring model, and the whole finite element model is shown in Figure 6-1(a). In the figure, the solid bodies

bonded with the upper-end face (Figure 6-1(b)) and the lower end face (Figure 6-1(c)) of the spring are the spring retainer and the valve seat, respectively. The lower surface of the valve seat is fixed on the ground, and the input is applied to the upper surface of the spring retainer. Besides, all the surfaces of the spring coils are defined by 'frictionless self-contact' to each other, as did in the static finite element spring model. This 'frictionless self-contact' condition allows the contacts between different elements. In other words, it enables the FE model to simulate the coil clash effects during dynamic simulations. Moverover, as 'transient' method is used in the dynamic FE model, the effects of velocities and accelerations of elements are considered. As a result, impact between coils is also included when the accelerations of coils are large.

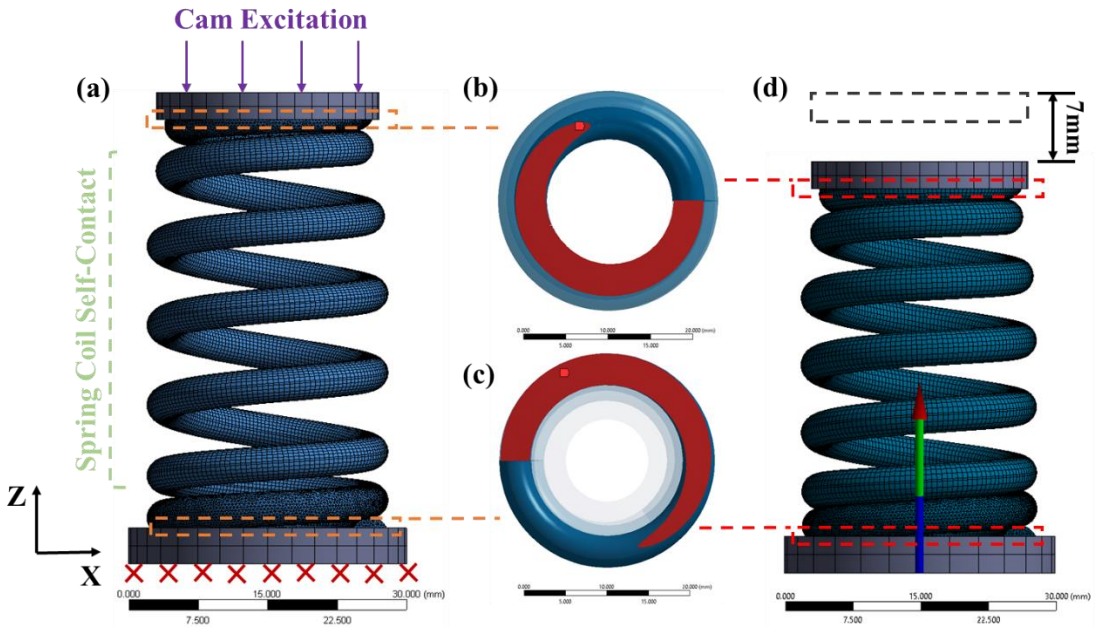


*Figure 6-1: (a). Boundary conditions of Modal FE model, and the fixed (b). the upper end and (c). the lower end of the spring. (d). The FE model with a 7mm pre-compression.*

The beehive spring is pre-compressed by 7mm to be installed into the valve train in the real engine. Therefore, the spring model is first compressed statically by 7mm before

conducting the dynamic simulation, as shown in Figure 6-1(d). This pre-compression is essential and cannot be neglected. Since it generates an extra static force that should be added into the overall dynamic force, it makes the lowest two coils of the spring closed so that the spring stiffness and, therefore, the spring's natural frequency becomes larger. Eventually, the pre-compressed spring model (Figure 6-1(d)) is used to implement the dynamic finite element simulation. As the cam profile directly actuates the spring retainer, the valve lift caused by the cam's rotation is the direct input on the spring retainer's upper surface, as shown in Figure 6-1(a). The input curve of the valve lift is shown in Figure 6-2. The valve lift curve can be divided into three stages: Stage I, Stage II and Stage III, which reflects the real profile of the cam. At Stage I, the cam starts to rotate but does not press the valve and the spring retainer until it rotates by around 90 degrees from where it presses the valve slightly by 1mm. Then, the cam continues rotating at Stage II, but it starts to push the valve significantly, and at 180 cam degrees, the valve lift reaches the maximum value of 11mm. After 180 cam degrees, the valve lift goes rapidly back to 1mm. Finally, the valve lift gradually drops from 1mm displacement to zero and remains unchanged until the next cam rotation cycle.

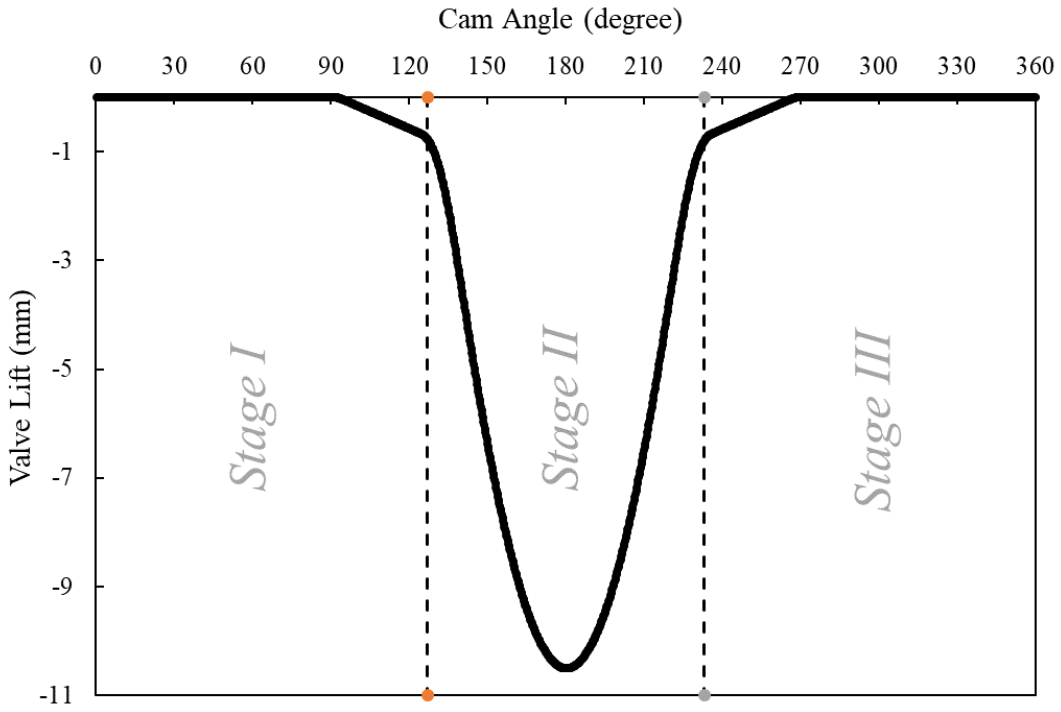


*Figure 6-2: Valve lift curve of the beehive valve spring in the real engine.*

In this finite element analysis, the internal damping (material and structure) of the spring is defined by the Rayleigh Damping method, which can be expressed by $\xi = \alpha/(2\omega_i) + \beta\omega_i/2$ where α and β are the Rayleigh coefficients that can be calculated by knowing the damping ratio ξ and the natural frequency $\omega_i$. In this study, the natural frequencies of the first three modes of the beehive spring are obtained from the modal finite element model in the previous section, and the values of them are 630Hz, 1120Hz and 1639Hz, respectively. The damping ratio is assumed to have the value of 0.016 empirically, which have been widely proved effective (Phlips et al., 1989, Kim and David, 1990, Liu and Kim, 2011).

In the analysis, one cam cycle is divided into 72 time steps, each of which is further averagely divided into 10 sub-steps. Hence, there are in total 720 sub-steps for an entire cam cycle. The dynamic finite element spring model is simulated under three different

engine speeds, namely 4200-rpm, 5600-rpm and 8000-rpm, of which the corresponding cam speeds and the time of each step are listed in Table 6-1. For each engine speed, two continuous cam cycles are simulated. However, only the results of the second cam cycle for each engine speed is analysed and compared.

The explanation for abandoning the first cam cycle is shown in Figure 6-3, which depicts typical dynamic spring force curves for two continuous cam cycles at 4200-rpm engine speed. It shows that the spring always starts from a stationary state at Stage I of Cycle I before being activated by the loading. However, at Stage I of Cycle II, the initial status of the spring is dominated by a residual vibration. It is because that the spring vibration cannot be fully dispersed at the end of Stage III of Cycle I. Therefore, only the second cam cycle (Cycle II) represents the real working status of a valve spring under dynamic loading. In this study, the simulation results of dynamic spring reaction forces generated on the upper surface of the valve seat at every engine speed are extracted. In addition, the nodes located at the centre of the cross-section of both the ends of coil 01 and coil 02 are named Node 01 and Node 02, respectively. The displacements, velocities and accelerations of Node 01 and Node 02 are obtained from the dynamic simulations to analyse the internal vibration of the spring and the effects of coil collision.

*Table 6-1: The engine speeds, cam speeds, time of each analysis step and time of each sub-step for the transient FE simulation*

| Engine Speed (rpm) | Cam Speed (rpm) | Time of each step (s) | Time of sub-step (s) |
|---|---|---|---|
| 4200 | 2100 | 396.8e-6 | 39.68e-6 |
| 5600 | 2800 | 297.6e-6 | 29.76e-6 |
| 8000 | 4000 | 208.3e-6 | 20.83e-6 |

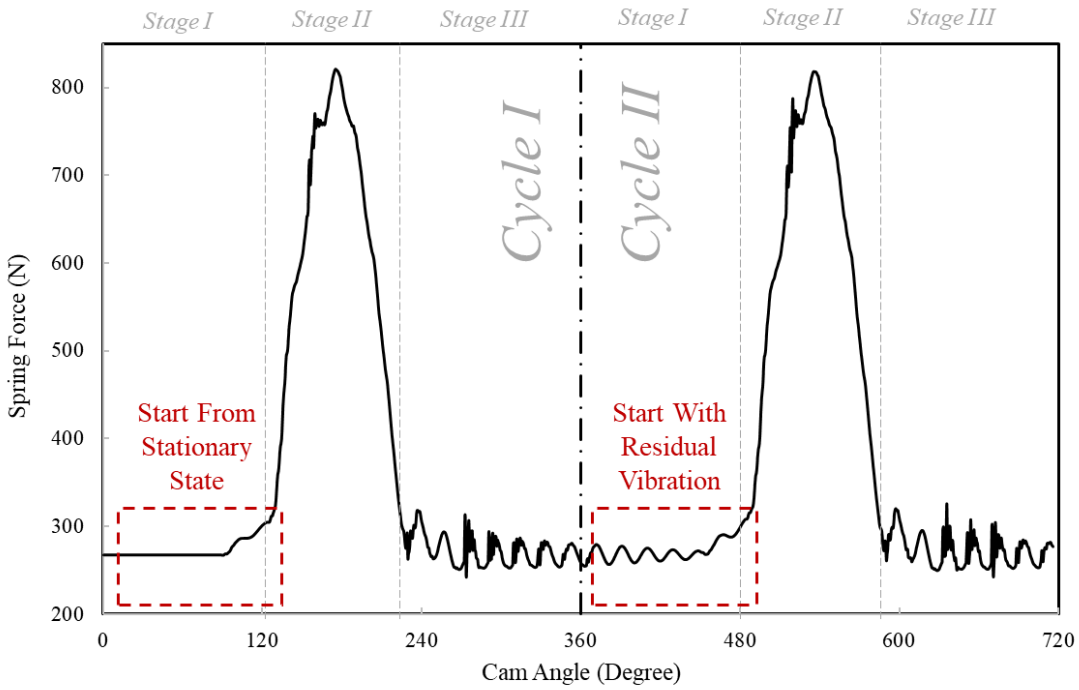


*Figure 6-3: A typical load and displacement relationship at engine speed: 4200-rpm*

## 6.2 Dynamic Spring Response at 4200-rpm Engine Speed

The dynamic spring model is firstly simulated at 4200-rpm engine speed, and the result of the spring force is plotted in Figure 6-4. Besides, the dynamic spring force at 4200-rpm of experimental data and analytical results are also shown in Figure 6-4 to compare with the finite element results. It is seen that the spring force oscillates over a range of 12N (from 270N to 282N) at stage I, which is a free vibration due to the residual energy from the previous cam cycle. With the rotation of the cam, the spring starts to be compressed by a large valve lift (Stage II) when the cam angle is 127 degrees. After that, the reaction force increases significantly until the cam angle is around 183 degrees, where peak forces are obtained. The magnitudes are 818N, 814N and 806N for the FE model, analytical model and experiment, respectively. Then, the reaction force decreases until the cam angle reaches 233 degrees (the end of Stage II). In general, both

the FE and the analytical models can describe the dynamic response of the spring with good agreement to the test results. However, according to the test results, there are high-frequency vibrations when the cam angle is around 235 degrees due to the internal contact of spring coils. As shown in Figure 6-4, the FE model can simulate this phenomenon, while the analytical model does not provide adequate detail of the occurrence.

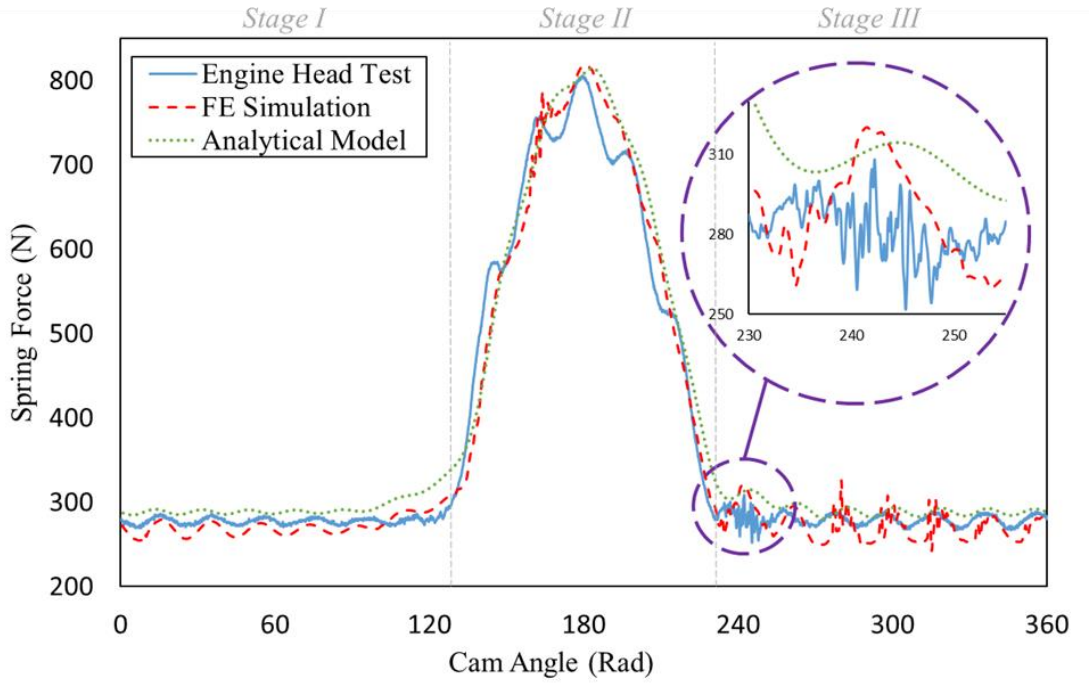


*Figure 6-4: Dynamic spring force curves of engine head test, FE simulation and analytical model at 4200-rpm engine speed.*

For analysing the internal motion of the spring coils, the simulation results of the two reference nodes: Node 01 and Node 02 are marked in the model. The accelerations, velocities and displacements of the nodes along the Z-axis at 4200-rpm are given in Figure 6-5. It is noteworthy that the displacement of Node 02 is obtained by recording the co-ordinate positions of Node 02, where the distance between coil 01 and coil 02 at all cam angles has been subtracted. Therefore, a zero value of it indicates that coil 02 is touching coil 01. Within the cycle, the displacement of Node 01 (Figure 6-5(a)) is

almost constant and close to zero, which means that coil 01 experiences no significant longitudinal motion. Node 02 (Figure 6-5(a)) oscillates freely at the beginning of stage I due to the residual vibrations from Cycle I. At the end of stage I, the effect of free vibration reduces due to the effects of damping and the compression of the external loading. At the beginning of Stage II, the compressive displacement is 0.07 mm, when coil 02 contacts coil 01. Both coils 01 and 02 deform elastically, which explains that the negative values in this stage. During Stage III, Node 02 starts to vibrate freely under a certain frequency.

As shown in Figure 6-5(b), the velocity of Node 01 keeps constant in the entire cam cycle, which shows that coil 01 does not move. For Node 02, its velocity varies slightly during Stage I and Stage II. It indicates that coil 02 moves due to the residual vibration at stage I and oscillates with a higher frequency due to the contact with coil 01. At Stage III, the velocity of Node 02 changes rapidly. The points of these rapid changes are also the ones where the displacement of Node 02 changes significantly (Figure 6-5(a)). The acceleration responses of Node 01 and Node 02 are presented in Figure 6-5(c). The acceleration of Node 01 keeps at a very low level during Stages I and II, although there are fluctuations around 140 degrees and 160 degrees. During Stage III, the acceleration varies at a higher level. The fluctuations are around 280 degrees, 300 degrees and 315 degrees. The peak acceleration of Node 01 is approximate -4.24e6 mm/s2 occurred at 315.5 degrees of cam angle at Stage III. For Node 2, the trend is similar to Node 1. However, the magnitudes of the fluctuations are higher than those of Node 01. The peak acceleration, approximate 5.49e6 mm/s2, of Node 02 occurs at around 314 degrees at Stage III. The peak accelerations of both Node 02 and Node 01 are consequences of the rapid velocities changes, which are due to the coil collisions between coil 01 and coil 02.

According to the results of the FE simulation, it can be concluded that coil 02 vibrates freely at Stage I and Stage III. During Stage II, it is compressed to contact coil 01 by the external loading, and there is no separation between the two coils. During Stage III, the rapid changes in velocity and acceleration of Node 02 are also caused by the contact between coils 1 and 2, which could explain the high-frequency fluctuations of the spring force around 165 degrees, 235 degrees, 280 degrees, 300 degrees and 315 degrees of cam angle.

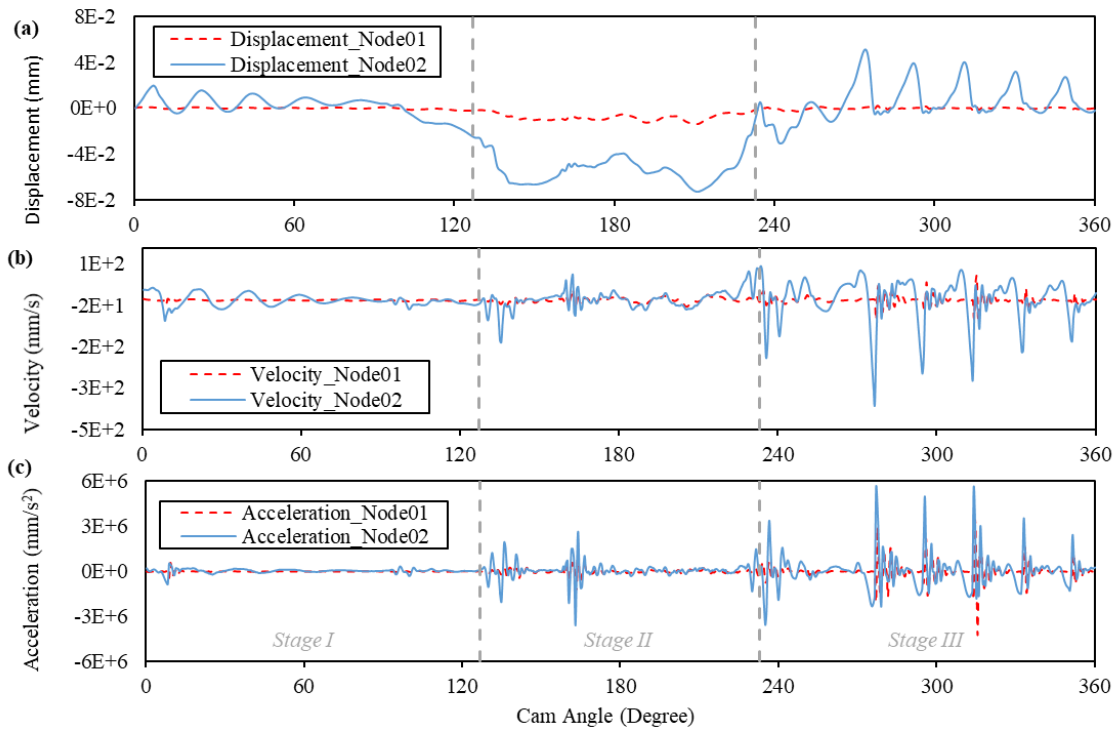


*Figure 6-5: (a). Displacements, (b). Velocities and (c). Accelerations of Node 01 and Node 02 along the Z-axis at 4200-rpm engine speed.*

## 6.3 Dynamic Spring Response at 5600-rpm Engine Speed

The results of the dynamic response of the valve spring are displayed in Figure 6-6. At Stage I, the spring force starts to oscillate between 250N and 350N, which is approximately 90 N larger than the one at 4200-rpm engine speed. Then, the spring is

compressed significantly at the beginning of Stage II (127 degrees of cam angle). The spring force increases until the cam angle is around 175 degrees, where the peak force is obtained. The magnitudes obtained from the FE model, the analytical model, and the experiment are 896N, 865N and 845N, respectively. It is clear that the peak forces in Stage II at 5600-rpm are about 60N higher on average than those at 4200-rpm. It means that the dynamic effects of both the natural vibration and the forced motion are greater due to the increase of engine speed. After 175 degrees of cam angle, the spring force decreases until the cam angle is 233 degrees (the end of Stage II). Finally, the loading starts to be removed at the beginning of Stage III, and the spring vibrates freely. However, high-frequency spring forces are detected in both the FE model and the experiment results around 240 degrees of cam angle, where the analytical model fails to show this. The maximum of these spike forces is as high as 620N, which is about 305N higher than that at 4200-rpm. The peak force obtained from the analytical model is 380N at this point of time.

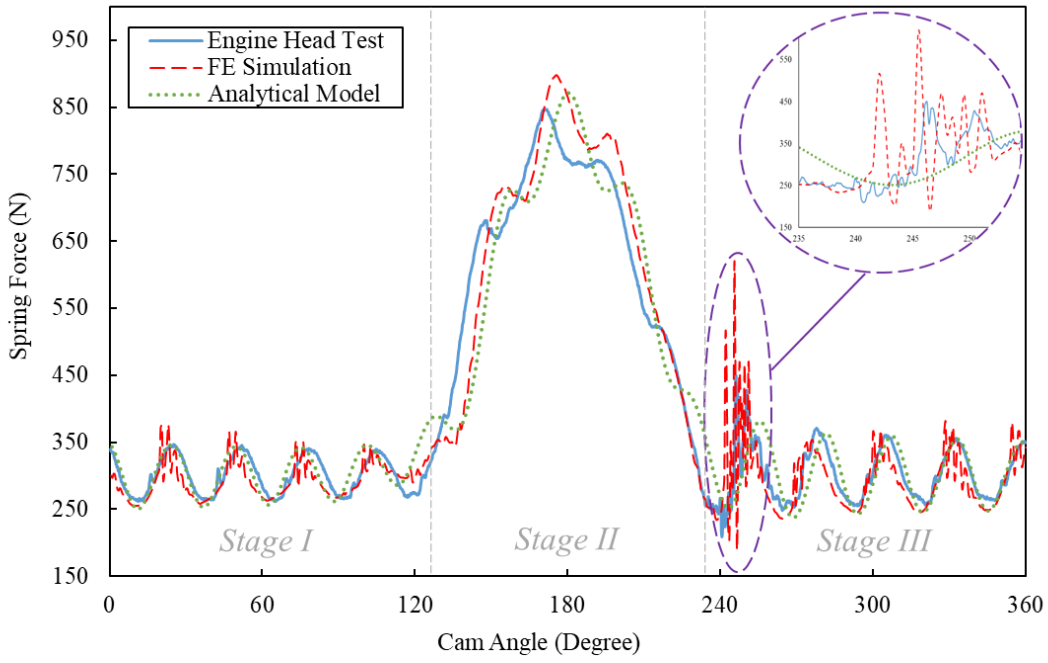


*Figure 6-6: Dynamic spring force curves of engine head test, FE simulation and analytical model at 5600-rpm engine speed*

The accelerations, velocities, and displacements of the reference nodes along the Z-axis at 5600-rpm are given in Figure 6-7. Similar to the results at 4200-rpm, the displacement of Node 01 keeps constant during the whole cam cycle in Figure 6-7(a) because the end of this coil is fixed. The displacement of Node 02 oscillates regularly during Stage I. It illustrates that coil two vibrates freely, starting with the residual vibration of the previous cam cycle. The magnitude of the displacement can reach as high as around 0.2 mm, which is nearly ten times the one at 4200-rpm. During Stage II, the displacement keeps nearly a constant. It is because coil 02 is pressed onto coil 01 by the external loading. At the beginning of Stage III, it starts to fluctuate at a high frequency.

As shown in Figure 6-7(b), the velocity of Node 01 is around zero during the whole cam cycle, which is corresponding to its constant displacement shown in Figure 6-7(a). On the other hand, the velocity of Node 02 fluctuates with a range of 1290N (from -742 mm/s to 548 mm/s) in Stage I. It is reduced, then, to zero during Stage II due to the external compressive loading. During Stage III, it reaches a peak velocity of 1352 N/mm at 241.5 degrees toward the negative direction of the Z-axis after a 1000 mm/s velocity toward the Z-axis. Then, it fluctuates with a range of 1598 mm/s (from -978 mm/s to 620 mm/s). The accelerations of Node 01 and Node 02 are displayed in Figure 6-7(c). The acceleration of Node 01 is nearly constant during Stage II while spike accelerations appear at 20 degrees, 46.5 degrees, 73 degrees, 100 degrees, around 245.5 degrees, 300 degrees, 328 degrees and 354.5 degrees, respectively, during Stage I and Stage III.

Another phenomenon is that the spike accelerations of Node 02 always appear at the same time. It means that coil collisions occur between coil 01 and 02 at those times. Contact status between coil 01 and coil 02 at three different cam angles is shown in

Figure 6-8. The areas where coil 02 contacts coil 01 are in pink. ‘Sliding’ indicates that there are transverse slides between contact surfaces. The yellow areas named ‘near’ indicate that coil 01 and 02 are close but still separated. From cam angle 240 degrees to 245.5 degrees, the two coils experience a contact-separation-contact process within a 0.327e-3 second. The process indicates a violent coil collision and explains the spike forces occurring at the time points.

Compared to the dynamic response at 4200-rpm, the spring force is generally higher due to the higher loading speed of 5600-rpm. The high-frequency fluctuations also appear at the beginning of Stage III. However, the spike forces are much higher than those at 4200-rpm, caused by the violent coil collisions.

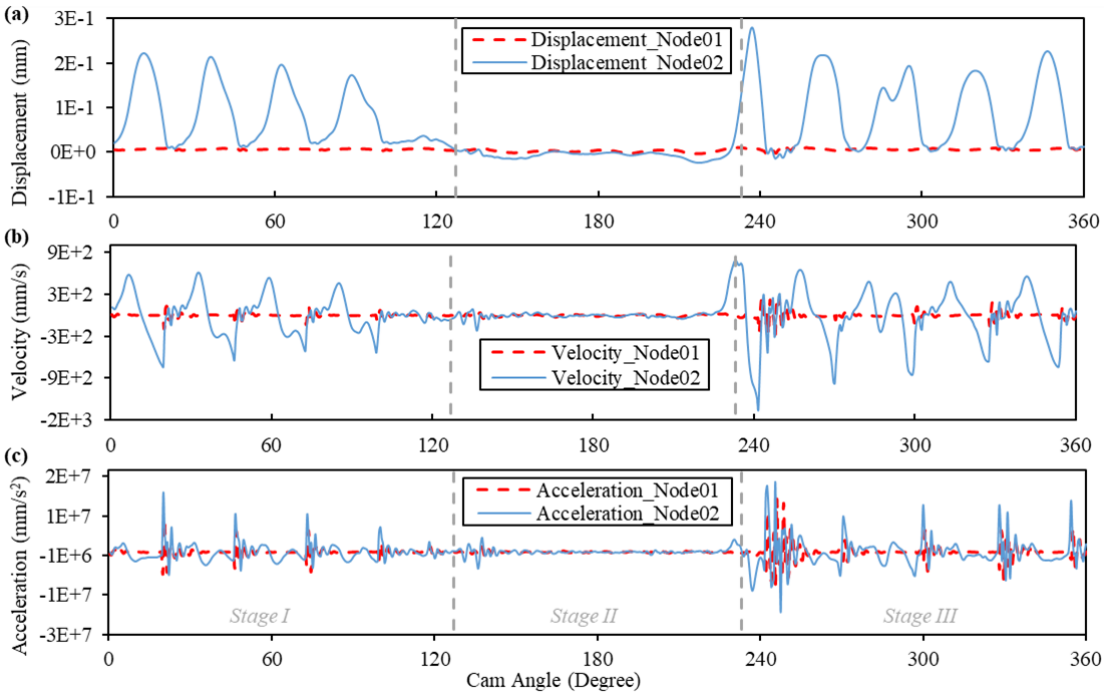


*Figure 6-7: Acceleration, velocity and deformation curves of Node 01, 02 and 03 at 5600-rpm engine speed.*

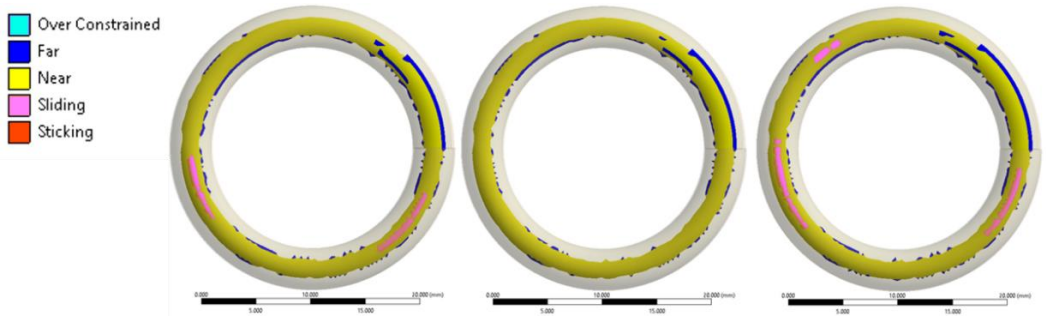


*Figure 6-8: Contact status of coil 1 and coil 2 at (a). 240 degree, (b). 243.5 degree and (c). 245.5 degrees under 5600-rpm engine speed.*

## 6.4 Dynamic Spring Response at 8000-rpm Engine Speed

Figure 6-9 shows the dynamic responses of the valve spring at 8000-rpm engine speed. The zoom-in area shown in Figure 6-10 displays a greater detail of Stage III, during which the peak forces occurred. At Stage I, the spring force oscillates at a range of 200N (between 250N and 450N), which is approximate 100N larger than the magnitude (100N) at 5600-rpm and 190N larger than the one (10N) at 4200-rpm engine speed. The frequencies of the vibration obtained from the FE model generally agree with the ones from experiments. However, a phase difference is observed in the result of the analytical model. For instance, the first three peak forces appear at 12.5 degrees, 42 degrees and 84.5 degrees from the FE model and test results, while they appear at 24 degrees, 58 degrees and 100 degrees in the analytical model. The phase difference is approximately 15 degrees.

When the spring is compressed at Stage II, the spring force increases to the first peak, around 940N in the FE model (895N from the test), at about 160 degrees of cam angle. However, the force curve of the analytical model reaches its peak force (880N) at 170 degrees of cam angle, thus, represents a phase lag of 10 degrees. With the rotation of the cam, the force decreases to around 580N in the FE model (581N from the test) at

approximately 172 degrees. When the cam angle is 186.5 degrees, the force increases again and reaches its second peak value, around 1200N in the FE model (1051N from the test). The second peak of the force based on the analytical model is 778N at 203 degrees, where the lag is 16.5 degrees compared with the FE model results and the experiment. After the second peak, the force decreases until 250N at the end of Stage II (233 degrees).

At Stage III, the change of the force is mainly dominated by a free vibration due to the low external loading. During this stage, very high spike forces are obtained. For instance, the spring force reaches as high as 1430N at 254.5 degrees from the FE model and the test results, which is even higher than the peak force in Stage II. However, the peak force calculated by the analytical model is only 360N when the cam angle is 270 degrees. The results show that the analytical model cannot simulate dynamic responses of the valve spring at a relatively high engine speed.

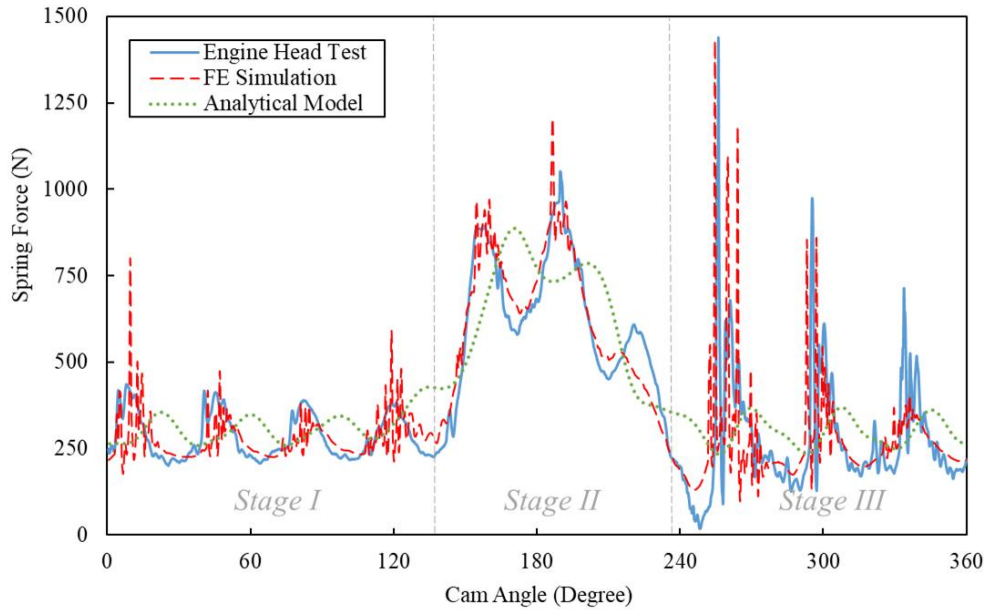


*Figure 6-9: Dynamic spring force curves of engine head test, FE simulation and analytical model at 8000-rpm engine speed.*

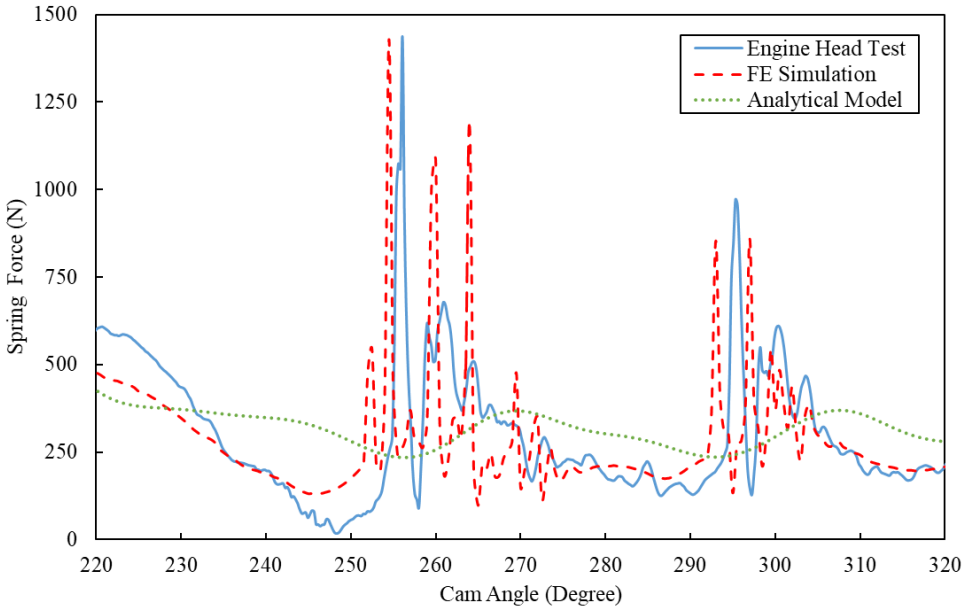


*Figure 6-10: Dynamic spring force curves of engine head test, FE simulation and analytical model at 8000-rpm engine speed between 220 degrees and 320 degrees cam angle.*

For understanding the internal vibrations of the spring at 8000-rpm engine speed, the accelerations, velocities and displacements of Node 01 and Node 02 are shown in Figure 6-11. At Stage I, the displacement of Node 01 (Figure 6-11(a)) remains constant and is close to 0 mm. The displacement of Node 02 (Figure 6-11(a)) oscillates in a range of 0.17 mm. Compared with the results at 4200-rpm and 5600-rpm, it appears more irregularly. At Stage II, there is nearly no movement when the external loading is executed. It illustrates that coil 02 is nearly compacted onto coil 01 despite very small vibrations at 155 degrees and 185 degrees.

At the end of Stage II (233 degrees), Node 02 begins to move upward. It reaches its maximum displacement of 0.68 mm when the cam angle is around 243 degrees (Stage III). It is about 0.4 mm and 0.63 mm higher than the magnitudes at 5600-rpm and 4200-rpm, respectively. Then, the force starts to oscillate irregularly. The velocities of Nodes 01 and 02 are displayed in Figure 6-11(b). The velocity of Node 01 remains nearly constant throughout the whole Stage I, II and III, though slight vibration was observed

at 270 degrees and 300 degrees in Stage III. For Node 02, the magnitude of velocity varies irregularly within 1320 mm/s at Stage I. It keeps nearly zero during Stage II except for two velocities fluctuations that occur at 155 degrees and 185 degrees. At the beginning of Stage III, the magnitude increases significantly from 0 mm/s (232 degrees) to 2130 mm/s (238.5 degrees) and then dramatically decreases by 4815 mm/s to -2685 mm/s at 251.5 degrees. With a further rotation of the cam (from 251.5 degrees to 252.5 degrees), the velocity increases rapidly again, which is from -2685 mm/s to 811 mm/s. This process occurs within 41.6e-6 seconds.

The magnitude varies arbitrarily during the rest of Stage III. Figure 6-11(c) shows the acceleration curves for Nodes 01 and 02. The acceleration of Node 01 has no obvious fluctuation in Stage I and Stage II. At stage III, there are some fluctuations where the peak values are 3.92e7 mm/s2, 1.53e7 mm/s2 and 3.07e7 mm/s2 at 254.5 degree and 297 degree, respectively. For Node 2, the fluctuations in Stage I and Stage II are lower than those in Stage III. When the cam angle is 254.5 degrees, the acceleration reaches its maximum of 1.03e8 mm/s2, corresponding to the peak spring force simultaneously. In addition, significant spike forces (Figure 6-9) also occur at these positions (254.5 degrees and 297 degrees). Therefore, it can be assumed that violent coil collisions occur between coil 01 and coil 02 at these times. The dynamic spring force is hugely lifted by these impact forces, which are shown by the significant spike forces in the final results.

Contact status between coil 01 and coil 02 at 8000-rpm is shown in Figure 6-12. It is shown that a contact-separation-contact process occurs when the cam angle increases from 253.5 degrees to 255.5 degrees. The process occurs within 0.0832e-3 seconds. The violent coil collision explains the spike spring force at 254.5 degrees. At 8000-rpm engine speed, the effects of coil collision on the spike forces are enhanced. The peak

force of the spring occurs during Stage III due to the coil collision rather than external loading. The results of modal analyses do not show the spike forces caused by coil collisions, and a certain phase difference is observed in the whole cam cycle. In sum, it shows that the FE model has a robust ability to simulate the dynamic effects of valve springs at this speed with a good agreement with the test results. On the contrary, the analytical modal model fails to be comparable with the test results at this speed.

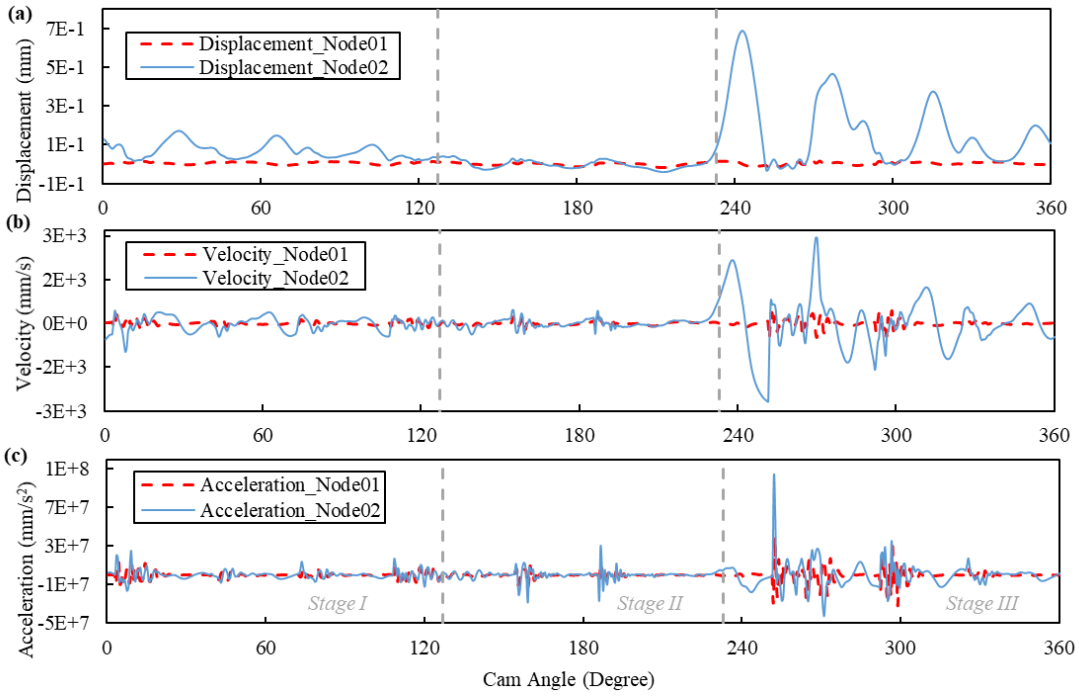


*Figure 6-11: Acceleration, velocity and deformation curves of Node 01, 02 and 03 at 8000-rpm engine speed.*

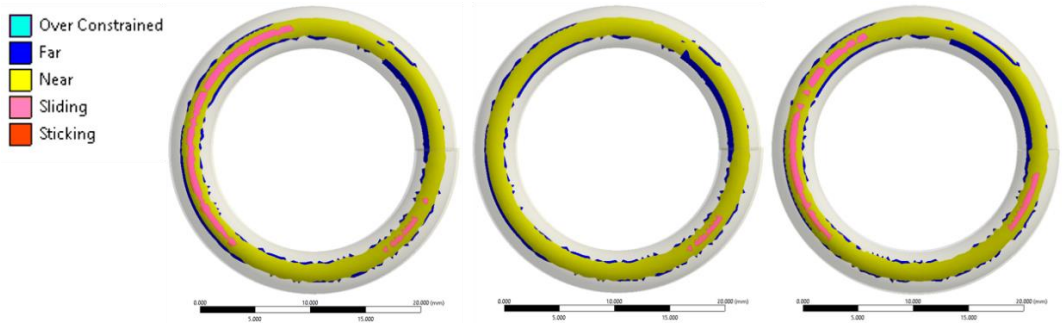


*Figure 6-12: Contact status of coil 1 and coil 2 at (a). 253.5 degree, (b). 254.5 degree and (c). 255.5 degrees under 8000-rpm engine speed.*

## 6.5 Summary

In this chapter, a dynamic FE model is developed to simulate the nonlinear dynamic response of the beehive valve spring at various engine speeds. Large deformations, varied spring diameter, varied spring pitch and therefore varied natural frequency, coil collisions are all considered in this model. The analytical spring model developed in the previous chapter is used to compare with the finite element model. A set of engine head test results was used to validate the computational results of both models. According to the analysis of the results, the main findings are made:

1. By comparing with engine test results, both the finite element model and the analytical models are able to simulate the reaction force of the spring at Stage II of the deformation when the engine speed is relatively low (4200-rpm). At this speed, the reaction force results from both the external loading and the internal vibrations of the coils. However, the finite element model can also simulate the high-frequency vibrations at the beginning of Stage III when the analytical model fails.

2. At relative higher engine speeds (5600-rpm), the external loading and natural frequency determine the peak reaction force. Both the analytical and finite element models can calculate the peak reaction force at Stage II accurately. However, the effects of coil collision become more significant with the increased engine speed. The unusual spike forces are observed at stage III of the deformation in both the finite element model and the testing results. Again, the analytical model cannot analyse the effects due to its intrinsic limitations.

3. At 8000-rpm engine speed, the peak dynamic force occurs at stage III of the deformation due to the dominating effect of coil collisions. The high-frequency contact force between the coils results in the extreme high spike reaction force absent from the

analytical model. In practice, the analytical model is still widely used in the design and analysis of valve springs. Therefore, the dynamic factor of the spring is likely to be underestimated by the analytical model, which may cause premature failure of the valve spring. For a more reliable spring design, the new finite element model developed in this paper can be used to predict the reaction forces at different engine speeds, including extreme high speeds.

# 7 Spring Design Method Based on Machine Learning Techniques

Helical spring, a common form of mechanical springs, is an essential component in many engineering applications such as vehicle suspension systems and valve train mechanisms. When the spring is serving in internal combustion (IC) engines, it is designed and called a valve spring. As the most flexible component in the valve train mechanism, valve springs should guarantee valves' precise and high-efficient return motions. Generally, a valve spring works in a high-speed status and sometimes bears high material stress. Therefore, poor designs of valve springs can lead to serving spring damage and malfunction of the engine. Good designs, on the contrary, can bring many benefits, for instance, high spring strength and low fuel consumption. The same problem also exists in other engineering applications with helical springs. For instance, a poor design of vehicle suspension spring could result in the spring vibrating in an undesired frequency and, therefore, extreme discomfort of passengers. Therefore, an increased interest in allowing better designs to meet these requirements is raised.

Traditional designs and optimizations of helical springs are usually based on theoretical and empirical equations that have been proposed for around a decade. The most commonly employed equations are the ones developed by Wahl (1944) for calculating the spring stiffness by Eq.(2.23), the first-order natural frequency by Eq.(2.40) and the maximum shear stress by Eq.(2.20), of which the details are also illustrated in the section of Elementary Theory of Helical Springs. These theoretical equations are available to implement the optimal design on helical springs. However, all these equations were proposed based on linear assumptions. For example, one

essential assumption is that the pitch angle is considered small, and another assumption is that the spring index D/d is assumed small. Besides, the accuracy of counting the number of active coils $N_a$ can significantly affect the accuracy of the analytical solutions. In fact, these assumptions make the design domain of helical springs very restricted. Generally, the current traditional design and optimization methods usually involve three simple categories of helical springs, and they are the standard type (Figure 3-2(a)), the conical type (Figure 3-2(b)) and the beehive type (Figure 3-2(c)). These helical springs possess linear geometry properties and linear variations of geometry properties. However, it has been proved in the research of Gu et al. (2020) that some inaccuracies can be introduced when formulating helical springs by these linear theories. Especially, the actual magnitude of spring forces can be three times larger than that calculated by the analytical model based on these linear spring theories.

In short, the linear empirical and theoretical equations for helical spring's designs are unable to describe the realistic nonlinear spring properties, which makes the mechanical properties of helical springs unrealistic. It is therefore urgent to develop a feasible approach for conducting designs and analysis on nonlinear helical springs. In this chapter, the finite element spring model is applied to generate numerical spring samples. In order to satisfy the requirement of sample numbers, an innovative DoE (Design of Experiments) technique cLHS (constrained Latin Hypercube Sampling) method that is more flexible than the normal LHS is also employed to generate design points for FE simulation. Furthermore, compression tests are conducted on the real manufactured spring part to validate the results of both FE simulations and the models based on GP. Finally, a sensitivity study for investigating the relationship between the geometric parameters of helical springs and their corresponding spring properties are also conducted.

## 7.1 Sampling Techniques

Sampling, which is usually used in statistics, quality assurance, and survey methodology, always refers to the techniques for selecting a subset of individuals from a statistical population and then estimating the characteristics of the whole population. The advantages of sampling lie in the low labour cost and the efficiency of data collection. It is extremely suitable for the cases in this study as for a helical spring, the amount of potential shapes in the whole design domain is infinite. Therefore, it becomes essential to employ sampling techniques to generate finite samples that can represent the characteristics of the infinite design domain. Every sample in the design domain should have its own unique features, which are called parameters. Therefore, the common method for selecting samples is first to define and select each sample's parameters.

In this study, a parametric model of spring geometry is developed to define geometric parameters on helical springs. First, the basic geometric model of the beehive spring is developed, and the detail is illustrated in the previous Chapter. Then, ten parameters are selected based on the spring geometry, as shown in Figure 7-1. They are P1, P2, P3, P4, P5, which are the pitches of coil 02, 03, 04, 05, 06 respectively, and P6, P7, P8, P9, P10, which are the diameter of coil 02, 03, 04, 05, 06 respectively. As a result, the ten parameters can be varied in the parametric spring model to generate various types of helical springs.

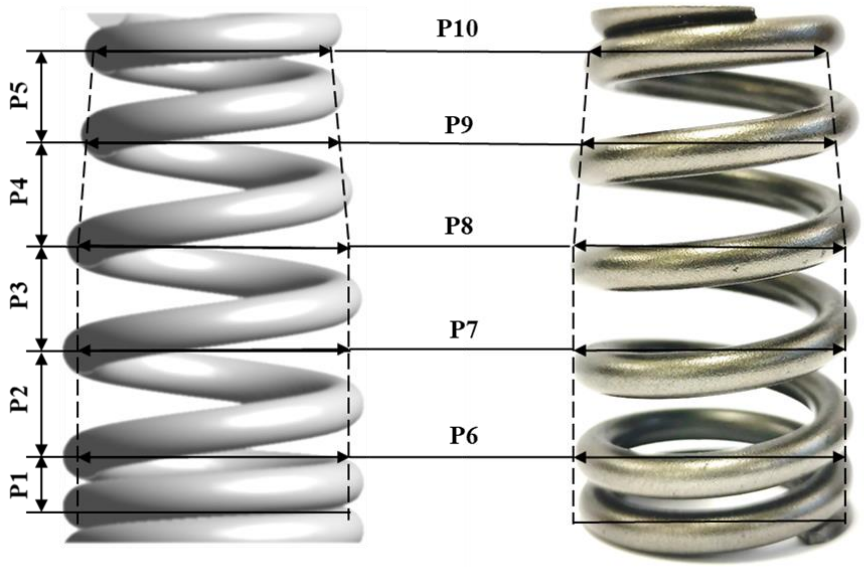


*Figure 7-1: Ten selected geometric parameters on the helical spring model and the beehive spring sample.*

### 7.1.1. Latin Hypercube sampling

The variable ranges for the ten selected geometric parameters are listed in Table 7-1, together with their default values for the original beehive spring sample. The whole design domain, in this case, is formed of these variable ranges. The geometry of the spring samples will be random combinations of arbitrary values of these parameters. Therefore, a good selection of spring samples can be more representative of the whole design domain. However, too many spring samples may bring more labour efforts and longer computing time.

*Table 7-1: Notations and ranges of the ten design parameters.*

| Name | Lower Bound | Upper Bound | Default Value (Beehive Spring) | Parameter |
|---|---|---|---|---|
| **P1** | 4 | 6 | 5.419 | Pitch of Coil 02 |
| **P2** | 7.5 | 9.5 | 8.777 | Pitch of Coil 03 |
| **P3** | 7.5 | 9.5 | 8.817 | Pitch of Coil 04 |
| **P4** | 7.5 | 9.5 | 8.622 | Pitch of Coil 05 |
| **P5** | 6.5 | 8.5 | 7.64 | Pitch of Coil 06 |
| **P6** | 9 | 12 | 11.075 | Diameter of Coil 02 |
| **P7** | 9 | 12 | 11.075 | Diameter of Coil 03 |
| **P8** | 9 | 12 | 11.075 | Diameter of Coil 04 |
| **P9** | 9 | 12 | 9.5085 | Diameter of Coil 05 |
| **P10** | 9 | 12 | 9.1725 | Diameter of Coil 06 |

In order to efficiently select samplings from the design domain, sampling techniques should be employed. One of the simplest sampling methods is the pure Monte Carlo sampling, of which basic theory is to randomly sample the desired numbers of input variables (Figure 7-3(a)). It is convenient to use; however, it usually contains poor sampling areas (Olsson et al., 2003). Therefore, another sampling method called Latin Hypercube Sampling (LHS) is suggested to use for generating input samples. LHS is initially derived from the idea of a Latin Square where samples are distributed evenly in a 2D space (Figure 7-3(b)). However, LHS extends this concept to a multi-dimensional space, which can be implemented by the process as follows.

*a.* Evenly divide the range of each variable $x_i$ into $n$ intervals $u_{ij}$, $i = 1, 2, \ldots, r$, $j = 1, 2, \ldots, n$.

*b.* Calculate the cumulative probability of the $j$ th interval of variable $x_i$ *as:*

$$P_{ij} = \frac{(j-1) + r_{ij}}{n}$$

*c.* Achieve the sample value $x_{ij}$ by the inverse of the distribution function $F(\cdot)$*:*

$$x_{ij} = F_i^{-1}(P_{ij})$$

*d.* The values for each variable $x_i$ are paired with those of other variables randomly or in certain orders.

### 7.1.2. Constrained Latin Hypercube Sampling

As features of some samples may not be desired for a specific problem, not all the samples selected from the design domain by LHS are favoured by engineers or designers. In this study, for instance, the combinations of variables that lead to the spring shapes, as shown in Figure 7-2(a), are not desired according to the experience of spring designers. The most important reason is that there are sudden changes of coil diameter, which may cause high shear stress in these areas and therefore results in pre-failure of the spring. On the contrary, the spring shown in Figure 7-2(b), which have a progressive change on the coil diameters, is usually acceptable. Therefore, it is essential to put constraints on the design parameters to samples only from the desired spring shapes. In other words, it is important to take into account inequality constraints between variables. However, these preferences cannot be achieved by simply including these considerations to determine variable ranges of parameters.

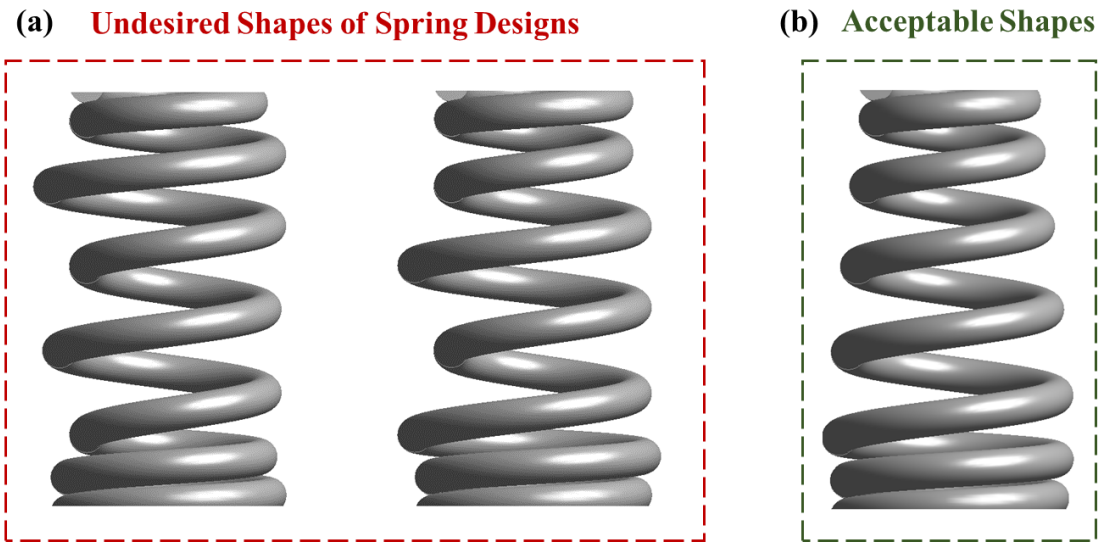


*Figure 7-2: The samples of spring designs with (a). undesired shapes (b). acceptable shapes.*

One method for achieving this is to employ the sampling technique called constrained Latin Hypercube sampling. It is an extension of existing normal LHS, which is also a stratified sampling technique. However, it has the advantage that it can search the variables space for the combinations of variables by defining inequality constraints. At the same, it is able to generate sample points more evenly than it does by the normal Monte Carlo sampling. Figure 7-3 shows 20 samples of two variables obtained with normal random sampling (Figure 7-3(a)), normal LHS (Figure 7-3(b)), constrained random sampling (Figure 7-3(c)), and cLHS (Figure 7-3(d)) respectively. It can be seen that cLHS can still generate even distribution of samples in every interval, though with inequality constraints.

In order to select samples from the design domain according to the variable ranges shown in Table 7-1, cLHS technique is employed. The constraints of the design parameters that are defined by inequality are shown in Table 7-2. Constraint C1 distributes the idea that only the spring geometry samples with a certain spring height are desired. Constraint C2 represents that the spring geometry samples are desired to have progressive values for the coil diameters from coil 01 to coil 07. Eventually, 300 spring geometry samples are generated from the design domain by these inequality constraints into cLHS.

Then, the 300 geometric models are imported into the static and modal finite element spring models, of which meshing strategy, analysis settings and validation have been discussed in the previous Chapter. Correspondingly, the spring forces at 7mm compression and the first-order natural frequency of the 300 spring models are obtained by conducting the static and modal finite element simulations, respectively. This thesis

aims to find and illustrate the relationships between the geometric parameters and their corresponding simulation results.

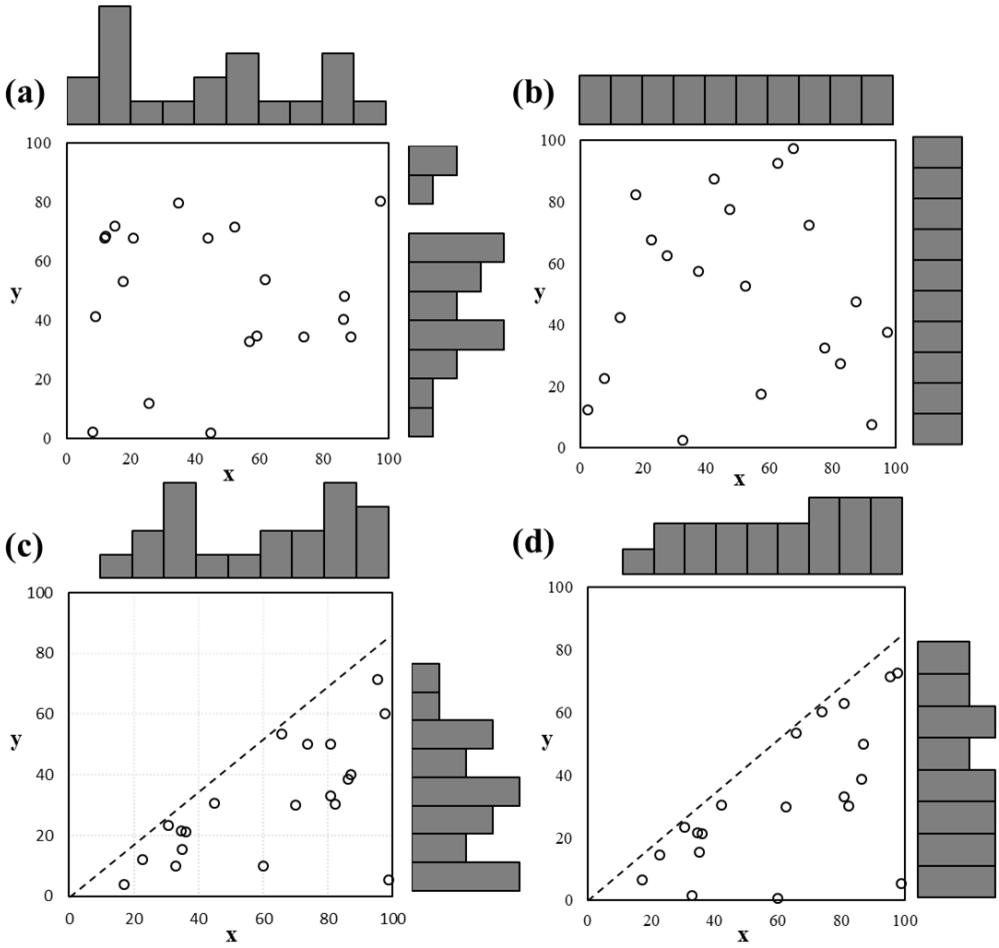


*Figure 7-3: Samples of design of experiments (20 points) generated by (a). normal random sampling (b). normal Latin Hypercube sampling (c). constrained random sampling (d). constrained Latin Hypercube sampling*

*Table 7-2: Constraints on the design domain by inequalities of design parameters.*

| Constraints Name | Description |
|---|---|
| **C1** | $39 < P1 + P2 + P3 + P4 + P5 < 39.275$ |
| **C2** | $P6 > P7 > P8 > P9 > P10$ |

## 7.2 Machine Learning Techniques for Design of Helical Springs

By employing the finite element models and the cLHS technique, 300 sets of spring parameters with their corresponding finite element results are obtained in the previous section. This section aims to find the relationships between the geometric parameters and the results of spring forces and natural frequencies. This task can be done by applying regression methods or machine learning techniques, for instance, the genetic algorithm and genetic programming methods used in this thesis. In our case, the ten geometric parameters and the corresponding finite element results for each spring sample are treated as a single feature in the regression model. It is expected that the regressed expression for describing the relationships between geometric parameters and finite element results is effective across all the 300 features. When applying the regressed expression, specific static forces and the natural frequency of helical springs can be obtained by defining the corresponding geometric parameters.

### 7.2.1. Genetic Algorithm

Genetic algorithm (GA) is inspired by Darwin's theory of natural selection and was firstly proposed by John Holland in 1960. It was then extended by the following researchers to be the current theory. The process flowchart of the generic algorithm is shown in Figure 7-4. Implementation of GA always starts with the generation of the initial population. According to the principles of 'survival of the fittest', the fittest generation becomes the parent generation. The individuals of the parent generations evolve by going through the processes of selection, crossover and mutation to generate children generations. The fitness of the children generation is also evaluated, and the individuals with better fitness will be stored for the next evolution. This process ensures

a more environmentally adaptive population can be evolved. In the end, the optimal individuals can be approximated as the optimal solution for the objective functions.

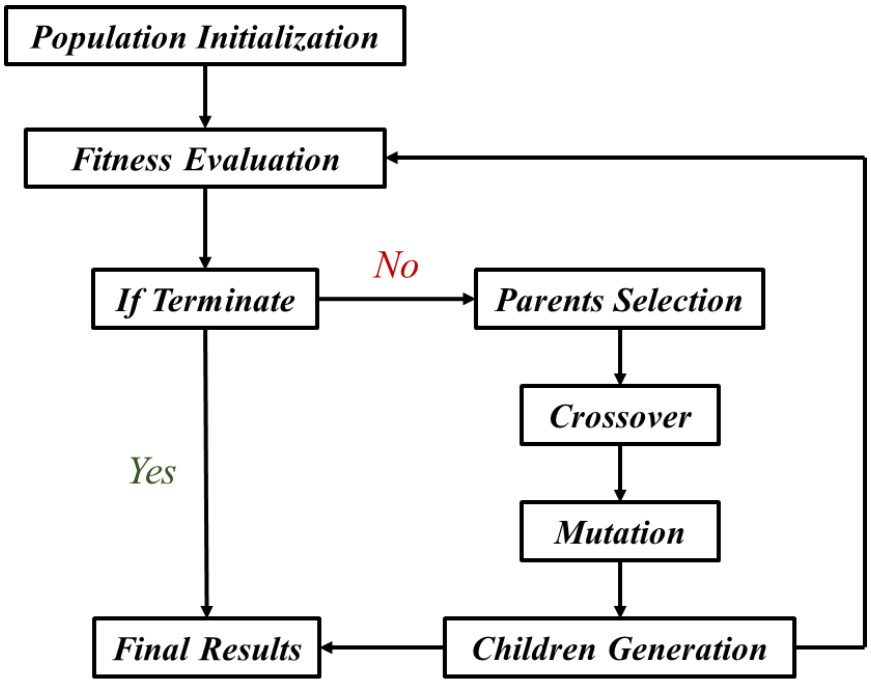


*Figure 7-4: The flowchart for the main process of the genetic algorithm*

### 7.2.2. Genetic Programming

Genetic programming is derived from and can be treated as a variant of a genetic algorithm. Instead of creating codes, genetic programming applies the basic genetic algorithm theory to a population of computer programs. To be specific, genetic programming adopts binary trees with branches and leaves to represent computer programs. It aims to evolve the computer programs to match as closely as possible to the desired objectives. For example, the function of Eq.(7.1) is the desired objective expression to approximate.

$$y = X_0^2 - 2X_1 + 1 \tag{7.1}$$

Firstly, genetic programming begins with initializing the population of randomly developed binary trees consist of functions and terminals. Functions that represent the

operators in equations and terminals are the end nodes of these trees. Next, the fitness of every single tree should be evaluated to determine if there is anyone who meets the terminate conditions. If not, these trees turn to be the parents' generation to go through crossover and mutation procedures based on the same methods as those in the genetic algorithm. The sub-tree mutation is based on the same logic but selects and replaces a random subtree instead of a random node. Consequently, GP accumulates these offspring of parent binary trees to form the new children generation. The fitness of every individual in the children generation should be evaluated. The children generation will then become the next parent generation to go through the procedures of crossover and mutation.

The crossover operates by randomly cutting two points from two trees and swapping the cut portions, producing crossover offspring, as shown in Figure 7-5(a). The mutation process is also employed in genetic programming for the purpose of eliminating trapping in a local optimum. An example of conducting point mutation can be found in Figure 7-5(b), where a random node is replaced by another random node. The average fitness of each generation can be improved by iterating this process. A stop criterion functions to cease the process as long as the evaluated fitness of an individual in the children generation exceeds the criterion. The best individual of the final generation provided by genetic programming is usually treated as one of the solutions in the researched problem.

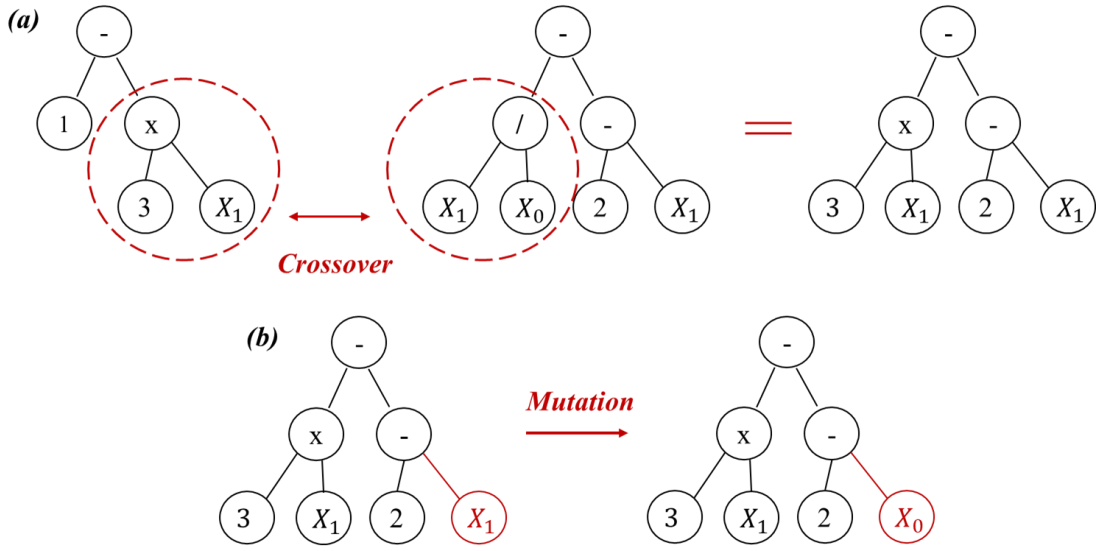


*Figure 7-5: Schematic of methods used in GP during producing children generations: (a). Crossover (b). Mutation for Equation 4.*

In this study, genetic programming techniques are employed to estimate the relationships between the parameters of the spring (Table 7-1) and the static compression forces of the spring. The python machine learning package 'GPlearn' is used to implement the genetic programming algorithm. In total, 300 sets of parameters selected by cLHS method and their corresponding finite element simulation results, 250 sets of which are training data and the other 50 sets are testing data, are used to train and test the genetic programming model. The parameters for developing the genetic programming model by GPlearn are listed in Table 7-3. In the table, the population size is used to initiate the structure of the genetic programming program. The genetic programming program solves for the desired solution and stops only when either the generations exceed 100, or the fitness is already lower than the stopping criteria 01. The parsimony coefficient is 0.008 in order to control the increasing size of the programs.

*Table 7-3: The parameters used for developing the GP model in 'GPlearn'*

| Parameters (GPlearn) | Value |
|---|---|
| Function set | '+', '-', '*', '/', '^' |
| Population size | 6000 |
| Generations | 100 |
| Stopping criteria | 0.1 |
| Crossover | 0.7 |
| Subtree mutation | 0.1 |
| Hoist mutation | 0.05 |
| Point mutation | 0.1 |
| Parsimony coefficient | 0.008 |

### 7.2.3. Helical Spring Formulas Regressed by Genetic Programming

By adopting the GPlearn package and using the parameters defined in Table 6-1, an explicit expression for describing the relationships between the spring parameters (P1-P10) and the compression force F is generated as shown below:

$$F = X_5 \cdot (X_4 + X_8) \cdot \frac{A_3 - X_1 - 0.765 \cdot X_3 \cdot (1 + \frac{A_5}{X_9})}{X_9} \tag{7.2}$$

where

$$A_1 = X_4 - 2X_5 + X_7 + \sqrt{X_3 X_8} - 0.398$$

$$A_2 = 2X_2 + X_5 - X_7 + 0.398$$

$$A_3 = 2X_4 + X_5 - X_6 + 3X_7 + 2X_8 - X_{10} + 1.53$$

$$A_4 = 2X_2 + X_5 - \sqrt{X_6} \cdot (X_8 - X_2)$$

$$A_5 = X_5 + 0.398 + \frac{A_1}{A_2} + \frac{A_4}{X_4(X_7 - X_6)}$$

In addition, another explicit expression for describing the relationships between the spring parameters (P1- P10) and the first-order natural frequency NF is modelled as shown below:

$$NF = \sqrt{X_5} \cdot (X_4 + \sqrt{B_1}) \cdot (X_2 + X_7 + X_8 - X_{10} + \sqrt{B_2} + \frac{X_8}{X_6}) \qquad (7.3)$$

where

$$B_1 = X_5 - X_1 - X_6 + X_7 + X_8 + X_{10} - 0.733 - \frac{X_3}{\sqrt{X_2}}$$

$$B_2 = X_2 - X_1 - X_6 + X_5 + \sqrt{X_7} + X_8 - X_9 + X_{10} - 0.733 - \frac{X_3}{\sqrt{X_2}}$$

In these two regressed expressions, the ten variables X0- X9 represent the ten selected parameters of the beehive spring P1-P10 (Table 7-1). They are simplified from the source results generated by genetic programming in Python (Appendix B). The correlation between the spring force results of training data for FE simulation and the GP model is illustrated in Figure 7-6(a). A large portion of the training data concentrates on the area where the spring forces stay between 240N and 400N. The same situation can be overserved in the correlation between the spring force results of testing data in Figure 7-6(b). However, it shows that though most of the testing data stay in this area where spring force is lower than 400N, the trained GP model is still able to predict well the spring force that is larger than 400N. Therefore, it can be concluded that the GP model is trained well to fit the data obtained from FE simulations, and it shows a high accuracy to predict the compression force according to the given spring parameters.

The correlation between the first-order natural frequency results of training data for FE simulation and the GP model is illustrated in Figure 7-7. Unlike those distributed in Figure 7-6(a), the training data in Figure 7-7(a) distributes averagely in the whole area between 450Hz and 600Hz of natural frequency. The testing data in Figure 7-7(b) also

distributes evenly in this whole area. It can be observed that both the training data and testing data in Figure 7-7 stay very close to the validation line. It means that the expression trained by GP is well trained to fit the natural frequency results obtained from the FE simulations. And the trained GP model can predict the 1st order natural frequency by given the values of the ten spring parameters.

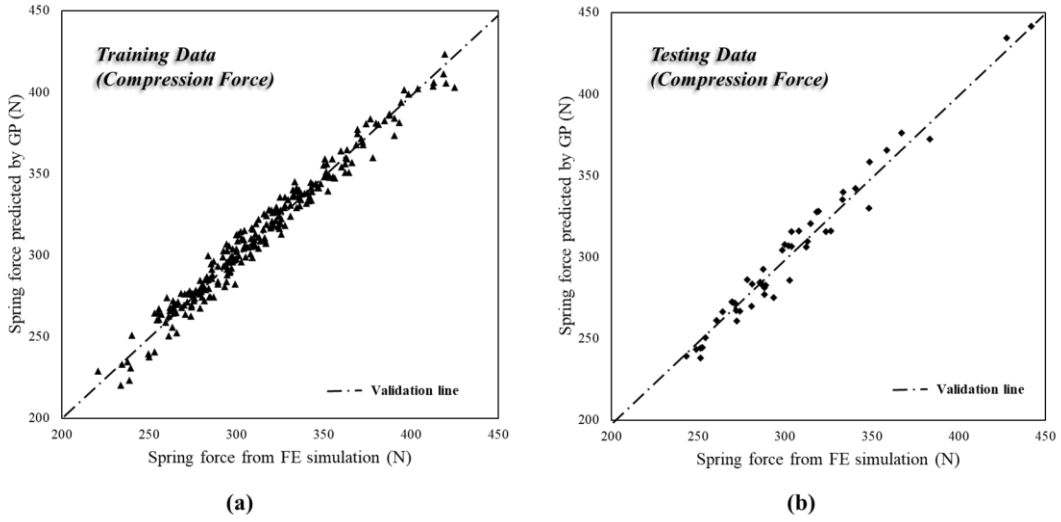


*Figure 7-6: The correlations between the spring forces obtained by the FE simulation and predicted by the GP model of (a). training data (b). testing data*

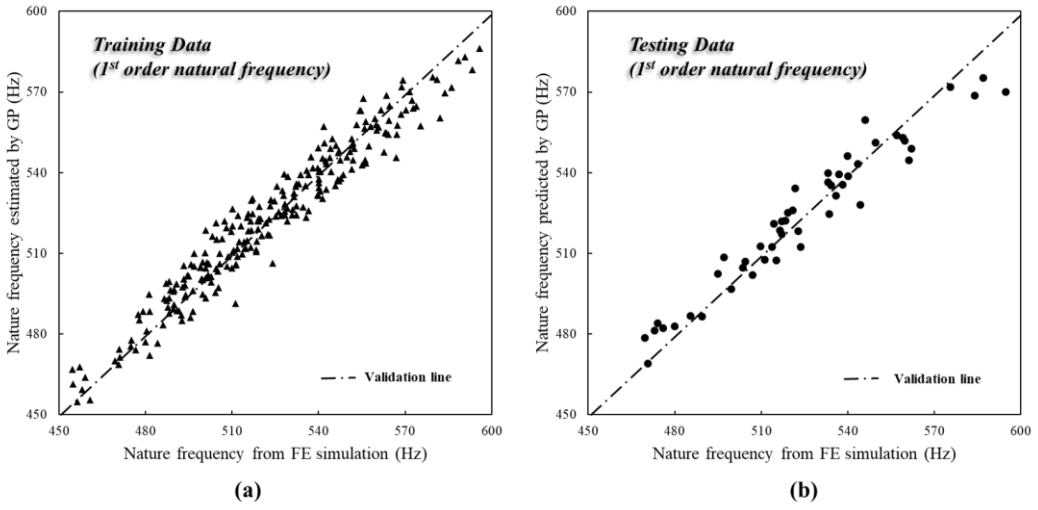


*Figure 7-7: The correlations between the first-order natural frequencies obtained by the FE simulation and predicted by the GP model of (a). training data (b). testing data*

### 7.2.4. Sensitivity Analysis of the Static Spring Formulas

The expressions for predicting the compression force and the first order natural frequency of a helical spring are regressed by employing genetic programming techniques. Then, a sensitivity analysis on the ten spring parameters can be conducted. To achieve this, the python package 'SALib' is used to implement the Sobol Sensitivity Analysis. The Sobol sensitivity analysis, or referred to the variance-based sensitivity analysis, is a method for analysing the global sensitivities of parameters. In the Sobol analysis, the bounds for the ten parameters are defined by the same values as those defined in Table 7-1. Then, the sampler in the 'SALib' generates a certain number of samples for the analysis. The inherent function of the sampler to calculate the number of samples is $N*(2D+2)$, where N is the argument coefficient, and $D$ is the number of input parameters ($D$=10 in this study). In the present study, the argument coefficient N is assigned the value 40000, which makes the total number of samples is 8.8e5.

The sensitivities of the ten spring parameters in the expression of predicting the compression force F is displayed in Figure 7-8(a). As defined in the previous section, the parameters P1-P5 represent the pitch of coils 02-06 and the parameters P6-P10 represent the diameters of coils 02-06. The parameters P2-P5 have higher sensitivities than those of the parameters P6-P10, which means that the value of the compression force is more sensitive to the changes of the spring pitch than to the changes of the diameters of the coils in the design domain. Theoretically, it is because that the changes of pitch can contribute to the change of the number of active coils $Na$, which will significantly increase the compression force of a helical spring. However, it is remarkable that the sensitivity of P1 is very small that has a value of 0.0004, which seems to conflict with this conclusion. In fact, the parameter P1, which represents the pitch of coil 02, is designed to be a damper pitch in the helical springs. In other words,

this pitch is always smaller than the others, making the coil 01 and the coil 02 closed at 7mm compression. Therefore, its changes affect little on the force at 7mm compression as it has nearly no contribution to the change of Na. Figure 7-8(b) illustrates the parameter sensitivities in the expression of predicting the first-order natural frequency NF. The parameters P1-P5 show much higher sensitivities than those of the parameters P6-P10. It can be explained that the changes of the spring pitches will alter the *Na*. At the free length, the change of Na has a significant effect on the result of the first-order natural frequency.

The sensitivities of the ten spring parameters to the compression force *F* is displayed in Figure 7-8a. As defined in the previous section, the parameters P1-P5 represent the pitch of coils 02-06 and the parameters P6-P10 represent the diameters of coils 02-06. The sensitivities of parameters P2-P5 are generally higher than those of parameters P6-P10. It means that the value of the compression force is more sensitive to the changes in spring pitch than to the changes in the diameters of the coils. Theoretically, it is because the pitch changes determine the change of the number of active coils *Na* during a compression, which will significantly increase the compression force of a helical spring. It is noticed that the sensitivity of P1 is very small that has a value of 0.0004, which is attributed to the fact that the parameter P1, which represents the pitch of coil 02 (4-6 mm), is designed to be a damper pitch in the helical springs. This pitch is always smaller than the others (7.5-9 mm), which makes coil 01 and coil 02 constantly closed at 7 mm compression. Therefore, the variation of P1 does not significantly affect the overall reaction force at 7mm compression as it has nearly no contribution to the change of *Na*.

Besides, it is observed that the sensitivity factor of P4 is 0.0093 in Figure 7-8a, which is slightly lower than the factors of P2, P3 and P5. The displacements of coils 02

– 06 of the beehive spring at 7mm compression are obtained to verify this phenomenon, as shown in Table 7-4. The displacements of coils 05 and 06 are smaller than those of coils 02, 03 and 04 due to the smaller coil diameters of coils 05 and 06, which is defined by the cLHS approach. This should have made the sensitivities of P4 and P5 lower than those of P2 and P3. However, coil 06 is directly connected to the fixed upper end of the spring, which means it will progressively contact the end of 07 during compression. As a result, the closure between coil 06 and coil 07 makes the sensitivity factor of P5 (coil 06) stay high in Figure 7-8a. Eventually, only the sensitivity of P4 (coil 05) is relatively small in Figure 7-8a.

*Table 7-4: The simulated displacements of coil 02 – 06 of the beehive spring at 7mm compression.*

| **Coil NO.** | **02** | **03** | **04** | **05** | **06** |
|---|---|---|---|---|---|
| **Displacement (mm)** | 1.545 | 1.597 | 1.485 | 1.254 | 1.01 |

Figure 7-8b illustrates the parameter sensitivities to the first-order natural frequency NF. The parameters P1-P5 show much higher sensitivities than those of the parameters P6-P10. It can be explained that the changes of the spring pitches will alter the *Na*. At the free length, the change of *Na* has a significant effect on the result of the first-order natural frequency.

In summary, the changes of spring pitches have more significant effects on both the results of the compression force and the first-order natural frequency than the changes of coil diameters do. However, the pitch of coil 02 (P1) has little effect on the force at 7mm compression due to the fact that the coil 01 and 02 are closed anyhow at that compression.

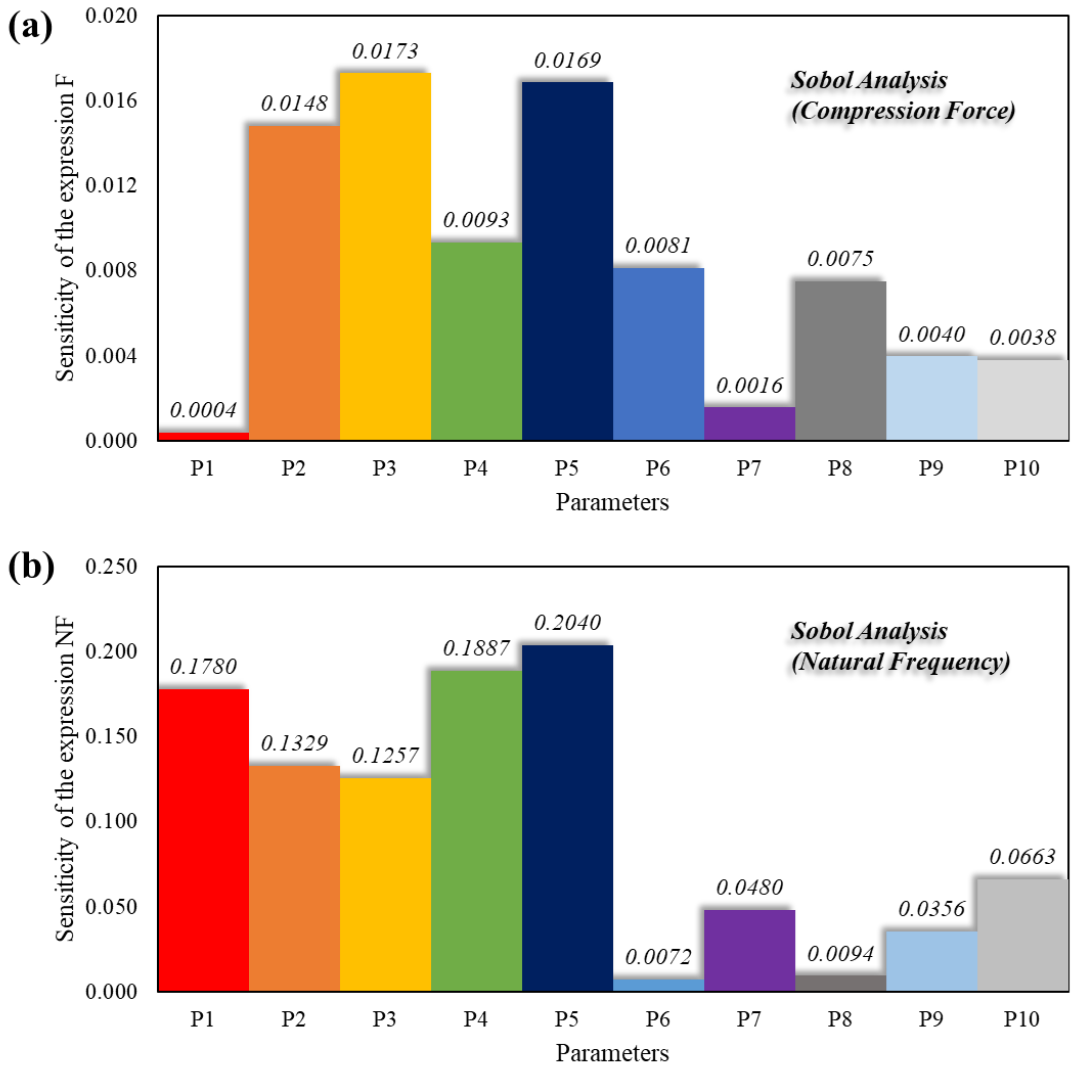


*Figure 7-8: The sensitivities of spring parameters on the GP models for (a). the spring compression force, and (b). the first-order natural frequency, respectively.*

## 7.3 Summary

In this chapter, an innovative study is conducted by combining the techniques of finite element analysis (FEA), constrained Latin Hypercube sampling (cLHS) and genetic programming (GP) to investigate the nonlinear relationships between design parameters and the mechanical properties of helical springs. The relationships between the spring parameters and the compression force, and the natural frequency of helical springs with

arbitrary shapes are successfully modelled for predicting the compression force and the natural frequency. The proposed method is proved to be a feasible and robust way to guide the design of helical springs of arbitrary shapes. The outcomes achieved by this study can be concluded as below.

Compared to the common LHS method, cLHS provides better flexibility and reliability in constraining an engineering design domain by defining inequalities between design parameters. It generates more representative samples for obtaining FE results and is then used by the GP model. The meta-models developed by GP describe the complicated relationships between the mechanical properties of helical springs and the multiple geometric parameters. It can also save a lot of computational time by avoiding the time-consuming FE simulations. Besides, according to the results of sensitivity studies, it is found that though both the spring pitch and the coil diameter can affect the compressive force and the natural frequency of helical springs, the spring pitch has higher sensitivities than the coil diameter does. An exception is that when the spring pitch is too narrow, the pitch will be closed at a certain compression. Then, the sensitivity of that pitch to the compressive force becomes extremely small as it does not contribute to the change of the number of active coils at that compression. In addition, the results also demonstrate that the spring pitch and the spring diameter also contribute to the amplitude of spring force and natural frequency. The narrow pitch significantly affects the compression force as the coils having narrow pitch are closed progressively during compression.

In summary, cLHS is an outstanding candidate for engineering design sampling where predefined constraints exist. GP technique has a strong ability in conducting multi-parameters modelling and analysis. By combining FEA, cLHS and GP techniques, the present model shows its robust ability in designing and analysing mechanical

devices with nonlinear programmed properties, which cannot be achieved by applying current existing engineering design and analysis methods. The method also shows big potential in aiding the process of engineering optimization by employing the meta-model in future works.

# 8 Conclusion and Future Works

## 8.1 Conclusion

In this thesis, an innovative spring formula is firstly developed to formulate the mechanical properties of a representative beehive helical spring with a highly nonlinear geometry. The new spring formula can consider the effects of variable coil diameter, variable spring pitch and, more importantly, the coil contact. A static compression test is conducted on the beehive spring to validate the results of the spring formula. It is found that the developed spring formula can better predict the stiffness and the first-order natural frequency of the beehive spring than the traditional spring formulas. Especially when several spring coils start to contact each other during the compression process, the developed spring formula shows its capability to include this effect and, therefore, accurately estimate the spring's mechanical properties. Besides the static model, a distributed parameter model is also developed and coupled with the developed spring formula to simulate the dynamic response of the beehive spring working in the real car engine. Correspondingly, the engine head tests are conducted to validate the analytical results obtained from the dynamic spring model. The analytical results show good agreement with the experimental results at both 4200-rpm and 5600-rpm engine speeds. However, significant high-frequency spring forces appear at the 5600-rpm engine, which cannot be well simulated by the dynamic analytical spring model. This phenomenon has also drawn the attention of researchers and engineers since these significant spring forces bring great danger to the car engine running at high speeds in practice.

For revealing the reasons causing the significant spring forces, a static FE model and a dynamic FE model are also developed to simulate the beehive valve spring's static

and dynamic responses. In the static FE analysis, the FE results are compared with both compression test results and the results of the developed analytical model. As a result, both the FE model and the developed spring formula can accurately predict the spring stiffness and the first-order natural frequency. In addition, the static FE model can accurately display the status of coil contacts at any loading step. These results illustrate that considering variable coil diameter, variable spring pitch, and coil contacts are essential for accurately predicting the mechanical properties of a nonlinear helical spring. These considerations can also contribute to the development of a successful dynamic spring model.

The dynamic analysis of the beehive spring is achieved by comparing the results of the dynamic FE model, the distribute parameter model and the engine head test. The dynamic FE results show excellent agreements with both analytical results and the experimental data at both 4200-rpm and 5600-rpm engine speeds. However, when the simulated engine speed is 8000-rpm, the abnormal high-frequency spring forces became significant and exceeded the maximum magnitude of the normal dynamic spring force. The dynamic FE model can still accurately simulate these abnormal spring forces, and however, the analytical model fails. One obvious conclusion is that the dynamic response of the valve spring becomes more significant when the engine speed is high. Then, by extracting the dynamic response of each spring coil in the FE simulations, it is found that these abnormal spring forces are caused by the violent impact between spring coils or saying by the coil clash. These conclusions present a better understanding of the effects of coil clashes on the application of high-speed valve springs and suggest a feasible spring design method for handling the nonlinear geometries of helical springs.

Finally, a machine learning model based on the genetic programming technique, the FE spring model, and constrained Latin Hypercube sampling is proposed to analyse

helical springs with highly nonlinear geometries. Instead of the time-consuming simulation models, it aims to use the data-driven model as a meta-model to predict the mechanical properties (spring stiffness and first-order natural frequency) of any helical springs in the design domain. The prediction results are validated by both the results of the FE spring model and experiments. In addition, a sensitivity study of spring geometric parameters is also conducted based on the developed machine learning models. The study reveals the importance of the narrow pitch to the mechanical properties and the combined effects of all these variable spring geometric parameters on the results. The machine learning model shows its ability as a tool for designing helical springs with highly nonlinear geometries.

In summary, beyond the traditional analysis of the most common linear helical spring, this thesis investigates nonlinear helical springs and their nonlinear static and dynamic responses from a comprehensive view using the analytical spring model, experimental validation, FE analysis and machine learning techniques. New spring formula and FE models are developed and validated by experiments to overcome the limitations of traditional spring models. The new spring formula successfully includes the effects of the nonlinear geometry (varied pitch and coil diameter), which can simulate nonlinear helical springs under static compression as accurately as the FE spring model. However, the results based on the commonly used spring formulas that exclude these nonlinear effects have significant departures from the test results. Therefore, nonlinear spring geometry, for instance, variable coil diameter, variable spring pitch and coil contact, are proved of great importance in analysing mechanical properties of nonlinear helical springs. More importantly, despite the success in simulating the spring dynamic responses at 4200-rpm and 5600-rpm engine speeds, the distributed parameter spring model coupled with the developed spring formula fails to

simulate the spring surge and coil clash phenomenon. These phenomena lead to the appearance of significant abnormal high-frequency spring forces, which plays an essential role in evaluating the performance of valve springs at high engine speeds. On the contrary, these phenomena are accurately simulated by the developed dynamic FE spring model by considering the varied natural frequency, varied spring stiffness and especially the violent impact between narrow coils. It demonstrates that the FE spring model shows better accuracy in simulating nonlinear springs while also taking extra computing time than the analytical spring model. Hence, in the last part of the study, a machine learning technique, genetic programming, is employed to develop a meta-model based on the FE results for the design of nonlinear helical springs. The developed visible formulas can precisely predict the spring stiffness and the first-order natural frequency of various nonlinear helical springs. Therefore, the mutual interactions of multiple spring geometry parameters on the mechanical performance of nonlinear springs can be analysed and studied based on these formulas. In addition, the visible spring formulas generated by GP models could be potentially used as a tool for the precise optimization of helical springs in practice.

## 8.2 Suggestions for Future Works

The distributed parameter model coupled with the new spring formula presents a good fitness compared with the experimental data at engine speeds lower than 5600-rpm. However, it fails to simulate the abnormal spring forces at higher speeds as it lacks the consideration of the coil clash at high loading speeds. Including the effects of the coil clash into the dynamic analytical model can be a good supplement for it. It would have a great potential to accurately predict the significant abnormal spring forces caused by

coil clash as the FE model does. Then, it will substantively accelerate the computing speed when ensuring accuracy at the same time.

Furthermore, the usage of the developed FE spring model cannot be limited to simulate the working status of valve springs. It should be widely applied in various categories of applications of helical springs, for instance, for suspension springs in vehicles. Besides, the FE model is also applicable for conducting studies on analysing dual spring systems, which usually use two different helical springs in one system.

Finally, the machine learning technique is always a data-driven method of which accuracy highly relies on the amount of training data. A straightforward method to predict the dynamic spring response at high-speed applications could be to develop a meta-model based on the dynamic FE simulation results. However, the current dynamic FE model is very time-consuming and therefore lowers the feasibility and efficiency of building up the meta-model. Therefore, methods for improving the efficiency of the developed dynamic FE model are incredibly beneficial for developing such a dynamic spring metal-model, or a dynamic analytical model for helical springs that can accurately predict the dynamic spring forces could also be another feasible way.

# References

ABIDIN, M. I. Z., MAHMUD, J., LATIF, M. J. A. & JUMAHAT, A. 2013. Experimental and numerical investigation of SUP12 steel coil spring. *Procedia Engineering*, 68**,** 251-257.

AL-MOSAWE, A., KALFAT, R. & AL-MAHAIDI, R. 2017. Strength of Cfrp-steel double strap joints under impact loads using genetic programming. *Composite Structures*, 160**,** 1205-1211.

ALVAREZ, L. 2000. Design optimization based on genetic programming. *University of Bradford, UK*.

ARMANI, U. 2014. *Development of a hybrid genetic programming technique for computationally expensive optimisation problems.* University of Leeds.

ASSIMI, H., JAMALI, A. & NARIMAN-ZADEH, N. 2017. Sizing and topology optimization of truss structures using genetic programming. *Swarm and evolutionary computation*, 37**,** 90-103.

AZAMATHULLA, H. M. & GHANI, A. A. 2010. Genetic programming to predict river pipeline scour. *Journal of Pipeline Systems Engineering and Practice*, 1**,** 127-132.

BAGHANI, M., NAGHDABADI, R. & ARGHAVANI, J. 2012. A semi-analytical study on helical springs made of shape memory polymer. *Smart Materials and Structures*, 21**,** 045014.

BAKHSHESH, M. & BAKHSHESH, M. 2012. Optimization of steel helical spring by composite spring. *International journal of multidisciplinary science and engineering*, 3.

BARBOSA, H. & BERNARDINO, H. 2010. Genetic Programming in Civil, Structural and Environmental Engineering. *Computational Technology Reviews,* 4**,** 115-45.

BAUMAL, A., MCPHEE, J. & CALAMAI, P. 1998. Application of genetic algorithms to the design optimization of an active vehicle suspension system. *Computer methods in applied mechanics and engineering,* 163**,** 87-94.

BERRY, W. 1938. Practical problems in spring design. *Proceedings of the Institution of Mechanical Engineers,* 139**,** 431-524.

BONTE, M., VAN DEN BOOGAARD, A. H. & HUÉTINK, J. 2005. Solving optimisation problems in metal forming using finite element simulation and metamodelling techniques. *Proceedings of APOMAT***,** 242-251.

BOX, G. E. & BEHNKEN, D. W. 1960. Some new three level designs for the study of quantitative variables. *Technometrics,* 2**,** 455-475.

CALABRETTA, M., CACCIATORE, D. & CARDEN, P. 2010. Valvetrain friction-modeling, analysis and measurement of a high performance engine valvetrain system. *SAE International Journal of Engines,* 3**,** 72-84.

CALDER, C. & JENKINS, C. 1988. Stress analysis of a helical coil automobile spring using rosettes. *Experimental Techniques,* 12**,** 17-20.

ÇALıM, F. F. 2009. Dynamic analysis of composite coil springs of arbitrary shape. *Composites Part B: Engineering,* 40**,** 741-757.

CEVIK, A. 2007. Genetic programming based formulation of rotation capacity of wide flange beams. *Journal of Constructional Steel Research,* 63**,** 884-893.

CEVIK, A., ARSLAN, M. H. & KÖROĞLU, M. A. 2010. Genetic-programming-based modeling of RC beam torsional strength. *KSCE Journal of Civil Engineering,* 14**,** 371-384.

CHAMPION, R. & CHAMPION, W. 2011. Departure from linear mechanical behaviour of a helical spring. *Mathematical and Computer Modelling,* 53**,** 915-926.

CHAN, C. & PISANO, A. P. 1987. Dynamic model of a fluctuating rocker-arm ratio cam system. *Journal of mechanisms, transmissions, and automation in design,* 109**,** 356-365.

CHAPMAN, C. D. 1994. *Structural topology optimization via the genetic algorithm.* Massachusetts Institute of Technology.

CHELLAPILLA, K. 1997. Evolving computer programs without subtree crossover. *IEEE Transactions on Evolutionary Computation,* 1**,** 209-216.

CHEN, F. Y. & POLVANICH, N. 1975. Dynamics of High-Speed Cam-Driven Mechanisms—Part 1: Linear System Models. *Journal of Engineering for Industry,* 97**,** 769-775.

CHEN, G. & ZHOU, J. 1993. *Vibration and damping in distributed systems,* Crc Press.

CLAUBERG, J., HUBER, B. & ULBRICH, H. Simulation and Validation of Valve Springs in Valve Train Simulations. Proceedings of the Eighth International Conference on Engineering Computational Technology, 2012.

CLAUBERG, J. & HUBER, R. 2013. Using non-smooth mechanics and parallelization techniques for the efficient simulation of different types of valve springs. SAE Technical Paper.

COOK, R. D. 1990. Finite element analysis of closely-coiled helical springs. *Computers & Structures,* 34**,** 179-180.

CORRIVEAU, G., GUILBAULT, R. & TAHAN, A. 2010. Genetic algorithms and finite element coupling for mechanical optimization. *Advances in Engineering Software,* 41**,** 422-426.

COSTELLO, G. 1975. Radial expansion of impacted helical springs. *Journal of Applied Mechanics,* 42**,** 789-792.

CRAMER, N. L. A representation for the adaptive generation of simple sequential programs. Proceedings of the first international conference on genetic algorithms, 1985. 183-187.

DALPIAZ, G. & RIVOLA, A. 2000. A non-linear elastodynamic model of a desmodromic valve train. *Mechanism and Machine Theory,* 35**,** 1551-1562.

DOS REIS NOGUEIRA, J. A. 2014. Dynamic analysis of a valve train system used in a four stroke engine.

DRAGONI, E. & BAGARIA, W. 2011. Mechanical design of bimaterial helical springs with circular cross-section. *The Journal of Strain Analysis for Engineering Design,* 46**,** 304-314.

DRESNER, T. & BARKAN, P. 1995. New methods for the dynamic analysis of flexible single-input and multi-input cam-follower systems. *Journal of Mechanical Design,* 117**,** 150-155.

DYM, C. L. 2009. Consistent derivations of spring rates for helical springs. *Journal of Mechanical Design,* 131**,** 071004.

FRENET, F. 1852. Sur les courbes a double courbure. *Journal de mathématiques pures et appliquées***,** 437-447.

FRIKHA, A., TREYSSEDE, F. & CARTRAUD, P. 2011. Effect of axial load on the propagation of elastic waves in helical beams. *Wave Motion,* 48**,** 83-92.

GAIKWAD, S. & KACHARE, P. 2013. Static analysis of helical compression spring used in two-wheeler horn. *IJEAT ISSN***,** 2249-8958.

GANDOMI, A. H. & ALAVI, A. H. 2011. Multi-stage genetic programming: a new strategy to nonlinear system modeling. *Information Sciences,* 181**,** 5227-5239.

GANDOMI, A. H. & ALAVI, A. H. 2012. A new multi-gene genetic programming approach to nonlinear system modeling. Part I: materials and structural engineering problems. *Neural Computing and Applications,* 21**,** 171-187.

GANDOMI, A. H., ALAVI, A. H. & SAHAB, M. G. 2010. New formulation for compressive strength of CFRP confined concrete cylinders using linear genetic programming. *Materials and Structures,* 43**,** 963-983.

GANDOMI, A. H., TABATABAEI, S. M., MORADIAN, M. H., RADFAR, A. & ALAVI, A. H. 2011. A new prediction model for the load capacity of castellated steel beams. *Journal of Constructional Steel Research,* 67**,** 1096-1105.

GARG, A., GARG, A. & TAI, K. 2014. A multi-gene genetic programming model for estimating stress-dependent soil water retention curves. *Computational Geosciences,* 18**,** 45-56.

GEBALLE, R. 1958. Statics and dynamics of a helical spring. *American Journal of Physics,* 26**,** 287-290.

GIRGIN, K. 2006. Free vibration analysis of non-cylindrical helices with, variable cross-section by using mixed FEM. *Journal of Sound and Vibration,* 297**,** 931-945.

GOLDBERG, D. E. 2006. *Genetic algorithms,* Pearson Education India.

GONZÁLEZ-TABOADA, I., GONZÁLEZ-FONTEBOA, B., MARTÍNEZ-ABELLA, F. & PÉREZ-ORDÓÑEZ, J. L. 2016. Prediction of the mechanical properties of structural recycled concrete using multivariable regression and genetic programming. *Construction and Building Materials,* 106**,** 480-499.

GU, Z., HOU, X., KEATING, E. & YE, J. 2020. Non-linear finite element model for dynamic analysis of high-speed valve train and coil collisions. *International Journal of Mechanical Sciences***,** 105476.

GUO, H. X., DAI, J., HU, G. Y. & CHENG, L. Z. Reliability-Based Design Optimization of Valve-Spring Using Evidence Theory and Genetic Algorithm. Applied Mechanics and Materials, 2010. Trans Tech Publ, 1258-1262.

GUO, J., ZHANG, W., ZHANG, X. & CAO, Y. 2014. Dynamic and exciting analysis with modal characteristics for valve train using a flexible model. *Mechanism and Machine Theory,* 78**,** 158-176.

GUO, J., ZHANG, W. & ZOU, D. 2011. Investigation of dynamic characteristics of a valve train system. *Mechanism and Machine Theory,* 46**,** 1950-1969.

GUSEL, L., BOSKOVIC, V., DOMITNER, J., FICKO, M. & BREZOCNIK, M. 2018. Genetic programming method for modelling of cup height in deep drawing process. *Advances in Production Engineering & Management,* 13**,** 358-365.

HAMZA, A., AYADI, S. & HADJ-TAIEB, E. 2015. Propagation of strain waves in cylindrical helical springs. *Journal of Vibration and Control,* 21**,** 1914-1929.

HAMZA, A., AYADI, S. & HADJ-TAÏEB, E. 2013a. The natural frequencies of waves in helical springs. *Comptes Rendus Mécanique,* 341**,** 672-686.

HAMZA, A., AYADI, S. & HADJ-TAÏEB, E. 2013b. Resonance phenomenon of strain waves in helical compression springs. *Mechanics & Industry,* 14**,** 253-265.

HE, C., LI, J., ZHAO, L., WANG, Y. & GU, W. 2017. The Combustion Modeling of the Heavy-Duty Diesel Engine Based on Genetic Programming. SAE Technical Paper.

HUBER, R., CLAUBERG, J. & ULBRICH, H. 2010. An efficient spring model based on a curved beam with non-smooth contact mechanics for valve train simulations. *SAE International Journal of Engines,* 3**,** 28-34.

JADHAV, T., ANGAJ, M. & KAPATKAR, V. 2019. Finite Element Analysis of Helical Coil Spring with Cushioning Buffer.

JAMALI, A., KHALEGHI, E., GHOLAMINEZHAD, I. & NARIMAN-ZADEH, N. 2016. Modelling and prediction of complex non-linear processes by using Pareto multi-objective genetic programming. *International Journal of Systems Science,* 47**,** 1675-1688.

JIANG, W. & HENSHALL, J. 2000. A novel finite element model for helical springs. *Finite Elements in Analysis and Design,* 35**,** 363-377.

JIANG, W., JONES, W., WANG, T. & WU, K. 1991. Free vibration of helical springs. *Journal of Applied Mechanics,* 58**,** 222-228.

JIANG, W., JONES, W., WU, K. & WANG, T. Non-linear and linear, static and dynamic analyses of helical springs. 30th Structures, Structural Dynamics and Materials Conference, 1989. 1200.

JIANG, W., WANG, T. & JONES, W. 1992. The forced vibration of helical springs. *International journal of mechanical sciences,* 34**,** 549-562.

JOHN, H. 1992. Holland. genetic algorithms. *Scientific american,* 267**,** 44-50.

JOHNSON, J. A., WIDENER, S., GITLOW, H. & POPOVICH, E. 2006. A "Six Sigma"© black belt case study: GEP Box's paper helicopter experiment part A. *Quality Engineering,* 18**,** 413-430.

KAGAWA, Y. 1968. On the dynamical properties of helical springs of finite length with small pitch. *Journal of Sound and Vibration,* 8**,** 1-15.

KANIMOZHI, J., JOTHI, J., SRINATH, T. J., JAYASIMMAN, M. & SRINIVASAN, D. K. 2018. Design and Analysis of Helical Springs with Non-Circular Cross Section. *International Journal of Latest Technology in Engineering, Management & Applied Science (IJLTEMAS).*

KAOUA, S. A., TAIBI, K., BENGHANEM, N., AZOUAOUI, K. & AZZAZ, M. 2011. Numerical modelling of twin helical spring under tensile loading. *Applied Mathematical Modelling,* 35**,** 1378-1387.

KARA, I. F. 2011. Prediction of shear strength of FRP-reinforced concrete beams without stirrups based on genetic programming. *Advances in Engineering Software,* 42**,** 295-304.

KATO, M. 1974. Study on Dynamic Properties of a Varying-Pitch Helical Compression Spring. *Bulletin of JSME,* 17**,** 1015-1022.

KELLY, A. & KNIGHT, C. 1992. Helical coil suspension springs in finite element models of compressors.

KHURD, S. N. & KULKARNI, P. P. 2014. Probabilistic Design of Helical Coil Spring for Longitudinal Invariance by Using Finite Element Method. Int. Journal of Engineering Research and Applications www. ijera. com ISSN.

KIM, D. Development of a finite element program for dynamic analysis of helical springs. Proceedings Third Russian-Korean International Symposium on Science and Technology. KORUS'99 (Cat. No. 99EX362), 1999. IEEE, 309-314.

KIM, D. & DAVID, J. W. 1990. A combined model for high speed valve train dynamics (partly linear and partly nonlinear). SAE Technical Paper.

KITADA, T. & KUCHITA, M. 2008. Development of vibration calculation code for engine valve-train. *Mitsubishi Motors Technical Review, Report***,** 74-82.

KOBELEV, V. 2014. Effect of static axial compression on the natural frequencies of helical springs. *Multidiscipline Modeling in Materials and Structures,* 10**,** 379-398.

KOSTER, M. 1975. Effect of flexibility of driving shaft on the dynamic behavior of a cam mechanism. *Journal of Engineering for Industry,* 97**,** 595-602.

KUMBHALKAR, M. A., BHOPE, D. & VANALKAR, A. 2017. Evaluation of frequency excitation of helical suspension spring using finite element analysis. *International Journal of Computer Aided Engineering and Technology,* 9**,** 420-433.

KURUGODU, H., BORDOLOI, S., HONG, Y., GARG, A., GARG, A., SREEDEEP, S. & GANDOMI, A. H. 2018. Genetic programming for soil-fiber composite assessment. *Advances in Engineering Software,* 122**,** 50-61.

KUSHWAHA, M., RAHNEJAT, H. & JIN, Z. 2000. Valve-train dynamics: a simplified tribo-elasto-multi-body analysis. *Proceedings of the Institution of Mechanical Engineers, Part K: Journal of Multi-body Dynamics,* 214**,** 95-110.

LAVANYA, N., RAO, P. S. & REDDY, M. P. 2014. Design and analysis of a suspension coil spring for automotive vehicle. *International Journal of Engineering Research and Applications,* 4**,** 151-157.

LEE, J. 2007a. Free vibration analysis of cylindrical helical springs by the pseudospectral method. *Journal of Sound and Vibration,* 302**,** 185-196.

LEE, J. 2007b. Free vibration analysis of non-cylindrical helical springs by the pseudospectral method. *Journal of Sound and Vibration,* 305**,** 543-551.

LEE, J. & PATTERSON, D. 1997. Nonlinear valve train dynamics simulation with a distributed parameter model of valve springs. *Journal of engineering for gas turbines and power,* 119**,** 692-698.

LEE, J. & THOMPSON, D. 2001. Dynamic stiffness formulation, free vibration and wave motion of helical springs. *Journal of Sound and Vibration,* 239**,** 297-320.

LEE, K. 2004. Dynamic contact analysis for the valvetrain dynamics of an internal combustion engine by finite element techniques. *Proceedings of the Institution of Mechanical Engineers, Part D: Journal of Automobile Engineering,* 218**,** 353-358.

LI, M., AZARM, S. & AUTE, V. A multi-objective genetic algorithm for robust design optimization. Proceedings of the 7th annual conference on Genetic and evolutionary computation, 2005. 771-778.

LIN, Y., CUI, W. M. & SONG, B. F. Reliability Optimization Design of Spacecraft Valve Spring. Advanced Materials Research, 2012. Trans Tech Publ, 851-857.

LIN, Y., HODGES, P. & PISANO, A. 1993. Optimal design of resonance suppression helical springs.

LIN, Y. & PISANO, A. 1990. Three-dimensional dynamic simulation of helical compression springs. *Journal of Mechanical Design,* 112**,** 529-537.

LIN, Y. & PISANO, A. P. 1987. General dynamic equations of helical springs with static solution and experimental verification. *Journal of applied mechanics,* 54**,** 910-917.

LIN, Y. & PISANO, A. P. 1988. The differential geometry of the general helix as applied to mechanical springs. *Journal of Applied Mechanics,* 55**,** 831-836.

LIU, D., ZHOU, X. & TOROPOV, V. 2016. Metamodels for composite lattice fuselage design. *International Journal of Materials, Mechanics and Manufacturing,* 4**,** 175-178.

LIU, F. C. & GENG, L. The Variation Coefficient Method for Reliability Sensitivity Analysis of Cylindrical Helical Spring. Applied Mechanics and Materials, 2011. Trans Tech Publ, 285-290.

LIU, H. & KIM, D. 2011. Estimation of valve spring surge amplitude using the variable natural frequency and the damping ratio. *International Journal of Automotive Technology,* 12**,** 631.

LOVE, A. E. H. 1972. *A treatise on the mathematical theory of elasticity*, Cambridge university press.

LOVESTEAD, R. L. & SAFAAI - JAZI, A. 2020. Optimum design of helical antennas by genetic algorithm. *Microwave and Optical Technology Letters,* 62**,** 425-431.

LUO, L., LIU, D., ZHU, M., LIU, Y. & YE, J. 2018. Maximum energy conversion from human motion using piezoelectric flex transducer: A multi-level surrogate modeling strategy. *Journal of Intelligent Material Systems and Structures,* 29**,** 3097-3107.

MAHADEVAN, N. K., GANESH, S. & VINODH, M. D. 2018. STRESS ANALYSIS OF COMPOSITE HELICAL SPRING (Cr-Va+ Low carbon steel & Cr-Va+ Stainless Steel). *International Journal of Pure and Applied Mathematics,* 119**,** 15855-15867.

MAHFOUD, S. W. Simple Analytical Models of Genetic Algorithms for Multimodal Function Optimization. ICGA, 1993. Citeseer, 643.

MANACHE, G. & MELCHING, C. S. 2004. Sensitivity analysis of a water-quality model using Latin hypercube sampling. *Journal of Water Resources Planning and Management,* 130**,** 232-242.

MCKAY, M. D., BECKMAN, R. J. & CONOVER, W. J. 1979. Comparison of three methods for selecting values of input variables in the analysis of output from a computer code. *Technometrics,* 21**,** 239-245.

MITRA, A. C., DESAI, G. J., PATWARDHAN, S. R., SHIRKE, P. H., KURNE, W. M. & BANERJEE, N. 2016. Optimization of passive vehicle suspension system by genetic algorithm. *Procedia Engineering,* 144**,** 1158-1166.

MORIO, J. & BALESDENT, M. 2015. *Estimation of rare event probabilities in complex aerospace and other systems: a practical approach*, Woodhead Publishing.

MOTTERSHEAD, J. E. 1980. Finite elements for dynamical analysis of helical rods. *International Journal of Mechanical Sciences,* 22**,** 267-283.

MUHR, T. H. 1993. New technologies for engine valve springs. *SAE Transactions***,** 1336-1345.

MULLA, T. M., KADAM, S. J. & KENGAR, V. S. 2012. Finite element analysis of helical coil compression spring for three wheeler automotive front suspension. *Int. J. Mech. Ind. Eng,* 2**,** 74-77.

NUO, L., HAO, C. & HAN, J.-Q. Application of Multigene Genetic Programming for Estimating Elastic Modulus of Reservoir Rocks. 2019 Symposium on Piezoelectrcity, Acoustic Waves and Device Applications (SPAWDA), 2019. IEEE, 1-4.

OKARMUS, M. M., KERIBAR, R., DASCALESCU, D.-L. & ZDRODOWSKI, R. 2013. An Efficient, One-Dimensional, Finite Element Helical Spring Model for Use in Planar Multi-Body Dynamics Simulation. *SAE International Journal of Engines,* 6**,** 979-989.

OLSSON, A., SANDBERG, G. & DAHLBLOM, O. 2003. On Latin hypercube sampling for structural reliability analysis. *Structural safety,* 25**,** 47-68.

OLSSON, A. M. & SANDBERG, G. E. 2002. Latin hypercube sampling for stochastic finite element analysis. *Journal of Engineering Mechanics,* 128**,** 121-125.

PALA, M. 2008. Genetic programming-based formulation for distortional buckling stress of cold-formed steel members. *Journal of Constructional Steel Research,* 64**,** 1495-1504.

PARANJPE, R. 1990. Dynamic analysis of a valve spring with a coulomb-friction damper. *Journal of Mechanical Design,* 112**,** 509-513.

PATTAR, S., SANJAY, S. & MATH, V. 2014. Static analysis of helical compression spring. *IJRET: International Journal of Research in Engineering and Technology,* 3.

PAWAR, H. & DESALE, D. 2018. Optimization of Three Wheeler Front Suspension Coil Spring. *Procedia Manufacturing,* 20**,** 428-433.

PHILLIPS, J. W. & COSTELLO, G. A. 1972. Large deflections of impacted helical springs. *the Journal of the Acoustical Society of America,* 51**,** 967-973.

PHLIPS, P., SCHAMEL, A. & MEYER, J. 1989. An efficient model for valvetrain and spring dynamics. SAE Technical Paper.

PISANO, A. & FREUDENSTEIN, F. 1983. An experimental and analytical investigation of the dynamic response of a high-speed cam-follower system. Part 2: a combined, lumped/distributed parameter dynamic model. *Journal of Mechanisms, Transmissions, and Automation in Design,* 105**,** 699-704.

PÖLLÄNEN, I. & MARTIKKA, H. 2010. Optimal re-design of helical springs using fuzzy design and FEM. *Advances in Engineering Software,* 41**,** 410-414.

QIMIN, X., LIWEI, L. & QILI, X. 2009a. The optimal design and simulation of helical spring based on particle swarm algorithm and MATLAB. *Wseas transactions on circuits and systems,* 8**,** 84-93.

QIMIN, X., LIWEI, L. & QILI, X. 2009b. The optimal design and simulation of helical spring based on particle swarm algorithm and MATLAB. *WSEAS Transactions on Circuits and Systems***,** 84-83.

QIN-MAN, F., YONG-HAI, W., KUN, L. & FENG, W. Multi-objective optimization design of automobile suspension helical spring. 2010 Third International Conference on Information and Computing, 2010. IEEE, 219-222.

RAMU, M., RAJA, V. P., THYLA, P. & GUNASEELAN, M. 2010. Design optimization of complex structures using metamodels. *Jordan Journal of Mechanical and Industrial Engineering,* 4**,** 653-664.

RASHIDI, M., BUDHABHATTI, S. P. & FRATER, J. L. Dynamics of a Coulomb Damped Helical Spring: A Finite Element Approach. ASME 2004 International Mechanical Engineering Congress and Exposition, 2004. American Society of Mechanical Engineers Digital Collection, 473-478.

RATLE, F., LECARPENTIER, B., LABIB, R. & TROCHU, F. Multi-objective optimization of a composite material spring design using an evolutionary algorithm. International Conference on Parallel Problem Solving from Nature, 2004. Springer, 803-811.

READMAN, M., MULDOON, M., REYNOLDS, L., MORRIS, R., BAYLISS, M., WOOD, D. & STEWART, I. 2001. Control of free length when coiling a helical spring. *IEE Proceedings-Control Theory and Applications,* 148**,** 239-244.

RENNO, J. M. & MACE, B. R. 2012. Vibration modelling of helical springs with non-uniform ends. *Journal of Sound and Vibration,* 331**,** 2809-2823.

ROß, J. & ARNOLD, M. 1993. Analysis of Dynamic Interactions in Valve Train Systems of IC-Engines by Using a Simulation Model. SAE Technical Paper.

ROSTAMI, A., ARABLOO, M. & EBADI, H. 2017. Genetic programming (GP) approach for prediction of supercritical CO2 thermal conductivity. *Chemical Engineering Research and Design*, 122**,** 164-175.

SAHOO, P. & BARMAN, T. K. 2012. ANN modelling of fractal dimension in machining. *Mechatronics and Manufacturing Engineering.* Elsevier.

SARKATE, T. S. A Finite Element Approach for Analysis of a Helical Coil Compression Spring Using CAE Tools. Applied Mechanics and Materials, 2013. Trans Tech Publ, 703-707.

SASTRY, M. N. P., DEVI, K. D., REDDY, K. H., REDDY, K. M. & KUMAR, V. S. Reliability based design optimization of helical compression spring using probabilistic response surface methodology. IEEE-International Conference On Advances In Engineering, Science And Management (ICAESM-2012), 2012. IEEE, 329-334.

SCHAMEL, A. 1993. *A frequency domain approach to the analysis and optimization of valve spring dynamics.* © A. Schamel.

SCHAMEL, A. R., HAMMACHER, J. & UTSCH, D. 1993. Modeling and measurement techniques for valve spring dynamics in high revving internal combustion engines. *SAE Transactions***,** 820-836.

SCHMIDT, M. & LIPSON, H. 2009. Distilling free-form natural laws from experimental data. *science,* 324**,** 81-85.

SEFLER, J. F. & PISANO, A. 1993. The design, experimentation, and simulation of a novel Coulomb friction device for automotive valve spring damping. *Journal of Mechanical Design,* 115**,** 871-876.

SEIDLITZ, S. 1989. Valve train dynamics-a computer study. SAE technical paper.

SEQUENZIA, G., OLIVERI, S., CALABRETTA, M., FATUZZO, G. & CALI, M. 2011. A new methodology for calculating and modelling non-linear springs in the valve train of internal combustion engines. SAE Technical Paper.

SERRET, J.-A. 1851. Sur quelques formules relatives à la théorie des courbes à double courbure. *Journal de mathématiques pures et appliquées***,** 193-207.

SHAO, K. L., WANG, F. & WU, Y. H. Optimization Design of Helical Spring based on Multi-objective Genetic Algorithm. Applied Mechanics and Materials, 2013. Trans Tech Publ, 1068-1071.

SHEVALE, D. V. & NIRANJAN, D. K. 2016. Analysis of Helical Compression Spring for Estimation of Fatigue Life. *Imperial Journal of Interdisciplinary Research (IJIR),* 2**,** 2088-2093.

SIMPSON, T. W., POPLINSKI, J., KOCH, P. N. & ALLEN, J. K. 2001. Metamodels for computer-based engineering design: survey and recommendations. *Engineering with computers,* 17**,** 129-150.

SIMS, K. 1993. Interactive evolution of equations for procedural models. *The Visual Computer,* 9**,** 466-476.

SOROKIN, S. V. 2009. Linear dynamics of elastic helical springs: asymptotic analysis of wave propagation. *Proceedings of the Royal Society A: Mathematical, Physical and Engineering Sciences,* 465**,** 1513-1537.

SOROKIN, S. V. 2011. The Green's matrix and the boundary integral equations for analysis of time-harmonic dynamics of elastic helical springs. *The Journal of the Acoustical Society of America,* 129**,** 1315-1323.

STANDER, N. & DU PREEZ, R. 1992. Vibration analysis of coil springs by means of isoparametric curved beam finite elements. *Communications in Applied Numerical Methods,* 8**,** 373-383.

STEPHEN, C., SELVAM, R. & SURANJAN, S. A Comparative Study of Steel and Composite Helical Springs Using Finite Element Analysis. 2019 Advances in Science and Engineering Technology International Conferences (ASET), 2019. IEEE, 1-6.

STOKES, V. K. 1974. On the dynamic radial expansion of helical springs due to longitudinal impact. *Journal of Sound Vibration,* 35**,** 77-99.

SUZUKI, S., KAMIYA, S., IMAIZUMI, T. & SANADA, Y. 1996. Approaches to minimizing side force of helical coil springs for riding comfort. SAE Technical Paper.

TAKTAK, M., OMHENI, K., ALOUI, A., DAMMAK, F. & HADDAR, M. 2014. Dynamic optimization design of a cylindrical helical spring. *Applied acoustics,* 77**,** 178-183.

TANYILDIZI, H. & ÇEVIK, A. 2010. Modeling mechanical performance of lightweight concrete containing silica fume exposed to high temperature using genetic programming. *Construction and Building Materials,* 24**,** 2612-2618.

TEMEL, B. & C¸ ALIM, F. 2003. Forced vibration of cylindrical helical rods subjected to impulsive loads. *J. Appl. Mech.,* 70**,** 281-291.

TEODORESCU, M., KUSHWAHA, M., RAHNEJAT, H. & ROTHBERG, S. 2007. Multi-physics analysis of valve train systems: from system level to microscale interactions. *Proceedings of the Institution of Mechanical Engineers, Part K: Journal of Multi-body Dynamics,* 221**,** 349-361.

TOGUN, N. & BAYSEC, S. 2010. Genetic programming approach to predict torque and brake specific fuel consumption of a gasoline engine. *Applied Energy,* 87**,** 3401-3408.

TSAI, H.-C. & LIAO, M.-C. 2019. Modeling Torsional Strength of Reinforced Concrete Beams using Genetic Programming Polynomials with Building Codes. *KSCE Journal of Civil Engineering,* 23**,** 3464-3475.

ÜNLÜSOY, Y. & TÜMER, S. 1994. Non-linear dynamic model and its solution for a high speed cam mechanism with coulomb friction. *Journal of sound and vibration,* 169**,** 395-407.

WAHL, A. M. 1944. *Mechanical springs,* Penton Publishing Company.

WANG, J., LUO, S. & SU, D. 2016. Multi-objective optimal design of cycloid speed reducer based on genetic algorithm. *Mechanism and Machine Theory,* 102**,** 135-148.

WANG, N. N., HOU, Y. F. & TIAN, Z. Z. Nonlinear vibration characteristics of helical spring. Applied Mechanics and Materials, 2010. Trans Tech Publ, 1317-1322.

WANG, S., XIAO, J., WANG, J., JIAN, G., WEN, J. & ZHANG, Z. 2018. Application of response surface method and multi-objective genetic algorithm to configuration optimization of Shell-and-tube heat exchanger with fold helical baffles. *Applied Thermal Engineering,* 129**,** 512-520.

WITTRICK, W. H. 1966. On elastic wave propagation in helical springs. *International Journal of Mechanical Sciences,* 8**,** 25-47.

WU, W., WANG, Z., ZHENG, M., GAO, Z. & SONG, W. 2017. Finite Element Simulation of Intake Valve Spring. *DEStech Transactions on Computer Science and Engineering*.

XI, P. Y. & ZHU, J. Simulated Annealing Optimization on Valve Spring of Diesel Engine. Applied Mechanics and Materials, 2011. Trans Tech Publ, 511-514.

YANG, O., ENGEL, P., PRASAD, B. & WOOLLATT, D. 1996. Dynamic response of compressor valve springs to impact loading.

YANG, Y. & SOH, C. K. 2002. Automated optimum design of structures using genetic programming. *Computers & Structures,* 80**,** 1537-1546.

YILDIRIM, V. 1996. Investigation of parameters affecting free vibration frequency of helical springs. *International Journal for Numerical Methods in Engineering,* 39**,** 99-114.

YILDIRIM, V. 2001. Free vibration of uniaxial composite cylindrical helical springs with circular section. *Journal of sound and vibration,* 239**,** 321-333.

YıLDıRıM, V. 2009. Numerical buckling analysis of cylindrical helical coil springs in a dynamic manner. *International Journal Of Engineering & Applied Sciences,* 1**,** 20-32.

YıLDıRıM, V. 2012. On the linearized disturbance dynamic equations for buckling and free vibration of cylindrical helical coil springs under combined compression and torsion. *Meccanica,* 47**,** 1015-1033.

YILDIRIM, V. & İNCE, N. 1997. Natural frequencies of helical springs of arbitrary shape. *Journal of Sound and Vibration,* 204**,** 311-329.

YOKOTA, T., TAGUCHI, T. & GEN, M. 1997. A solution method for optimal weight design problem of herical spring using genetic algorithms. *Computers & industrial engineering,* 33**,** 71-76.

YU, A. & HAO, Y. 2011. Free vibration analysis of cylindrical helical springs with noncircular cross-sections. *Journal of Sound and Vibration,* 330**,** 2628-2639.

YUNUS, M. & ALSOUFI, M. S. 2017. Prediction of mechanical properties of plasma sprayed thermal barrier coatings (TBCs) with genetic programming (GP). *International Journal of Engineering Trends and Technology,* 47**,** 139-145.

ZHANFANG, L. & JUNLING, T. Study on the optimization design of hydro-pneumatic spring based on genetic algorithm. 2011 Third International Conference on Measuring Technology and Mechatronics Automation, 2011. IEEE, 568-571.

ZHANG, L. Robust design of valve spring based on Taught method. 2nd International Conference on Electronic & Mechanical Engineering and Information Technology, 2012. Atlantis Press.

ZHENG, H., YAN, F., LU, C., XU, F., LI, Q. & TIAN, W. 2017. Optimization design of the valve spring for abnormal noise control in a single-cylinder gasoline

engine. *Proceedings of the Institution of Mechanical Engineers, Part D: Journal of Automobile Engineering*, 231**,** 204-213.

# Appendix A

***Python codes for fitting 3D scan data of the beehive spring***

```
import numpy as np

import pandas as pd

import matplotlib.pyplot as plt


# directories


# read x and y data

def read_data(path, title):

    lines = pd.read_csv(path)

    data = np.array(lines[title])

    return data


# function fitting

def fun_fit(x_data, y_data, deg):

    fit_coefs = np.polyfit(x_data, y_data, deg=deg)

    fit_val = np.polyval(fit_coefs, x_data)

    return fit_coefs, fit_val


def fit_c_dia(x):

    ''' represent the fitting funtions'''

    power = len(fit_coefs_cd) - 1

    fit_f = 0
```

```
    for num in range(len(fit_coefs_cd)):
        y_item = fit_coefs_cd[num]*x**power
        power -= 1
        fit_f += y_item
    return (fit_f*1e-3)**3


def fit_p_add(x):
    ''' represent the fitting funtions'''
    power = len(fit_coefs_pv) - 1
    fit_f = 0
    for num in range(len(fit_coefs_pv)):
        y_item = fit_coefs_pv[num]*x**power
        power -= 1
        fit_f += y_item
    return fit_f*1e-3


def plot_fit(x_data, y_data, fit_val, pos):
    ‘’’ plot the original points vs. fitting curve’’’
    plot1 = plt.plot(x_data, y_data, 's', label = 'Oiginal Points')
    plot2 = plt.plot(x_data, fit_val, 'r', label = 'Fitting Data')
    plt.xlabel('X')
    plt.ylabel('Y')
    plt.legend(loc=pos)
    plt.title('Original Points vs. Fitting Curve')
    plt.show()
```

```
    return


# directories
path_cd = ‘coil_diameter.csv'
path_sp = ‘spring_pitch.csv'


# fitting results
c_rad, c_dia = read_data(path_cd, 'Rad'), read_data(path_cd, 'coil_diamter(mm)')
rad, pitch = read_data(path_sp, 'Rad'), read_data(path_sp, 'spring_pitch(mm)')


fit_coefs_cd, fit_val_cd = fun_fit(c_rad, c_dia, deg=15)
fit_coefs_pv, fit_val_pv = fun_fit(rad, pitch, deg=15)


plot_fit(c_rad, c_dia, fit_val_cd, 3)
plot_fit(rad, pitch, fit_val_pv, 2)
```

# Appendix B

***1. Source result codes of spring force generated by GPlearn in Python:***

*F = div(add(X3, X7), div(div(X8, add(X6, add(add(sub(add(X6, sub(add(X6, sub(add(X3, sub(add(X3, X7), sub(X0, 0.765))), mul(X2, 0.765))), div(mul(X2, 0.765), div(X8, add(add(X4, add(0.398, div(div(add(add(X4, add(sub(X1, X4), X1)), sub(X4, mul(sqrt(X5), sub(X7, X1)))), sub(X6, X5)), X3))), div(sub(add(X3, sqrt(mul(X2, X7))), add(X4, add(0.398, sub(X4, X6)))), add(add(X4, add(sub(X1, X4), X1)), add(0.398, sub(X4, X6))))))))), sub(X9, 0.765)), X7), sub(X4, X5)))), X4))*

***2. Source result codes of first order natural frequency generated by GPlearn in Python:***

*NF = mul(mul(add(sqrt(sub(sub(X4, X0), sub(sub(div(X2, sqrt(X1)), sub(sub(X7, X5), sub(sub(sqrt(X6), sqrt(X6)), add(-0.733, X9)))), X6))), X3), sqrt(X4)), add(add(sub(X6, X9), add(X7, X1)), add(div(X7, X5), sqrt(sub(sub(X4, X0), sub(sub(div(X2, sqrt(X1)), sub(sub(X7, X5), sub(sub(sub(X8, X1), sqrt(X6)), add(-0.733, X9)))), X6))))))*

*Note: The symbols 'add', 'sub', 'mul', 'div' and 'sqrt' represent for the math operators '+', '-', '*', '/', '^' respectively.*